A Thesis

entitled

Evaluation of Spatial Interpolation Techniques Built in the Geostatistical Analyst Using

Indoor Radon Data for Ohio, USA

by

Dipsikha Sarmah

Submitted to the Graduate Faculty as partial fulfillment of the requirements for the

Master of Science Degree in Civil Engineering

_____
Dr. Ashok Kumar, Committee Chair

_____
Dr. Brian W. Randolph, Committee Member

_____
Dr. Matthew Franchetti, Committee Member

_____
Dr. Patricia R. Komuniecki, Dean
College of Graduate Studies

The University of Toledo

December 2012

An Abstract of

Evaluation of Spatial Interpolation Techniques Built in the Geostatistical Analyst Using

Indoor Radon Data for Ohio, USA

by

Dipsikha Sarmah

Submitted to the Graduate Faculty as partial fulfillment of the requirements for the
Master of Science Degree in Civil Engineering

The University of Toledo

December 2012

According to the United States Environmental Protection Agency, radon is the number

one cause of lung cancer among non-smokers, and it is responsible for about 21,000 lung

cancer deaths every year in the United States. In the State of Ohio, 14% of lung cancer

deaths are caused due to radon. It is essential to have the radon concentration data for

every location (i.e., zip codes) so that necessary preventive measures can be taken up.

Measuring the radon concentration across the entire State of Ohio will be very expensive

and time consuming. This research focuses on the application of six geographical

information system (GIS) based interpolation techniques to estimate the radon

concentration in the unmeasured zip codes in the State of Ohio. The radon concentration

in homes has been obtained by The University of Toledo researchers from various

commercial testing services, university researchers, and county health departments. The

data are divided into two sets. The first set uses 80% of the data for training different

interpolation schemes, and the second data set includes 20% of the data to evaluate the

interpolation techniques. Statistical performance measures such as coefficient of

correlation (r), Spearman correlation coefficient (ρ), slope of the regression line (m), ratio of the intercept of the regression line to the average observed concentrations (b/C_o), fractional variance (FV), fraction of prediction within a factor of two of the observations (FA$_2$), model comparison measure (MCM$_2$), geometric mean bias (MG), geometric mean variance (VG), normalized mean square error (NMSE), fractional bias (FB), revised index of agreement (IOA$_r$), accuracy for paired peak (A$_p$), maximum ratio (R$_{max}$), scatter plots, quantile – quantile (QQ) plots and bootstrap 95% confidence interval estimates based on extreme-end concentrations (i.e., peak-end/low-end), and the mid-range concentrations of indoor air quality (IAQ) models are performed on the predicted data points to evaluate the best interpolation technique.

Considering the statistical indicators for peak-end, low-end and mid-range estimates, it has been found that cokriging is a suitable technique for peak-end estimates, and the radial basis function (RBF) technique meets all the acceptable criteria for low-end and mid-range estimates. After considering the closeness of the greater number of measures to their respective ideal values, graphical representations of the scatter plots and QQ plots, the RBF technique surpasses the other six interpolation techniques. Again, the summary of the bootstrap confidence interval estimates among the techniques indicate that the RBF technique is not significantly different from the other five interpolation techniques under all situations. Therefore, the RBF technique may not be the best technique always when applied to similar sets of dataset from other states and countries. The RBF technique is tentatively suggested in this thesis to perform the interpolation of radon concentration for the unmeasured zip codes in the State of Ohio. This technique is

used to understand the extent of radon problems in Ohio. This approach provides a complete picture of radon distribution in the state. It has been found from the zip code based analysis that the number of zip codes exceeding 2.7 pCi/l (World Health Organization (WHO) recommended limit), 4 pCi/l (US Environmental Protection Agency (EPA) action limit), 8 pCi/l and 20 pCi/l are 1300, 693, 28, and 2, respectively after prediction using the RBF technique.

This thesis is dedicated to my husband, Mr. Anujit Barooah for his love, support, and encouragement

Acknowledgements

Table of Contents

List of Tables

List of Figures

Chapter 1

Introduction

1.1 Overview

Radon is a colorless chemically – unreactive inert gas and it was discovered by English physicist Ernest Rutherford in 1899. Radon is produced by the radioactive decay of the element uranium. The atomic radius of radon is 1.34 angstrom, and it is the heaviest known gas; radon is nine times denser than air. Radon is a single atom gas, so it can easily penetrate many common materials like paper, leather, and building materials like gypsum board, concrete block, and mortar, sheathing paper, wood paneling, and most insulation. Figure 1-1 shows the concentration of radon in outdoor air, indoor air, soil air, and ground water. Radon concentration is commonly expressed in terms of the alpha particles it generates, and the unit of concentration is "picocuries per liter of air" (pCi/l). Radon exposure is the second major cause of lung cancer in the general population after smoking. The lung cancer deaths due to radon in the US are around 15,000 to 22,000 annually according to the National Cancer Institute. The lung cancer cases each year in Ohio are about 7,700 and 900 of them are caused due to the radon gas. Different devices are available to measure the radon concentrations, and those are charcoal canisters, alpha-track detectors, scintillation counters, ionization chambers, positive barrier, two-filter

method, electrostatic radon monitor etc. It is time consuming, and the investment will be very high to measure the radon concentration for the entire State of Ohio. Different geographic information system (GIS) based interpolation techniques could be used to predict the concentration in the unknown places for the State of Ohio.

Geographic information systems have emerged as widely used software systems for input, storage, manipulation, and output of geographically referenced data over the past couple of years. A set of sample points representing changes in the environment, landscape, or population can be used to visualize the continuity and variability of observed data across a surface using interpolation tools. A powerful collection of tools is provided by the geographical information system for the management, collection, and analysis of spatial data. The ArcGIS geostatistical analyst tool which can be used for spatial data exploration and surface generation using sophisticated statistical methods, and which allows for creating a surface from data measurements is used for this study.
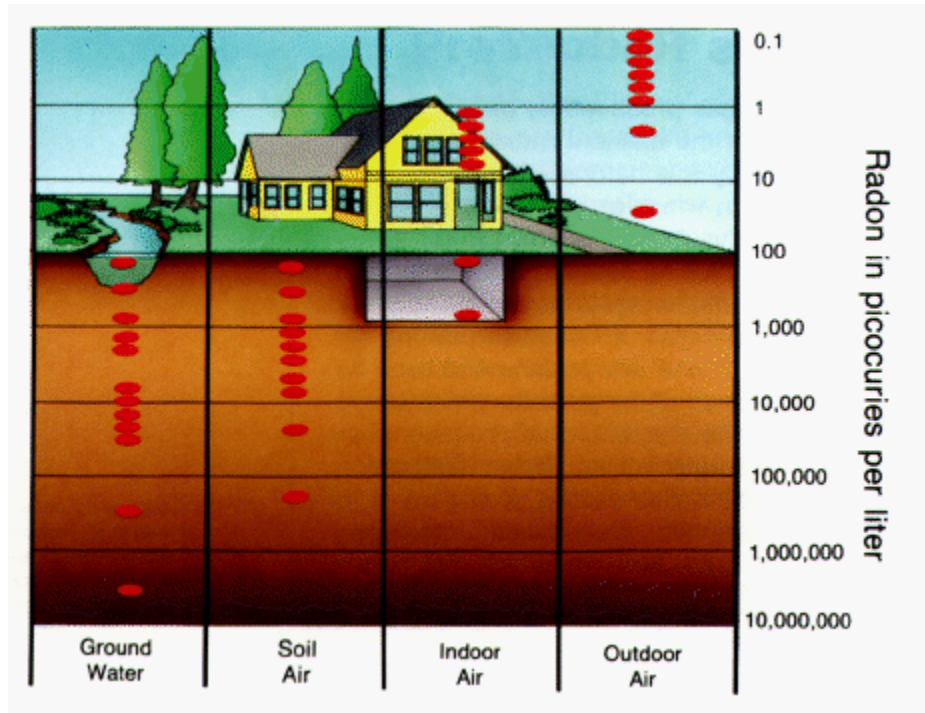
**Figure 1-1: Radon levels in outdoor air, indoor air, soil air, and ground water
(http://energy.cr.usgs.gov/radon/georadon/page4.gif)**

1.2 Problem Statement

The aim of the thesis is to evaluate the interpolation techniques in order to estimate the radon concentrations in the unmeasured zip codes where no data have been collected. The thesis is divided into three main objectives as presented below:

- The first objective is to evaluate the interpolation techniques depending on how radon data is distributed. This is done by dividing a radon data set into an 80% training data set and a 20% test data set. The geographical information system based interpolation techniques: inverse distance weighting (IDW), global polynomial interpolation (GPI), local polynomial interpolation (LPI), radial basis function (RBF), ordinary kriging, and ordinary cokriging are used on the training data set to evaluate the prediction for the test data points. The bootstrap application and the model evaluation parameters

suggested by Kadiyala and Kumar, 2012 are used to evaluate the six different interpolation techniques.

- The second objective is to perform the interpolation with the whole radon data set for the State of Ohio using the best interpolation technique and to calculate the geometric mean of radon concentrations in the unmeasured zip codes by the best interpolation technique

- The third objective can be divided in to two parts as follows:

  1) To calculate the number of zip codes having radon concentrations exceeding 2.7 pCi/l (World Health Organization (WHO) recommended limit), 4 pCi/l (US EPA action limit), 8 pCi/l, and 20 pCi/l, respectively.

  2) To calculate the percentage increase/decrease in radon concentration after prediction by the best interpolation technique for the counties in Ohio.

Chapter 2

Literature Review

2.1 Background

Interpolation is a method or mathematical function that estimates the values at locations where no measured values are available. Spatial Interpolation is widely used for creating continuous data when data are collected at discrete locations i.e., at points. For example, the precipitation maps provided by the National Weather Service (NWS) are generated from NWS stations. Some of the fields that have benefited by the use of spatial interpolation are agricultural production, temperature data, soil contamination, mining, health care, and meteorology. Various studies based on the geostatistical interpolation techniques are summarized below:

In the study by Erxleben et al. (2002), the relative performances of four spatial interpolation methods were evaluated to estimate snow water equivalent for three 1-km^2 study sites in the Colorado Rocky Mountains. Four analytical methods - inverse distance weighting, ordinary kriging, modified residual kriging, and cokriging and a combined method using binary regression trees and geostatistical methods were used to estimate snow depth over the 1-km^2 areas. Each method was assessed for accuracy using cross-

validation procedures. Cross-validation was accomplished by removing each data point and then using the remaining observations to estimate the data value. This procedure was repeated for all observations in the data set. The tree-based models provided the most accurate estimates for all the study sites.

In the study by Salih M et al. (2002), three interpolation methods: kriging, cokriging, and IDW were tested to determine the extent of spatial correlation of radon in water with bedrock radioactivity. First maps of radon concentrations in water were created from point measurements and which were then matched with existing bedrock uranium maps. Two approaches were investigated for mapping radon in ground water. The first approach treated the whole dataset as one unit creating one layer, while in the second approach the data were split into sub regions according to the distribution of the samples. Inverse distance weighting (IDW) and the kriging method were employed in both the approaches.

In the study by Sabit (2003), spatial variability in the field measured infiltration rate (IR) and soil properties having significant spatial correlation to IR were studied using kriging and cokriging procedures. The study was conducted to evaluate and compare kriging and cokriging to estimate IR using limited available data on an 8.5 Ha alluvial field. Three approaches were used to estimate the IR values within a 25 by 25 grid. These approaches were (a) Kriging using 50, 45, 40, 35 and 30 measured values of IR, (b) Cokriging using 50 measured IR values along with 60, 70, 80, 90, 100, 120, and 140 measured bulk density values and (c) Cokriging using 50, 45, 40 and 35 measured IR values along with 120 bulk density values. The study area was divided into five equal sub areas to

determine the data points to omit, and each time a datum was removed randomly from each subarea. Both kriging and cokriging estimates with original and reduced datasets were subjected to the procedure cross validation that resulted in the smallest neighborhood. Kriging and cokriging procedures were used along with isotropic semivariograms and cross-semivariograms to estimate IR values at 90 unobserved points. It was found that cokriging is superior to kriging in estimating Infiltration Rate in the case of limited available data, and results showed that cokriging provided no advantage over kriging when data were sufficient.

In the study by Yang et al. (2004), four spatial interpolation methods, inverse distance weighting (IDW), spline, kriging and cokriging, were tested to interpolate land surface temperature (LST) in Southern New England using ground temperatures measured at national weather stations in the summer of 2001. The study showed a method to estimate LST by calibrating spatial interpolation using satellite-derived surface emissivity. It was concluded that kriging interpolation could be recommended due to the considerations of prediction confidence in error maps and spatial auto-correlation between sampling sites and cokriging could be recommended for areas having rough terrains and large variation in elevation.

In the study by Li et al. (2005), the spatial distribution of surface air temperature on the Qinghai-Tibet Plateau was estimated using different interpolation methods. Inverse distance weight, ordinary kriging, ordinary cokriging, and a combined method were used to estimate the spatial distribution of the 1961-1990 January mean air temperature in the

Qinghai –Tibet Plateau. The combined method was a combination of ordinary kriging and correction of altitude effect by using the lapse rate of air temperature. The results showed that some spatial pattern can be manifested by ordinary kriging but the performance was not improved much. Although cokriging to a certain extent was an improvement over kriging, due to limited altitude information in the co-variable, the results were not in accordance with the actual situation. The combined method was found to be superior to the other methods as the interpolation results were reasonable as proved by both subjective analysis and by many earlier works.

Ustrnul et al. (2005) examined the mean monthly temperatures from 168 stations located across the entire territory of Poland and from 55 stations located in bordering zones were used to construct air temperature maps for the territory of Poland through the application of contemporary GIS techniques. Various interpolation methods: ordinary kriging, cokriging, universal kriging, and residual kriging were tested. Residual kriging was chosen for map construction, and it produces the exact mean temperature maps for territory of Poland and Central Europe.

In the study by Liu et al. (2006), four hundred and fifty soil samples in topsoil of the Hangzhou-Jiaxing-Huzhou (HJH) plain were selected to characterize the spatial variability of Cu, Zn, Pb, Cr and Cd. Ordinary kriging and logonormal kriging were carried out to map the spatial patterns of heavy metals. Disjunctive kriging was used to quantify the probability of heavy metal concentration higher than their guide value and the Cokriging method was used to minimize the sampling density for Cu, Zn, and Cr. The

Cation Exchange Capacity (CEC) of the heavy metals was used as a co-variable for cokriging and the overall estimated quality of Cu, Zn, and Cr by cokriging was better than that by kriging. The results showed that Cu, Zn, and Cd had high risk for causing environmental pollution and human health.

In the study by Luo et al. (2008), seven methods of spatial interpolation: trend surface analysis, inverse distance weighting, local polynomial, thin plate spline, ordinary kriging, universal kriging, and ordinary cokriging were compared to determine their suitability for estimating daily wind speed surfaces from the data recorded at nearly 190 locations across England and Wales. The results showed that the cokriging method was most likely to produce the best estimation of a continuous surface for wind speed, and the result had temporal consistency. The cokriging maps showed more details than the kriging maps due to the inclusion of the co-variable, elevation, in the estimation.

In the study by Ahmadi et al. (2008), geostatistical methods: kriging and cokriging were applied on the maximum, minimum and mean ground water depths of 39 wells. Results showed that ground water depths were all spatially correlated. To check the accuracy of the kriging and cokriging methods, the known ground water depth points were estimated by kriging and cokriging with cross-validation. The root mean square error (RMSE) was used to evaluate the precision of the two methods and it was seen that cokriging had less RMSE error as compared to kriging. The result showed that cokriging gives a more accurate estimation than kriging.

In the study by Moral et al. (2010), the ordinary kriging (OK), simple kriging (SK) and universal kriging (UK) methods were compared with three multivariate algorithms: collocated ordinary kriging (OCK), simple kriging with varying local means (SKV) and regression kriging (RK) which take into account the altitude. The different techniques were applied to monthly and annual precipitation data measured at 136 meteorological stations in a region of southwestern Spain. The results of the analysis showed that all the multivariate techniques (OCK, SKV & RK) excelled over the univariate methods (OK, SK & UK), yet cross-validation had shown that prediction performances vary among algorithms. SKV and RK had the smallest mean square error; therefore, performance was better than the OCK.

In the study by Sarmadian et al. (2010), continuous mapping was carried out to evaluate the accuracy of different techniques including kriging and cokriging methods for prediction of spatial distribution of topsoil calcium carbonate in Zanjan province, Central Iran. In order to carry out geostatistical analysis, the sampling was done with stratified random methods and soil samples from 0 to 15 cm depth were collected from 23 soil profiles located in Zanjan province. Cross validation and statistical parameters such as the correlation coefficient and RMSE were used for comparing and evaluating statistical methods. The results showed that the cokriging method has the higher correlation coefficient and less RMSE, which implies that the cokriging method had the higher accuracy than kriging method to predict calcium carbonate content.

In the study by Akkala et al. (2010), several interpolation techniques and available software were reviewed. A comparative study of generally used techniques and a review of geographic information system software were done to interpolate environmental data. Eleven interpolation techniques were obtained from the existing literature for the interpolation of environmental data. Some of these techniques such as kriging, inverse distance weighting, splines etc. were applied to estimate the unknown environmental data e.g. temperature, rainfall and toxic substance concentrations. It had been recommended that research and development of knowledge based technique e.g. knowledge based neural networks could result in a new-generation of interpolation schemes that would go beyond the extent of the traditional interpolation techniques.

In the study by Nas, Bilegehan et al. (2011), the ground water quality of Konya city was mapped by using GIS and geostatistics techniques. The quality of ground water was determined by taking samples from 177 wells within the study area. The spatial distribution of ground water quality parameters were found through GIS and geostatistical techniques. Ordinary kriging was used to obtain the spatial distribution of ground water quality parameters.

In the study by Hooshmand et al. (2011), two geostatistic methods, kriging and cokriging, were applied to estimate chloride content and sodium adsorption ratio (SAR) of ground water in the Boukan area, Iran. The performance of the interpolation methods were evaluated by cross validation method. The results obtained from both the methods were

compared, and it was seen that the cokriging method was more accurate than the kriging method.

In the study by Akkala et al. (2011a), different spatial interpolation schemes for the use of environmental data are discussed together with the introduction of the concept of spatial data processing system (SDPS). The spatial interpolation techniques that are covered in the paper are nearest neighbor, thiessen polygons, triangulated irregular network, spline, inverse distance weighting, radial basis functions, global polynomial interpolation, local polynomial interpolation, trend surface analysis, kriging and its variations, cokriging, and artificial neural networks. It was observed that there was no particular technique, which was suitable for all interpolation problems related to environmental data.

2.2 Prior studies on Radon

Kumar et al (2007) applied the kriging interpolation technique, built in the ArcGIS geostatistical analyst to the radon data to predict the geometric mean of radon concentrations for the unmeasured zip codes in Ohio. Using the radon data in Ohio, the application of an interpolation technique with the help of ArcGIS geostatistical analyst was illustrated. It was found that kriging technique was convenient for providing the information on radon concentration in the unmeasured zip codes.

In the study by Manthena et al. (2009), the spatial interpolation techniques, kriging and cokriging were used to estimate the radon concentrations in the unknown zip codes for the State of Ohio. It was found that cokriging technique produced less errors compared to

kriging technique based on the comparison of the prediction errors of both the interpolation techniques. Although the differences between prediction errors for the two techniques were minimal, it was noticed that cokriging interpolation technique showed better results with less data.

In the study by Kumar et al. (2011), the growth of Ohio Radon Information System (ORIS), which includes five databases namely "Homes", "Water", "Schools", "Mitigation", and "Tester" and the corresponding results from the analysis of radon gas data for the counties and zip codes in the State of Ohio, are discussed. A clear picture of the radon gas problems across Ohio can be assessed from the analysis and results. The degree of the radon problems in the homes, public water systems, and schools can be determined from the information available in the database. The best mitigation system along with the counties and zip codes with radon concentration greater than 4 pCi/l was also determined from the available information.

In the study by Akkala et al. (2011b), a new interpolation technique was discussed based on Artificial Neural Network (ANN) for modeling and predicting radon concentrations in the State of Ohio. By using the available data, different ANNs were first trained and then validated. The model with the lowest validation error was selected from the resulting model. It was found that the ANN models showed comparatively better accuracies as compared to the conventional interpolation techniques. The best neural model, the ANN model with 60 hidden neuron, was chosen to estimate the radon concentrations in the unknown zip codes.

In the study by Manthena et al. (2011), two geostatistical interpolation techniques, kriging, and cokriging were used to predict radon gas concentrations in the unmeasured zip codes in Ohio. Statistical performance measures: mean bias (MB), normalized mean square error (NMSE), coefficient of correlation (r), factor of two (FA_2), fractional standard deviation (FS), and fractional bias (FB) were used to evaluate the performance of the two interpolation techniques. In addition, the confidence limits for NMSE, r, and FB were found using "Bootstrap" method. The cokriging technique showed better performance compared to the kriging technique based on the comparison of the performance measures and their respective confidence limits.

Akkala et al. (2012) applied different knowledge based neural models for modeling and predicting the radon concentrations. The application of knowledge based neural network approaches: prior knowledge input method, source difference method, and space-mapped neural network method were suggested in order to model and predict radon concentrations. Various models were trained and validated in order to find the best model for each of the three techniques and these models were compared with multi-layer perceptions (MLP) and the traditional interpolation techniques. The results showed that for five out of the six model evaluation parameters, both SDM (Source Difference Method) network with coarse model having 10 hidden neurons and the difference model having 20 hidden neurons gave the best performance.

2.3 Conclusions from Literature Review

It is seen from the literature that several studies have been done using geostatistical interpolation techniques addressing different variables of concern and evaluating these

techniques using general statistical parameters. However, none of the studies has used a comprehensive set of statistical parameters suggested for model evaluations by Kadiyala and Kumar, 2012 to examine and assess six major interpolation schemes built in the geographical information systems. In this study, the statistical parameters suggested by Kadiyala and Kumar, 2012 are used to determine the best interpolation technique.

Chapter 3

Data Collection

3.1 Radon Data

The data for radon concentration in homes have been obtained from various county health departments, commercial testing services, and university researchers. The database has been compiled for more than 20 years. The initial database with 50,000 observations was arranged by Kumar et al. (1990) for the Ohio radon information system (ORIS) discussed by Heydinger et al. (1991). The database reached the total observations of 82,000 in 1997. Sud (1998) analyzed 80,436 observations in her thesis. The database is updated continuously with new data. Kumar and Varadarajan (2005) reported the analysis of 121,959 data points. Kumar et al. (2010) has extended the database to 159,340. In this thesis, 208,097 data points for 708 zip codes where number of radon concentration records are more than 20 are used for the analysis. None of the previous studies on interpolation schemes has used a database of this size. Radon data is heavily skewed towards higher concentrations, so geometric mean of radon data is used to input as point sources. Of the 708 zip codes, 22 zip codes are not shown in the Ohio zip code shape file, which is collected from ESRI website. Therefore, 686 zip codes from the original dataset

of 708 zip codes are used as inputs for the point sources data for analyzing the interpolation techniques.

3.2 Uranium data

The Uranium data is obtained from the map published by Duval (1985) as shown in Figure 3-1. The map provides the uranium concentration in Ohio's soil zone as measured from an airplane. A map of Ohio's zip code areas was drawn to the same scale and overlaid on the uranium map with the uranium data then extracted by hand for each zip code areas. Each line of the uranium data file contains the zip code followed by three coded numbers representing, modal uranium concentration, maximum uranium concentration, and minimum uranium concentrations. The uranium data is used as co-variable in the cokriging interpolation techniques.
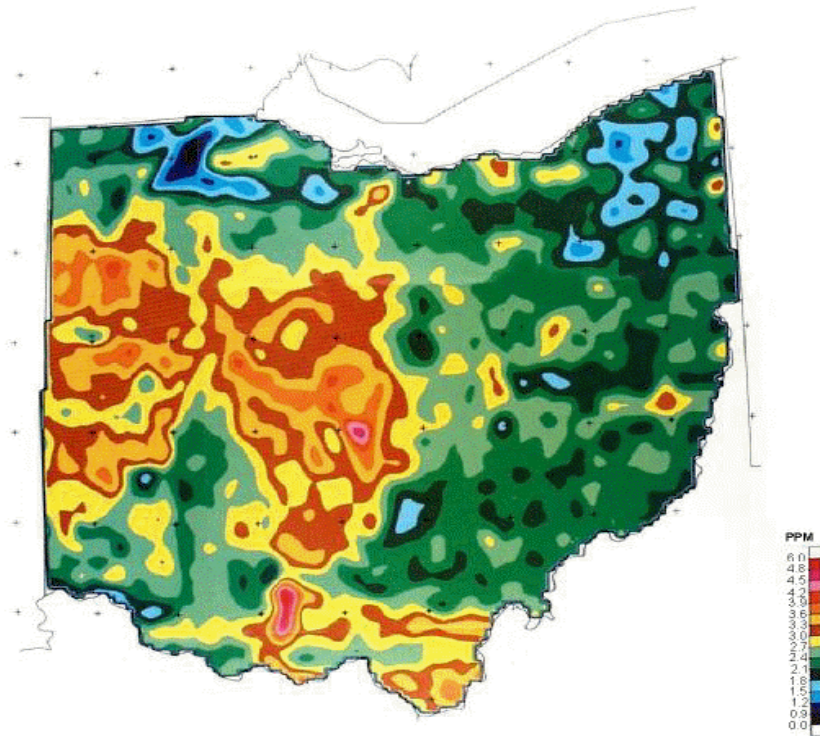
Figure 3-1: Aerial radiometric map of Ohio showing the concentration of uranium in surficial sediments and soils (in parts per million) (http://www.eng.utoledo.edu/aprg/radon/fig5new.html)

Chapter 4

Methodology

4.1 Geostatistical Analyst

The geostatistical analyst is an ArcMap extension that provides a wide variety of tools for spatial data exploration, identification of data anomalies and evaluation of error in prediction surface models, statistical estimation, and optimal surface creation. The geostatistical analyst determines the probability of certain variables occurring over an area where identifying every possible location would be impossible. It can be explained with the help of an example: in Ohio, particulate matter monitoring stations are set up around the state, and these monitoring stations measure the amount of particulates in the air. The geostatistical analyst can determine the approximate amount of particulates in the area of interest and can determine where these particulates may be moving by creating an optimal interpolated surface. The geostatistical analyst provides a multitude of powerful interpolation methods with advanced analytical tools for generating optimal interpolated surfaces from discrete spatial data measurements. There are mainly two groups of interpolation techniques: deterministic and geostatistical. Deterministic techniques use mathematical functions that form weighted averages of nearby measured values to create surface, while geostatistical techniques use both mathematical and statistical methods.

The geostatistical analyst also provides many supporting tools in addition to providing various interpolation techniques. The geostatistical analyst provides a full suite of exploratory spatial data analysis (ESDA). Each tool provides a view of the data in a separate window, and each tool is linked to every other and with the map. The ESDA tools allow the user to explore the distribution of the data, look for global trends in the data, identify local and global outliers, and understand the spatial structure of the data.

4.1.1 Exploratory Spatial Data Analysis

ESDA tools allow one to examine the data in more quantitative ways. The different tools to view the data are:

- Histogram

- Normal QQ plot

- Trend analysis

- Semivariogram/Covariance cloud

4.1.1.1 Histogram

The histogram tool provides a univariate (one-variable) description of the data and it displays the frequency distribution for the dataset of interest and calculates the summary statistics. The frequency distribution is a bar graph that displays how often observed values fall within certain intervals or classes, and one can specify the number of classes of equal width that are used in the histogram. The relative proportion of data that falls in each class is represented by the height of each bar. The different interpolation methods give the best results when the data is normally distributed. The following plots (Figure 4-1 and Figure 4-2) show the frequency distribution for radon dataset. It can be seen from

the first plot (Figure 4-1) that data is not normally distributed, and it has to be transformed to a normal distribution in order to get better results. The second plot (Figure 4-2) shows the normal distribution of data after the log transformation.
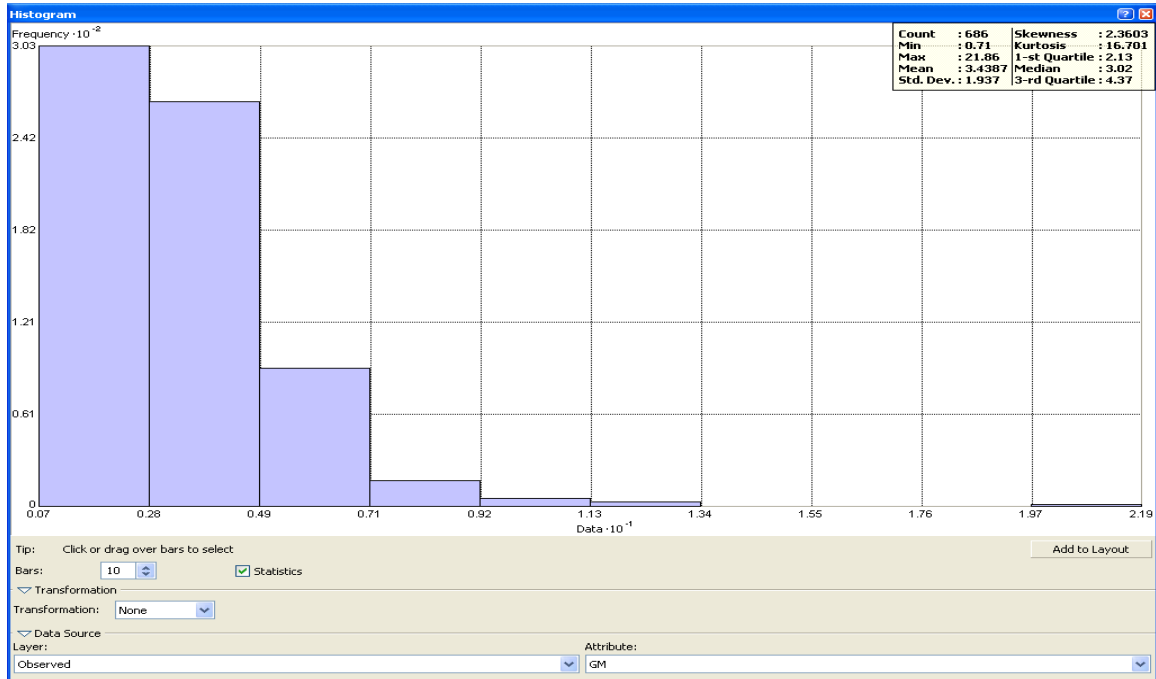
Figure 4-1: Frequency distribution of the radon dataset

Figure 4-2: Frequency distribution of the radon dataset after log transformation

4.1.1.2 Normal QQ Plot

QQ plots are graphs on which quantiles from two distributions are plotted relative to each other. General QQ plots are used to assess the similarity of the distributions of the two datasets. Points on the normal QQ plots provide an indication of the univariate normality of the dataset. If the data is normally distributed, the points will fall on a 45-degree reference line, and if the data is not normally distributed, the points will deviate from the reference line. The first plot (Figure 4-3) shows that data is not normally distributed as the radon data points deviate from the reference line at the low and the high values. The second plot (Figure 4-4) shows that the data is normally distributed after the log transformation.
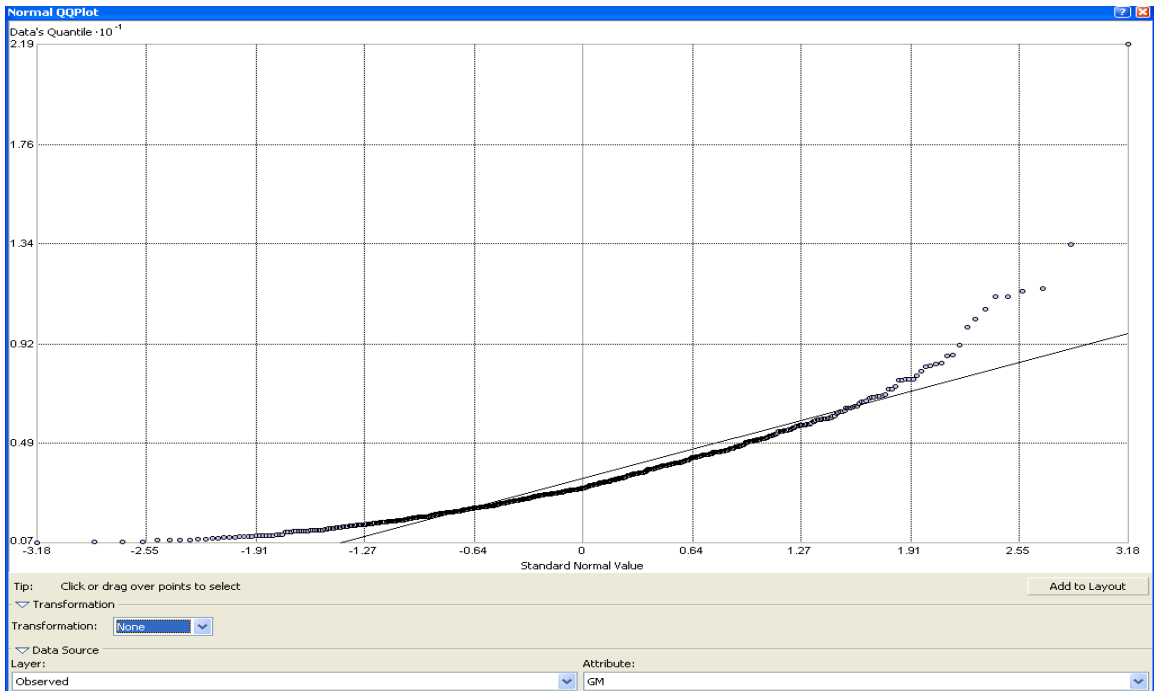
Figure 4-3: Normal QQ plot for radon dataset

Figure 4-4: Normal QQ Plot for Radon data set after log transformation

4.1.1.3 Trend Analysis

The trend analysis tool helps to identify the trends in the input dataset. The tool provides

a three dimensional perspective of the data as shown in figure 4-5. The locations of the

sample points are plotted on the x, y plane. The value is given by the height of a stick in

the z dimension above each sample point. A unique feature of the trend analysis tool is

that the values are then projected on to the x, z plane, and y, z plane as scatterplots. This

can be thought of as sideways views through the three-dimensional data. Polynomials are

then fitted through the scatter plots on the projected plane. An additional feature is that

data can be rotated to isolate directional trends. This tool also includes other features that

allow users to rotate and vary the perspectives of the whole image, change size and color

of points and lines, remove planes and points and selects the order of the polynomial, that

is to be fitted the scatterplots.
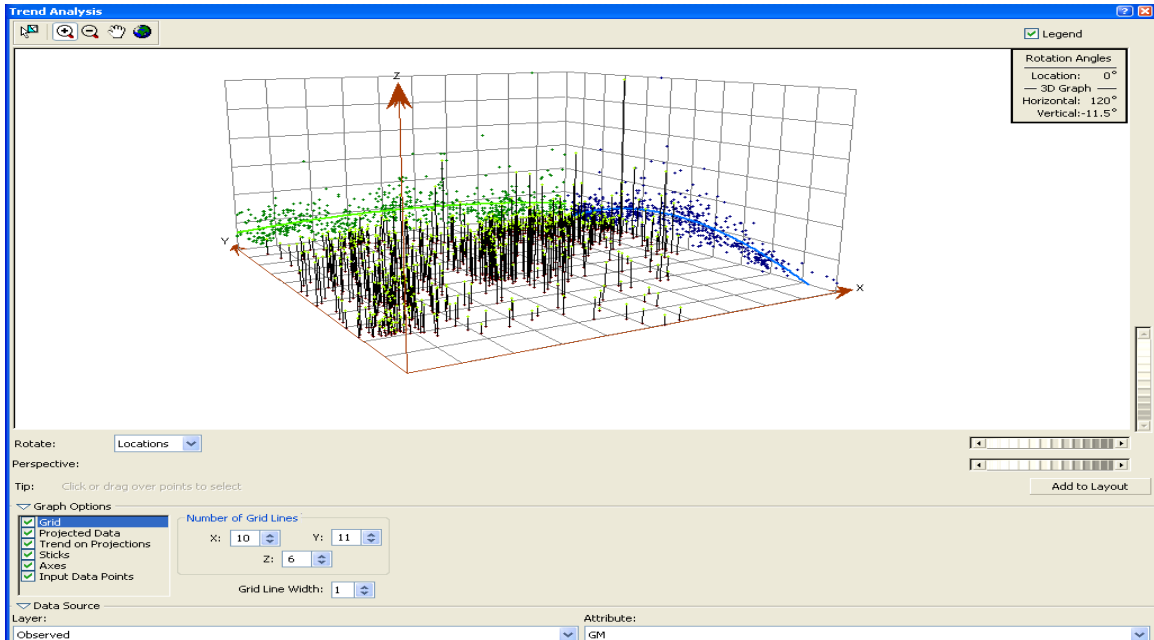
Figure 4-5: Trend analysis dialogue box

The X-axis is the East–West axis and the Y-axis is the North–South axis. The polynomials drawn through the projected points shows that the model trends in specific directions. The green line is an East–West trend line and the blue line is a North–South trend line. There is no trend when the lines are flat. However, the blue line in the image shows that it starts with low values and increases as it moves towards North and then decreases from the center. This demonstrates that there is a strong trend in the North-South direction and a weaker trend in the East-West direction. It seems that radon concentration values are higher near the Central Ohio and then decrease towards North and South.

4.1.1.4 The Semivariogram/Covariance Cloud

The semivariogram/covariance cloud is used to examine the spatial autocorrelation between the measured sample points. It is assumed that things that are close to one another are more alike. This relationship can be examined by the semivariogram /covariance cloud. A semivariogram value (squared difference between the values of each pair of locations) is plotted on the y-axis, and the distance separating each pair of locations is plotted on the x-axis as shown in Figure 4-6.
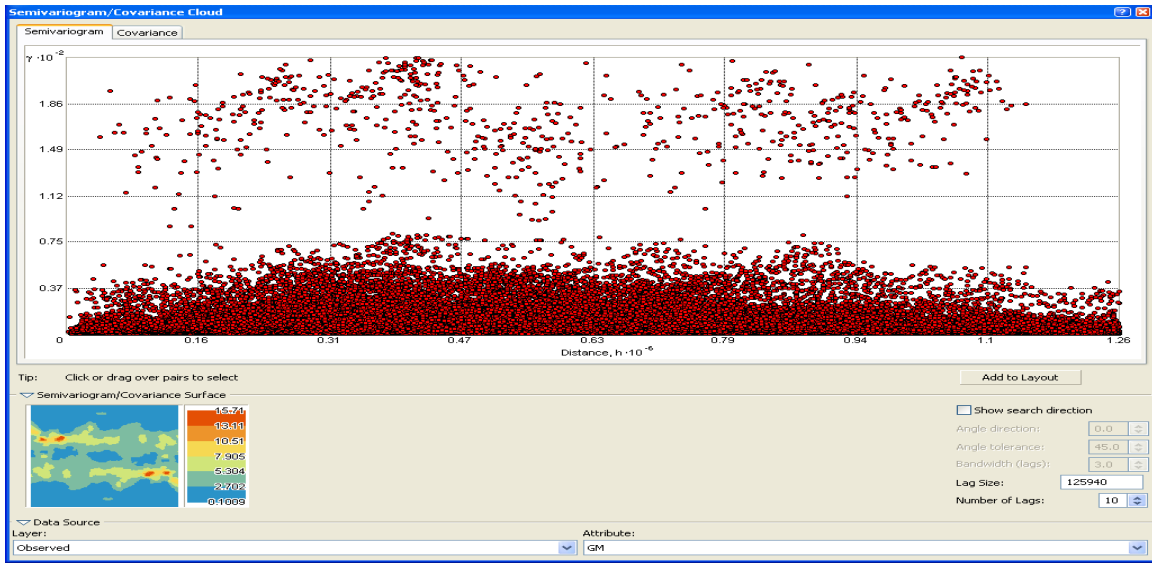
Figure 4-6: Semivariogram/Covariance cloud dialogue box

Each red dot represents a pair of locations in the Semivariogram/Covariance cloud. As the locations that are close to each other are more alike, the locations that are far left on the X-axis will have low semivariogram values on the Y-axis. As we move towards the right of the X-axis, the distance between the pair of locations also increases, and the semivariogram values increase on the Y-axis. However, a certain distance is reached where the cloud flattens out, indicating that the values of the pair of points separated by more than this distance are no longer correlated.

4.2 Deterministic Interpolation Technique

Deterministic interpolation techniques create surfaces from measured points based on either the extent of similarity (Inverse Distance Weighting) or the degree of smoothing (Radial Basis Function). A deterministic interpolation can either force the resulting surface to pass through the data values or not. An interpolation technique that predicts a value that is identical to the measured value at a sample location is known as an exact interpolator and the technique that predicts a value that is different from the measured

value is an inexact interpolator. Inverse distance weighting and radial basis functions are exact interpolators while global Polynomial, local polynomial, kernel interpolation with barriers, and diffusion interpolation with barriers are inexact interpolators.

4.2.1 Inverse Distance Weighting (IDW)

IDW interpolation explicitly implements the assumption that things that are close to one another are more alike than that are farther apart. IDW uses the measured values surrounding the prediction location to predict a value for any unmeasured location. The measured values closest to the prediction location have more influence on the predicted value than those farther away. IDW assumes that each measured point has a local influence that diminishes with distance. It gives greater weights to points closest to the prediction location, and the weights diminish as a function of distance.

A simple IDW weighting function as defined by Shepard (1968) is

$$\mathbf{w(d)} = \frac{1}{\mathbf{d^p}} \qquad\qquad \textbf{(1) (http://help.arcgis.com)}$$

where, w (d) is the weighting factor applied to a known value, d is the distance from the known value to the unknown value, and p is the positive real number, which is called the power parameter. Here weights decreases as distance increases from the interpolated points. Greater values of p assign greater influence to values closest to the interpolated point. The most common value of p is 2. The usual expression for IDW is as below:

$$\mathbf{Z_{(s_0)}} = \mathbf{\sum_{i=1}^{N} \lambda_i \cdot \hat{Z}(s_i)} \qquad\qquad \textbf{(2) (http://help.arcgis.com)}$$

where, $Z_{(s_0)}$ is the value to be predicted for location s_0 , N is the number of measured sample points surrounding the prediction location that will be used in the prediction, and

λ_i is the weight assigned to each measured point to be used. The weights will decrease with distance. $\hat{Z}(s_i)$, is the observed value at location, s_i.

4.2.2 Radial basis functions (RBF)

RBF methods are a series of exact interpolation techniques; i.e., the surface must pass through each measured sample value. There are five different basis functions:

- Thin-plate spline

- Spline with tension

- Completely regularized spline

- Multiquadric function

- Inverse multiquadric function

Each basis function has a different shape and results in a different interpolation surface. RBF methods are a special case of splines. RBFs are conceptually similar to fitting a rubber membrane through the measured sample values while minimizing the total curvature of the surface. The basis function that one selects determines how the rubber membrane will fit between the values. Figure 4-7, as shown below, illustrates how a RBF surface fits through a series of elevation sample values. It can be seen that the surface passes through the data values.
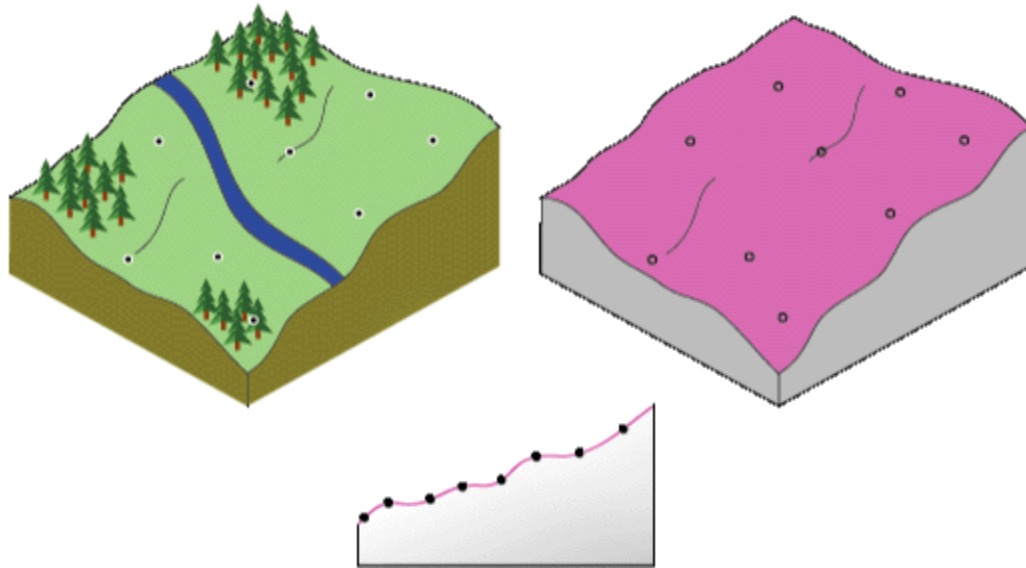
**Figure 4-7: RBF surface fits through a series of sample points
(http://help.arcgis.com)**

As exact interpolators, the RBF methods are different from the global and local polynomial interpolators, which are both inexact interpolators that do not require the surface to pass through the measured points. While comparing RBF to IDW, IDW does not predict values above the maximum measured value or below the minimum measured value, but the RBFs can predict values above the maximum and below the minimum values.

4.2.3 Global Polynomial Interpolation (GPI)

A smooth surface is fitted by global polynomial interpolation, which is defined by a mathematical function, a polynomial, to the input sample points. The surface changes gradually and exerts a coarse scale pattern in the data. Global polynomial interpolation is like taking a piece of paper and fitting it between the raised points. This is shown in Figure 4-8, for a set of sample points of elevation taken on a gently sloping hill (the piece of the sample paper is magenta).
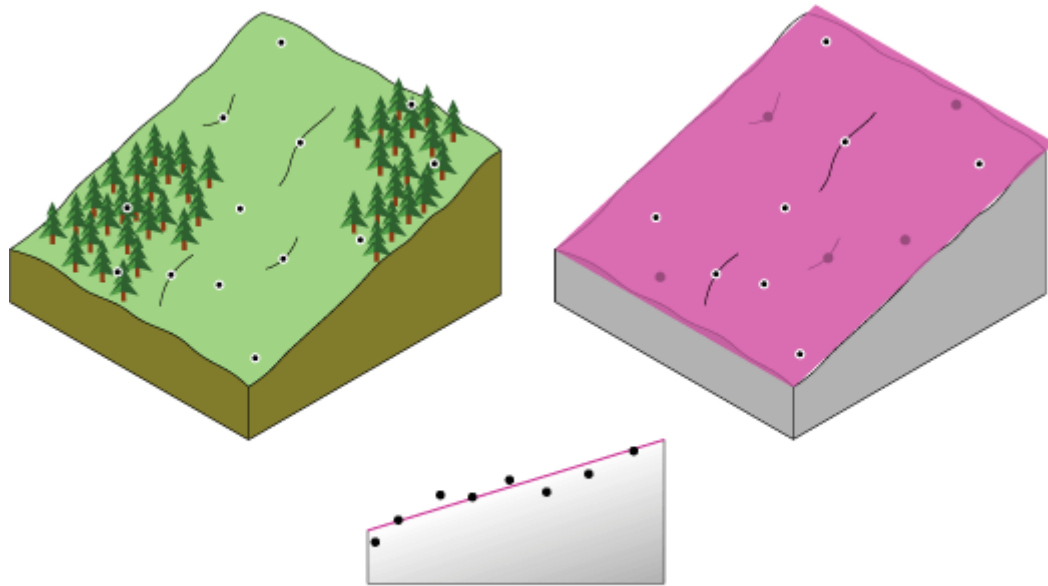
Figure 4-8: Global Polynomial Interpolation fitting through sample points of Elevation on Gently Sloping Hill. (http://help.arcgis.com)

A landscape containing a valley will not be captured by a flat piece of paper. However, the fit will be much better if one is allowed to bend the piece of paper. A similar result is produced by adding a term to the mathematical formula, a bend in the plane. A flat plane is a first-order polynomial, allowing for one bend is a second order polynomial, two bends a third order and so forth; up to 10 are allowed in Geostatistical Analyst. Figure 4-9 below represents a second-order polynomial fitted to a valley.
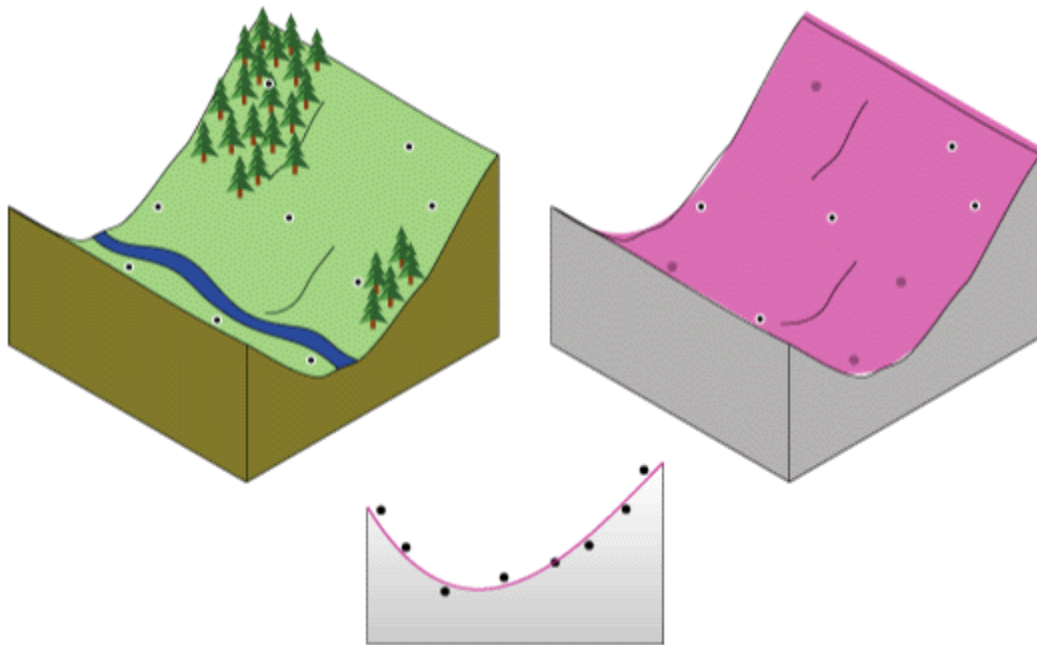
Figure 4-9: Global Polynomial Interpolation fitted to a valley using Second Order Polynomial (http://help.arcgis.com)

The piece of paper will rarely go through the actual measured points, which makes the global polynomial interpolation an inexact interpolator. Some points will be above the piece of paper and others will be below the piece of paper. However, if one adds up the height of each point above the piece of paper and adds up the height of each point below the piece of paper, then the two sums should be similar. The surface, in magenta is obtained by using a least –squares regression fit. The resulting surface minimizes the squared differences among the raised values and the sheet of paper.

4.2.4 Local Polynomial Interpolation (LPI)

Local polynomial interpolation fits many polynomials that are within the specified overlapping neighborhoods. By using the size and shape, number of neighbors and sector configuration, the search neighborhood can be defined. A first-order global polynomial

31

fits a single plane through the data; a second- order global polynomial fits a surface with a bend in it, allowing surfaces representing valleys, a third-order global polynomial allows for two bends and so forth. A surface that has varying shapes will not be fitted by a single global polynomial. Multiple polynomial planes can represent the surface more accurately as shown in Figure 4-10 below.
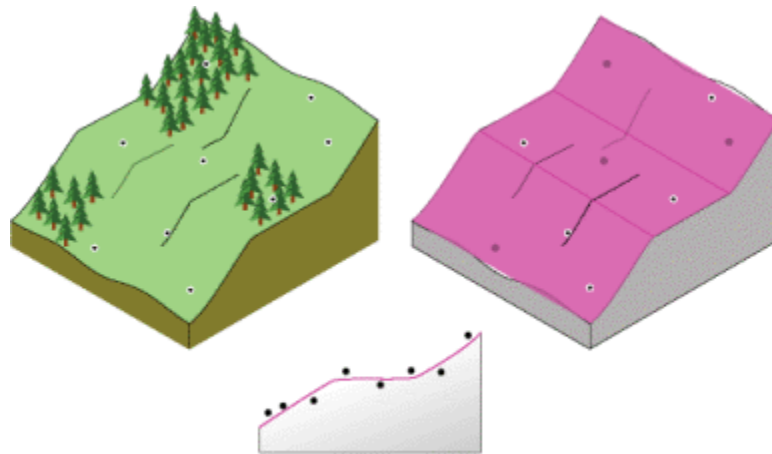
Figure 4-10: Multiple polynomial planes to represent surface with varying shape (http://help.arcgis.com)

Local polynomial interpolation, on the other hand, fits the specified order polynomial using points only within the neighborhood. The neighborhood coincides, and the value of the fitted polynomial at the center of the neighborhood is the value used for each prediction.

4.3 Geostatistical Interpolation Techniques

Geostatistical methods are based on statistical models that include autocorrelation; i.e., statistical relationship among the measured points. These techniques have the capability of producing prediction surfaces, and they can provide the measure of the accuracy of

these predictions. Geostatistics was originally synonymous with kriging in spatial statistics. Kriging is a statistical version of interpolation.

4.3.1 Kriging

Kriging assumes that at least some of the spatial variation observed in natural phenomena can be modeled by random processes with spatial autocorrelation and requires that spatial autocorrelation can be explicitly modeled. Kriging techniques can be used to describe and model spatial patterns, predict values at unmeasured locations and assess the uncertainty associated with predicted value at the unmeasured location. Kriging methods depend on mathematical and statistical models. The addition of a statistical model includes the probability that separates kriging methods from the deterministic methods. Kriging methods rely on the idea of autocorrelation. Correlation is usually thought of as the tendency for two types of variables to be related. Autocorrelation is a function of distance, and this is the defining feature of geostatistics. It can be expressed in the following mathematical formula:

$$Z(s) = \mu(s) + \varepsilon(s) \qquad\qquad \textbf{(3) (http://help.arcgis.com)}$$

Where, $Z(s)$ is the variable of interest, decomposed into a deterministic trend $\mu(s)$ and a random auto correlated errors form $\varepsilon(s)$. The symbol s indicates the location, and it can be thought as containing spatial x (longitude) and y (latitude) coordinates. Variation in the formula forms the basis for all the different types of kriging.

4.3.1.1 Ordinary Kriging

Ordinary Kriging assumes the model as

$$Z(s) = \mu + \varepsilon(s) \qquad\qquad \textbf{(4) (http://help.arcgis.com)}$$

33

Where, μ is an unknown constant.

The main issue concerning ordinary kriging is whether the assumption of a constant mean is reasonable. Sometimes, there are good scientific reasons to reject this assumption, but as a simple prediction method, ordinary kriging has remarkable flexibility. The following Figure 4-11 is an example in one spatial dimension.
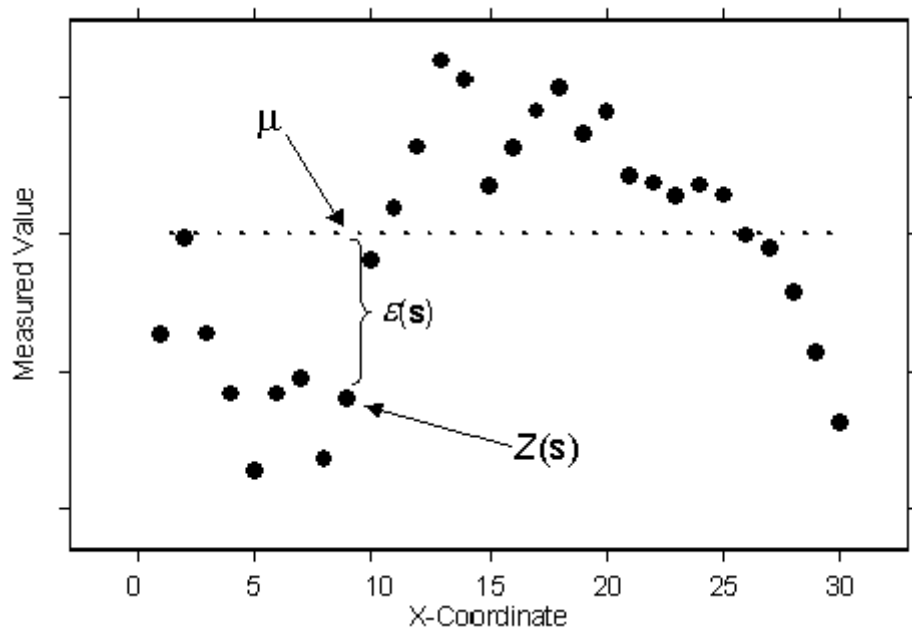
Figure 4-11: Ordinary kriging in one spatial dimension (http://help.arcgis.com)

It seems (Figure 4-11) that the data is elevation values collected from a line transect through a valley and over a mountain. It is also seen that the data is more variable on the left and becomes smoother on the right. The data was simulated from the ordinary kriging model with a constant mean μ .The true but unknown mean is given by the dashed line. Thus, it is seen that ordinary kriging can be used for data that seems to have a trend.

4.3.2 Cokriging

The cokriging technique uses information for several variable types. The main variable of interest is Z_1 and both autocorrelation for Z_1, and cross-correlations between Z_1 and all other variable types are used to make better predictions. Cokriging requires lot of information including estimating the autocorrelation for each variable as well as cross-correlations. Theoretically, when there is no cross-correlation, cokriging will do the autocorrelation for Z_1.

4.3.2.1 Ordinary Cokriging

The ordinary cokriging assumes the models given by the equation below:

$$Z_1(s) = \mu_1 + \varepsilon_1(s) \qquad\qquad \textbf{(5) (http://help.arcgis.com)}$$

$$Z_2(s) = \mu_2 + \varepsilon_2(s) \qquad\qquad \textbf{(6) (http://help.arcgis.com)}$$

Where, μ_1 and μ_2 are unknown constants. There are two types of random errors, $\varepsilon_1(s)$ and $\varepsilon_2(s)$, so there is autocorrelation for each of the errors and cross correlation between them. Ordinary cokriging attempts to predict $Z_1(s_0)$ like ordinary kriging, but the difference is that it uses information in the covariate $Z_2(s)$ to do a better prediction. It can be seen from Figure 4-12 that it has the same data which was used for ordinary kriging (Figure 4-11), but a second variable has been added.
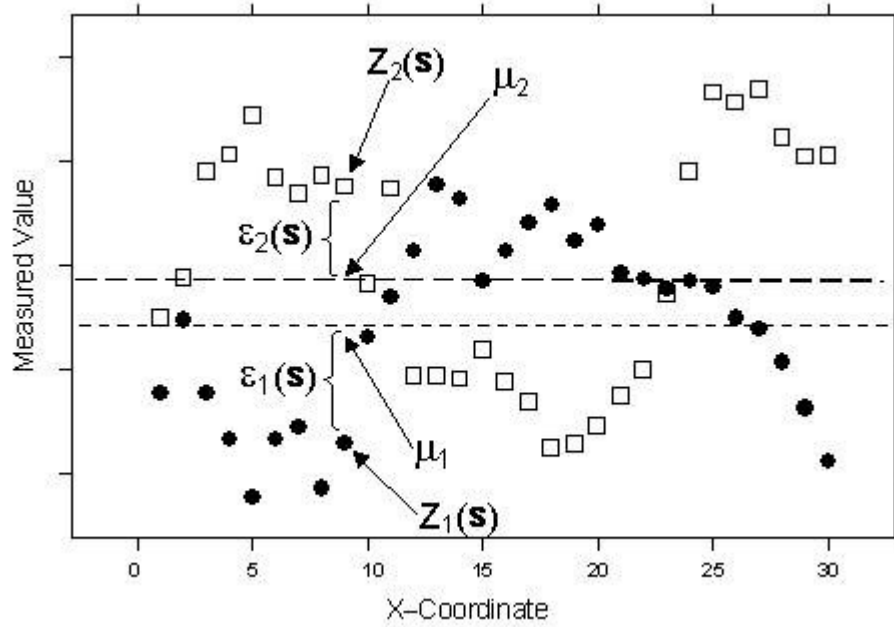
**Figure 4-12: Ordinary Cokriging with two variables $Z_1(s)$ and $Z_2(s)$
(http://help.arcgis.com)**

Chapter 5

Approach

5.1 Procedure

The geostatistical analysis aims at predicting values for the unknown areas. The Ohio zip code shape file collected from ESRI website consists of 1862 zip codes. In this study, 686 zip codes with number of radon concentration records more than 20 are used as input data for the interpolation techniques. The ArcGIS geostatistical analyst is used to predict the radon concentration data for the unmeasured 1176 zip codes by using the different interpolation methods: IDW, GPI, LPI, RBF, ordinary kriging, and ordinary cokriging. In the Ohio zip code shape file, the geometric mean of the radon concentration data is inputted into the attribute table for each zip code, and zero values are assigned to the zip codes that are not measured. Then the polygon features of the Ohio zip code shape file are converted into point features using the data management tool available in the ArcGIS. The point featured shape file is then divided into two shape files, one having 686 zip codes with radon concentration data and the other shape file containing1176 zip codes with no measured radon concentration data.

The first approach is to evaluate the best interpolation technique. The point shape file with 686 zip codes is divided into 80% training data points, which is used for modeling to create the output surface, and the remaining 20% is used to validate the output surface by comparing the measured and predicted values. The sensitivity analysis for the possible divisions of 90-10, 80-20, 70-30 and 60-40, the 80-20 division had less root mean square error as showed by Maroju (2007) and Manthena et al. (2011).

To make the validation of the surface significant and to create a surface, a sufficient number of data points are required. Then different interpolation techniques can be applied to evaluate the best interpolation technique from the surface created and validation of the test data points.

The second approach is to evaluate the radon concentrations in the unmeasured zip codes by the best interpolation technique. Modeling is done for whole radon data set, which creates a surface of spatial variation of radon concentrations. Then the predictions for the unmeasured zip codes, where there is no data will be evaluated from the surface created.

5.2 Application of interpolation techniques

The different interpolation techniques to be performed on the training and test data sets are given below:

- Ordinary Kriging

- Ordinary Cokriging

- Inverse Distance Weighting

- Radial Basis Function

- Global Polynomial

- Local Polynomial

5.2.1 Ordinary Kriging

At first kriging type "Ordinary" and output type "Prediction" is selected in the geostatistical wizard option of the ArcGIS as shown in Figure 5-1. Log transformation is applied as radon data is skewed which is shown in the ESDA tool, and the first order trend removal is selected as it was showing trend in the North-South direction as shown in Figure 5-1.
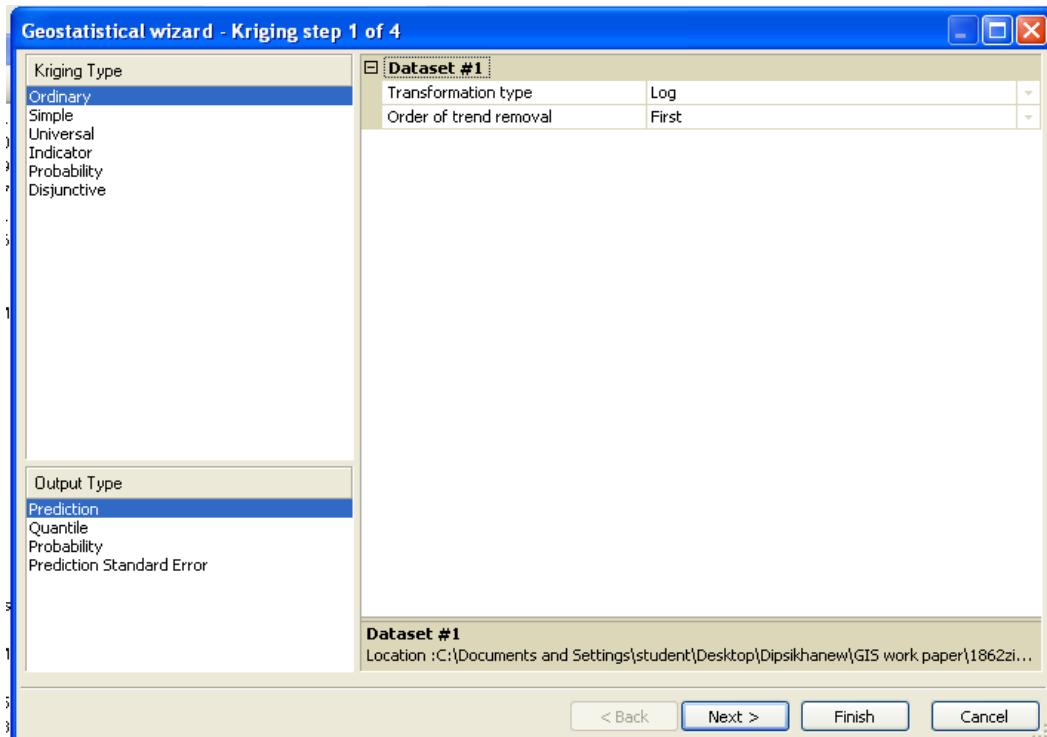
Figure 5-1: Geostatistical Method Selection Dialogue Box

In the next step, spatial autocorrelation of the transformed data is modeled using semivariogram/covariance modeling. Semivariogram depicts the spatial autocorrelation of the measured sample points. The similarity between the data points decreases as the

distance between the data points increases. Red dots in Figure 5-2 are the binned values and are generated by grouping (binning) semivariogram/covariance points together using square cells that are one lag wide. Blue crosses represent the average points, and these are generated by binning empirical semivariogram/covariance points that fall within angular sectors. Local variation in the semivariogram/covariance values is shown by binned points, and smooth semivariogram/covariance value variation is shown by average values. After calculating the empirical variogram for the measured data points, a model is fitted to fit through the points. The stable type model (dark blue line) is fitted as shown in Figure 5-2.
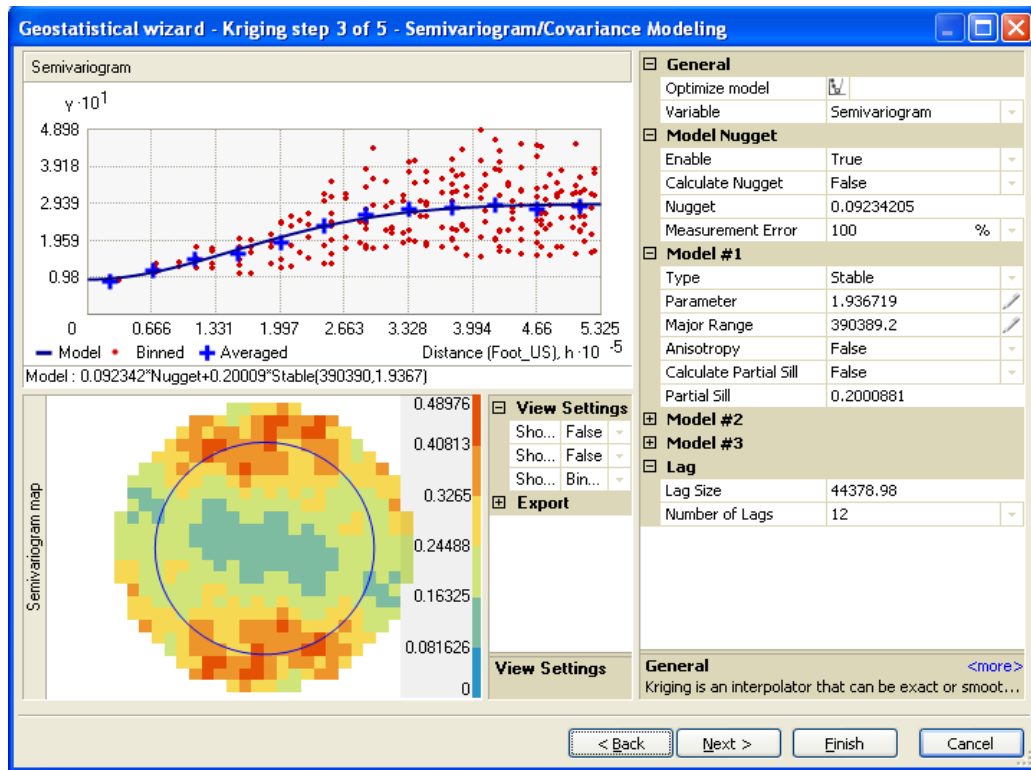
Figure 5-2: Semivariogram/Covariance Modeling

At zero separation distance ($h = 0$), the semivariogram value should be zero. However, at an infinitesimally small separation distance, the semivariogram often exhibits a nugget

effect, which is some value greater than zero. In this case, the nugget effect exists which is 0.09234. It is seen that at a certain distance the model levels out. The distance at which the model first flattens out is known as the range, which is equal to 390389.20. Sample locations separated by distances closer than the range are spatially auto correlated, whereas locations farther apart than the range are not. The value that the semivariogram model attains at the range (the value on the y-axis) is called the sill. The partial sill is the sill minus the nugget, which is 0.20002. The lag size is the size of a distance class into which pairs of locations are grouped. The automated lag size and the number of lags generated are 44378.98 and 12.

The calculated semivariogram value is represented by the color scale as shown in Figure 5-2. It provides a direct link to the semivariogram values on the graph and those on the semivariogram surface. The higher values are in orange and red, and the lower values are in blue and green.

The next step in kriging is the searching neighborhood. As the locations get father from the prediction location, the measured values will have less spatial auto correlation with the prediction location. As these points will have little or no effect on the predicted value, they can be eliminated from the calculation of that particular point by defining a search neighborhood. Therefore, it is necessary to provide the (1) adjacent points, (2) the searching radius, and (3) the number of sectors of the circle (or ellipse) which should be specified in predicting the radon concentration. As shown in Figure 5-3, five neighboring points are selected and a circle with four sectors is selected. The points highlighted in the

data give an indicator of the weights associated with each point, and these weights are used to estimate the value at the unknown location, which is at the center of the crosshair.
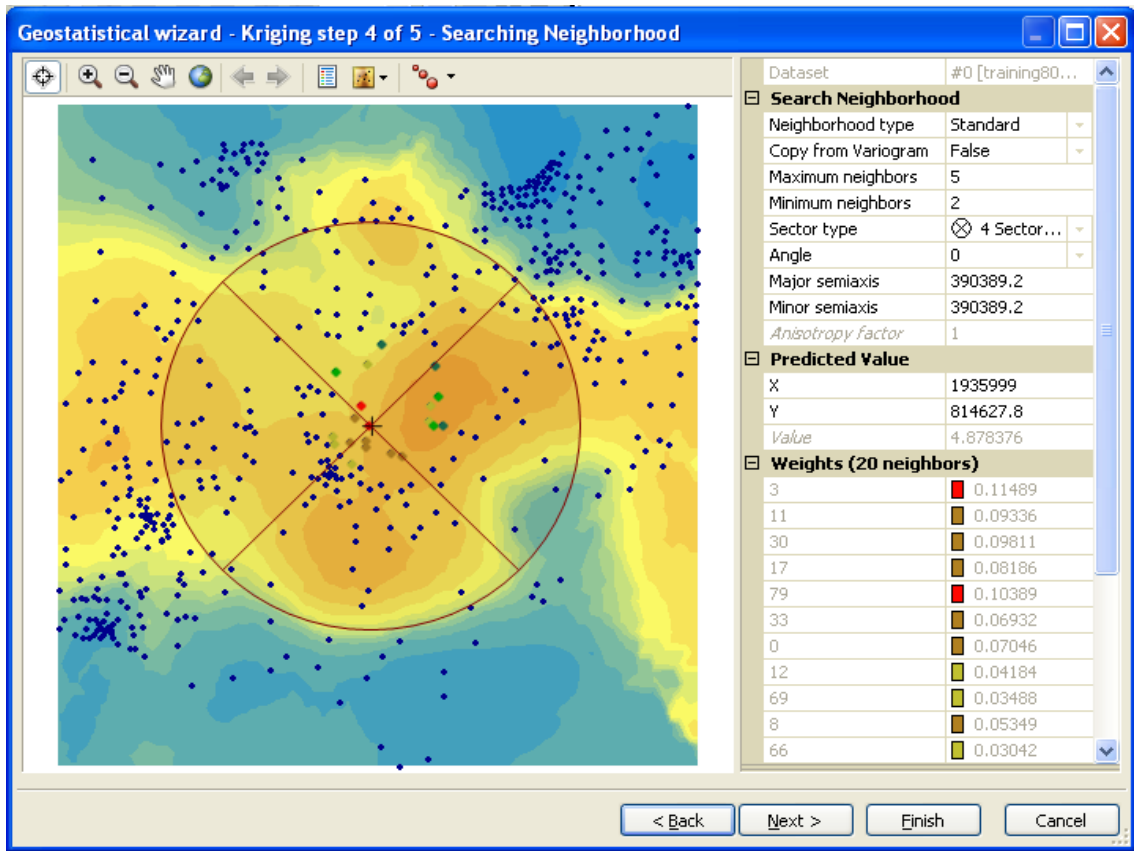
Figure 5-3: Searching Neighborhood Dialog Box of Ordinary Kriging

The last step in kriging is the cross validation tool. Before the final surface is produced, how well the models will predict the unknown values can be assessed from the cross validation tool. The concept of cross-validation is that data is removed from one or more locations, and their associated data is predicted using the data at the rest of the locations. The cross validation tool compares the measured radon value with the predicted radon value, and statistical measures are used to assess the performance of the surface model. The accuracy of the surface model and its predictions are derived by the statistical measures. Figure 5-4 represents the graphical comparison between measured and

predicted values. The cross validation dialogue box also displays the scatter plots that show the error, standardized error, and normal QQ plot for each data point.
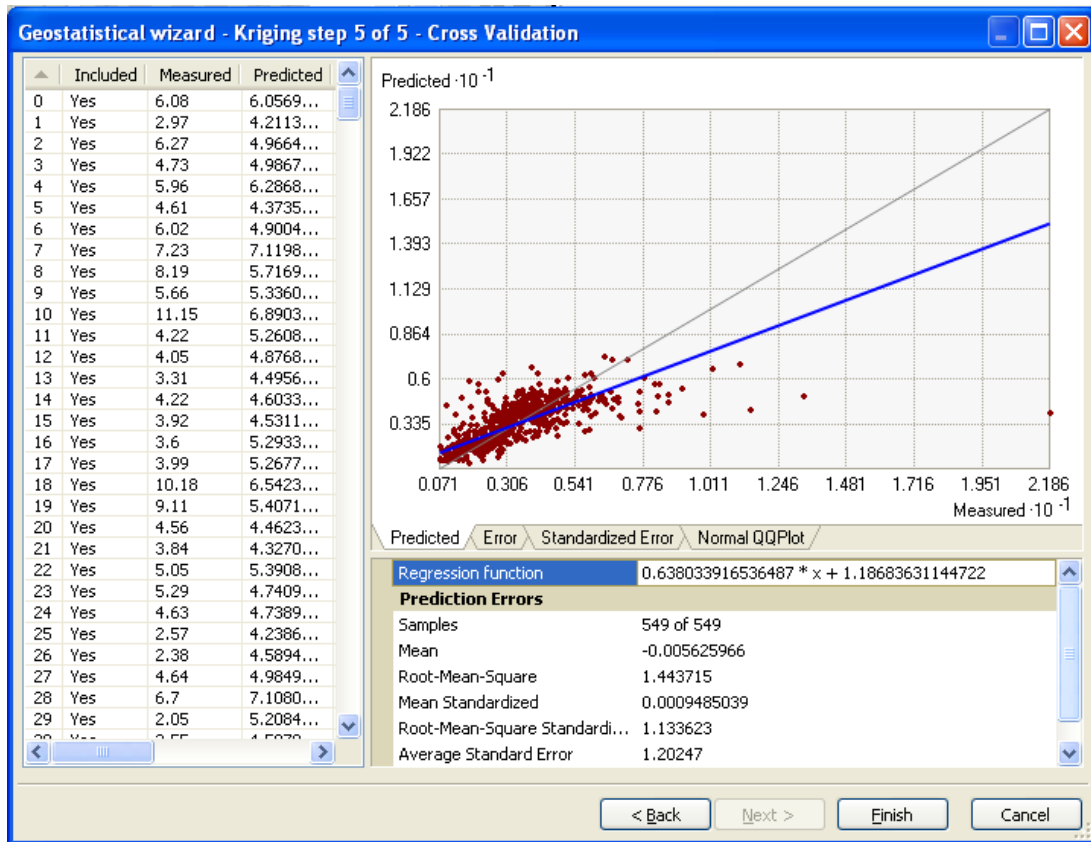
Figure 5-4: Predicted plot of Ordinary Kriging (Predicted values vs. Measured values)

The red dot represents the predicted values after cross validation. The blue line is the fitted line and the grey line is the 1:1 line. Ideally, the predicted values should be same as the measured ones, and all the points should form the 1:1 line. However, in reality, all the data points would scatter around the 1:1 plot due to natural variation and uncertainties. The prediction error is used to describe the difference between the prediction and actual measured values. Mean and mean standardized error should be close to zero, the root mean square error and the average standardized error should be as small as possible and

the root mean square standardized error should be close to unity for the accurate predictions of a surface model.

Prediction errors of ordinary kriging available using the radon concentration training dataset is presented in Table 5.1.

Table 5.1: Prediction errors using Ordinary Kriging

Error	Value
Mean	-0.00563
Root Mean Square	1.44372
Mean Standardized	0.00095
Root Mean Square Standardized	1.33623
Average Satndard Error	1.20247

Figure 5-5 represents the graphical representation between errors and measured values. The error plot is the same as the prediction plot, except the measured values are subtracted from the predicted values. The mean prediction error should be near zero if the prediction errors are unbiased.
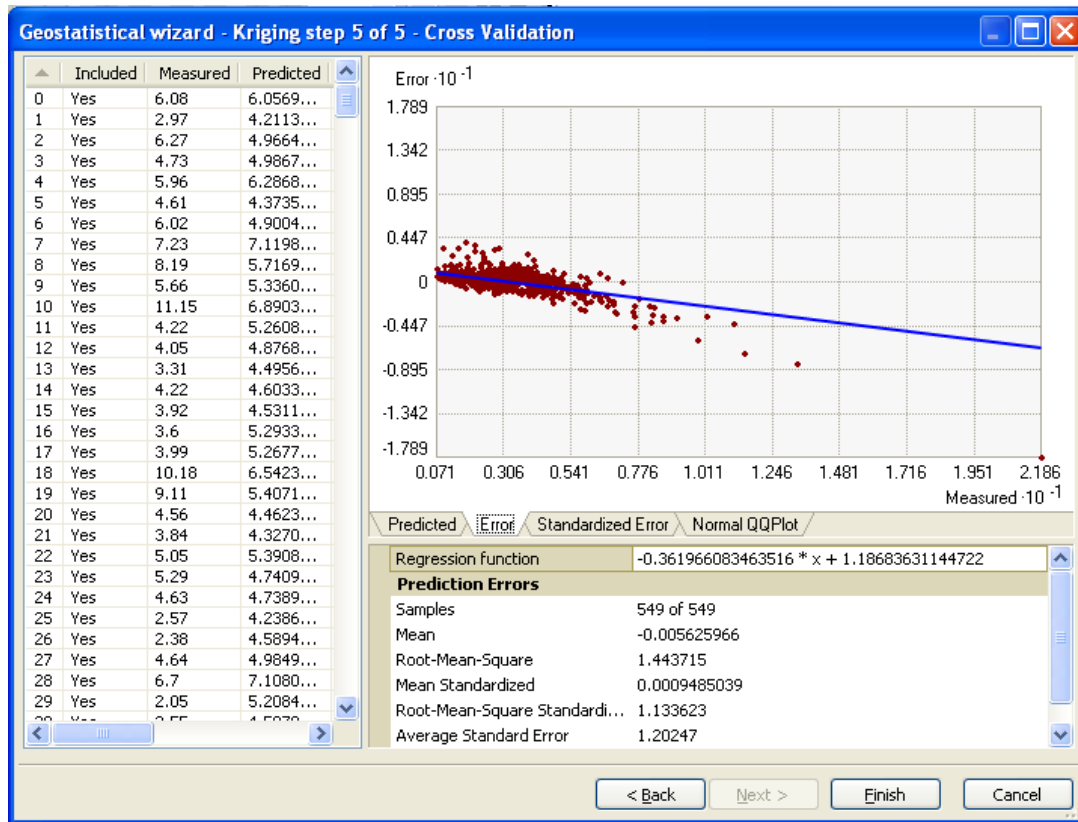
Figure 5-5: Error plot of Ordinary Kriging (Error vs. Measured values)

Figure 5-6 represents the graphical representation between standardized error and the measured values. The measured values are subtracted from the predicted values and divided by the estimated kriging standard errors for the standardized error plot.
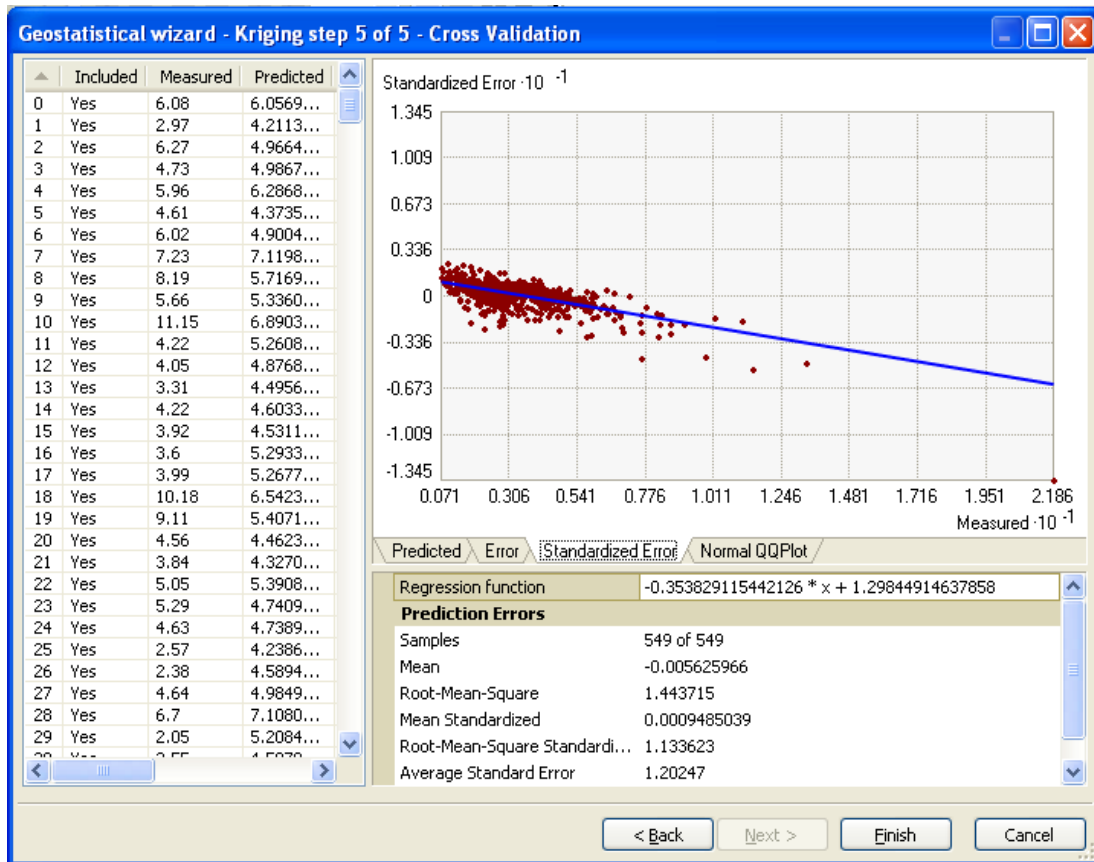
Figure 5-6: Standardized Error Plot of Ordinary Kriging (Standardized Error vs. Measured values)

Figure 5-7 shows the normal QQ plot. The QQ plot shows the quantiles of the difference between the predicted and measured values and the corresponding quantiles from a standard normal distribution. The points should roughly lie along the grey line if the errors of the predictions are normally distributed. It can be seen from the plot that the errors of the prediction are normally distributed.

46
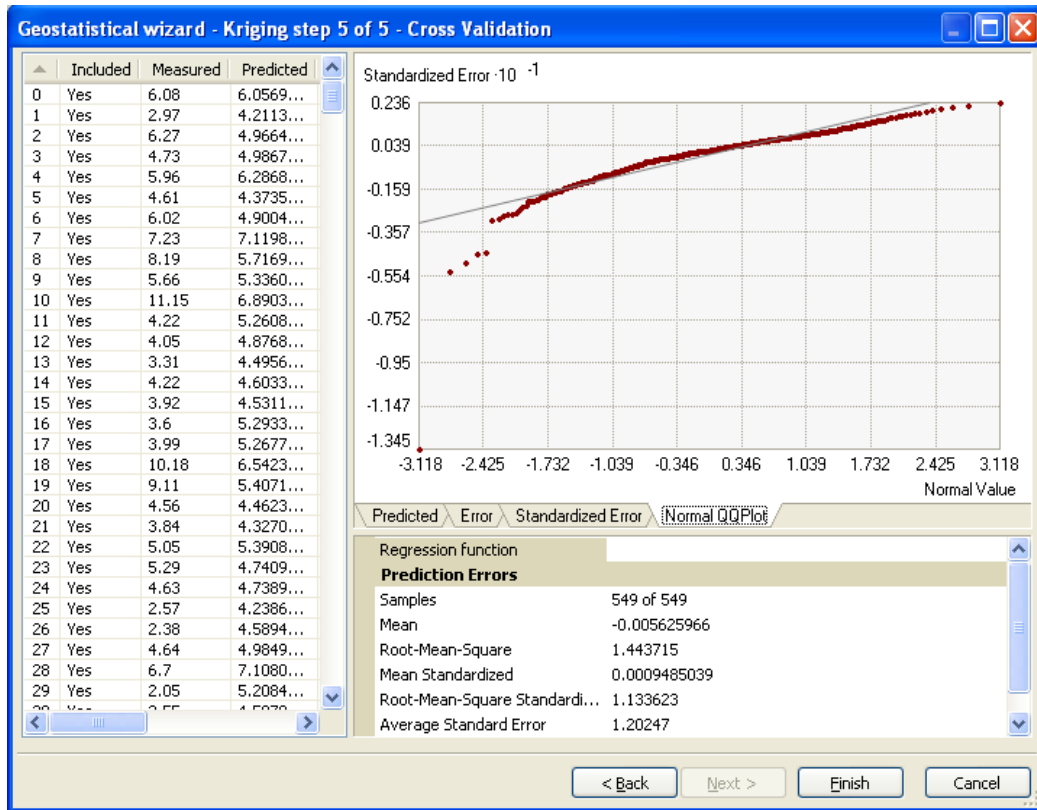
Figure 5-7: QQ plot of Ordinary Kriging

After the cross validation process, the next step is the generation of the surface map. The prediction map is created using the measured radon concentration. Figure 5-8 shows the distribution of radon concentration for the State of Ohio using the training dataset. The higher concentrations are represented by dark colors, and the lower concentrations are represented by light colors.

Estimated Radon Concentration (pCi/L)

- 0.71 - 1.90
- 1.90 - 2.49
- 2.49 – 2.78
- 2.78 - 2.92
- 2.92 - 3.22
- 3.22 - 3.81
- 3.81 - 4.99
- 4.99 - 7.38
- 7.38 – 12.19
- 12.19 - 21.86
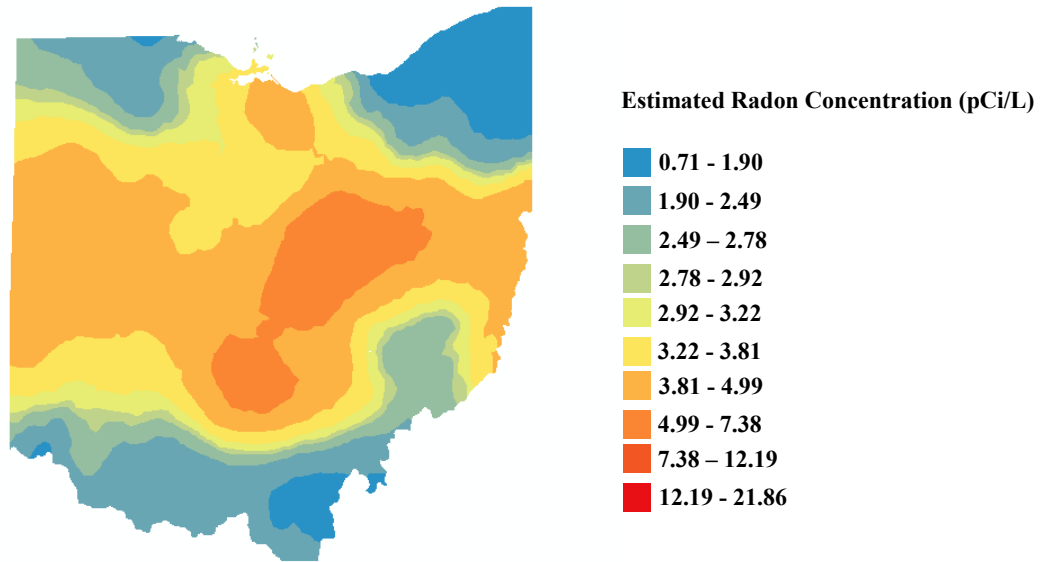
Figure 5-8: Prediction Map of Ordinary Kriging using the Radon Concentration Training Data Set.

5.2.2 Ordinary Cokriging

The procedure used for performing cokriging is similar to kriging except two variables are used in cokriging. In this case, uranium concentration is used as co-variable. In the geostatistical wizard dialogue box (kriging/cokriging), at first the radon concentration training point file is selected from the "Dataset" option in the "Source Dataset" drop down menu, and GM is selected as the first set of variable in the "Data Field" option. Secondly, the uranium point file is selected from the "Dataset 2" option in the "Source Dataset" drop down menu, and UR_GM is selected in the "Data Field" option for the second set of variable as shown in Figure 5-9. Log transformation is applied to the first set of variable, and first order trend removal is selected which is similar to ordinary kriging.
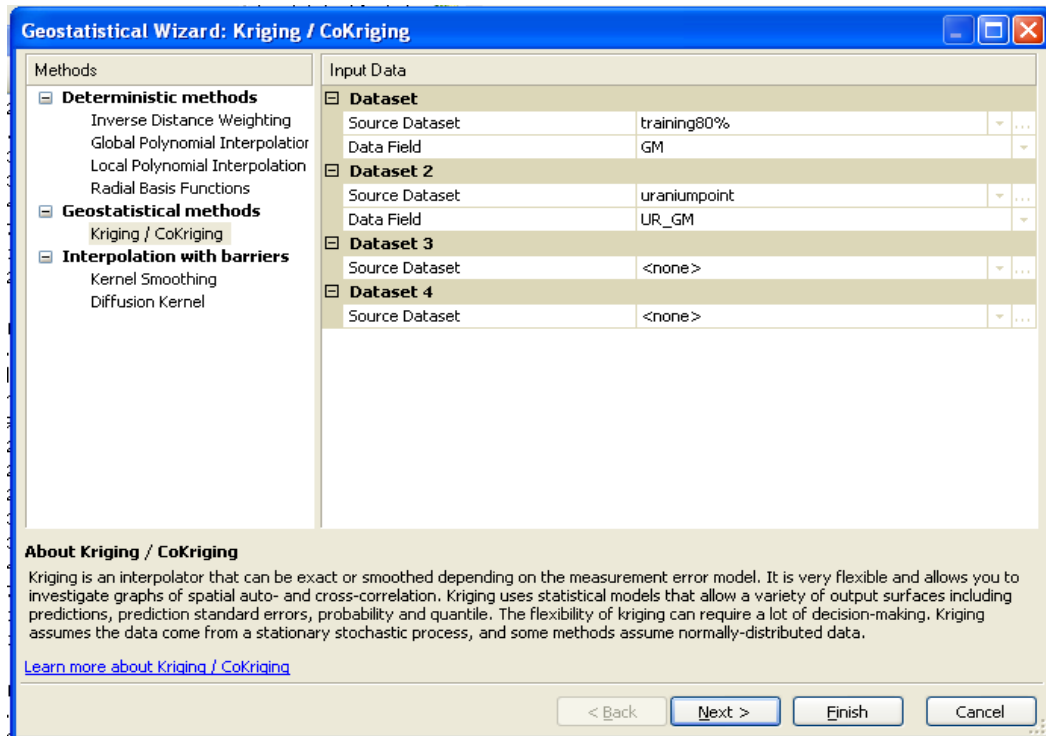
Figure 5-9: Geostatistical Method Selection Dialogue Box

The next step is semivariogram/covariance modeling. After calculating the empirical variogram for the measured data points, a stable type model is selected as shown in the figure (dark blue line). The nugget value, range, and sill parameters are 0.1092, 467689.38, and 0.19462 respectively.
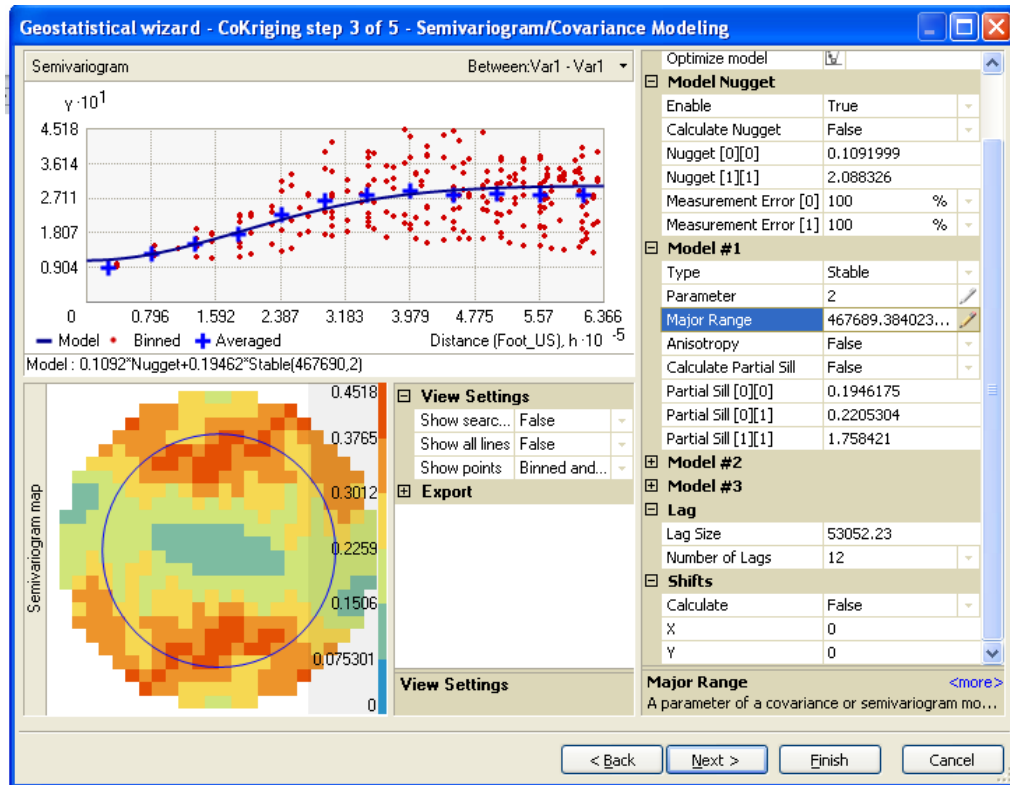
Figure 5-10: Semivariogram/Covariance Modeling dialogue box of Ordinary Cokriging.

The next step in cokriging is searching neighborhood. As shown in Figure 5-11, five neighboring points are selected, and a circle with four sectors is selected. The points highlighted in the data give an indicator of the weights associated with each point, and these weights are used to estimate the value at the unknown location, which is at the center of the crosshair.
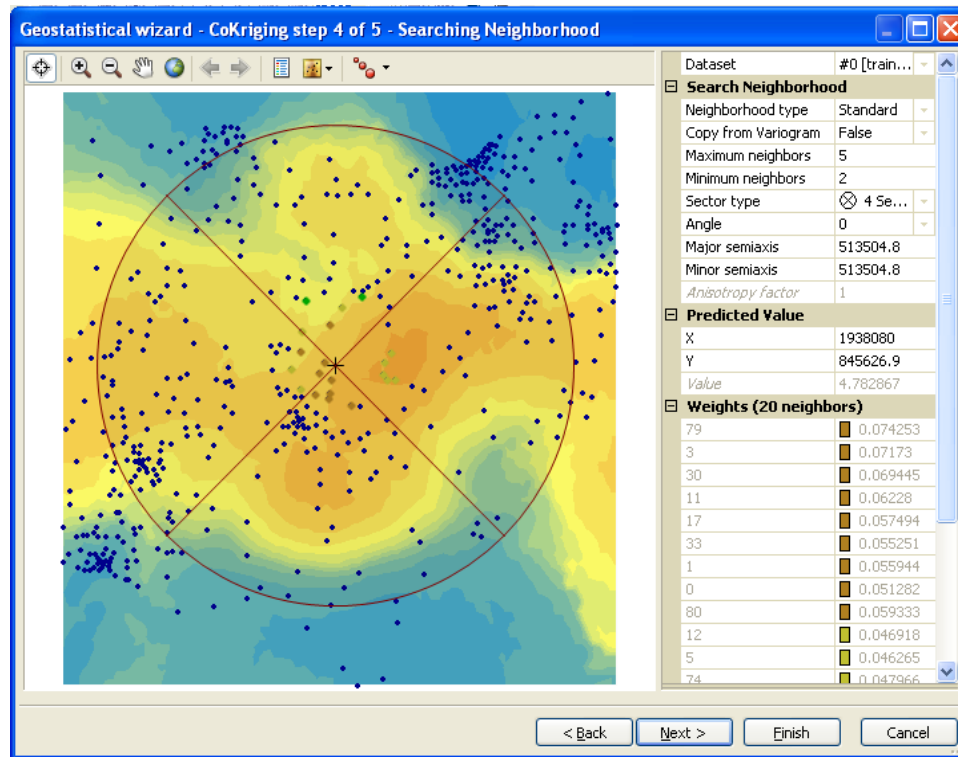
Figure 5-11: Searching Neighborhood Dialogue Box of Ordinary Cokriging.

The last step in cokriging is cross validation. The cross validation dialogue box displays

the predicted, error, standardized error, and normal QQ plot for each data point as shown

in Figure 5-12, Figure 5-13, Figure 5-14, and Figure 5-15, respectively.
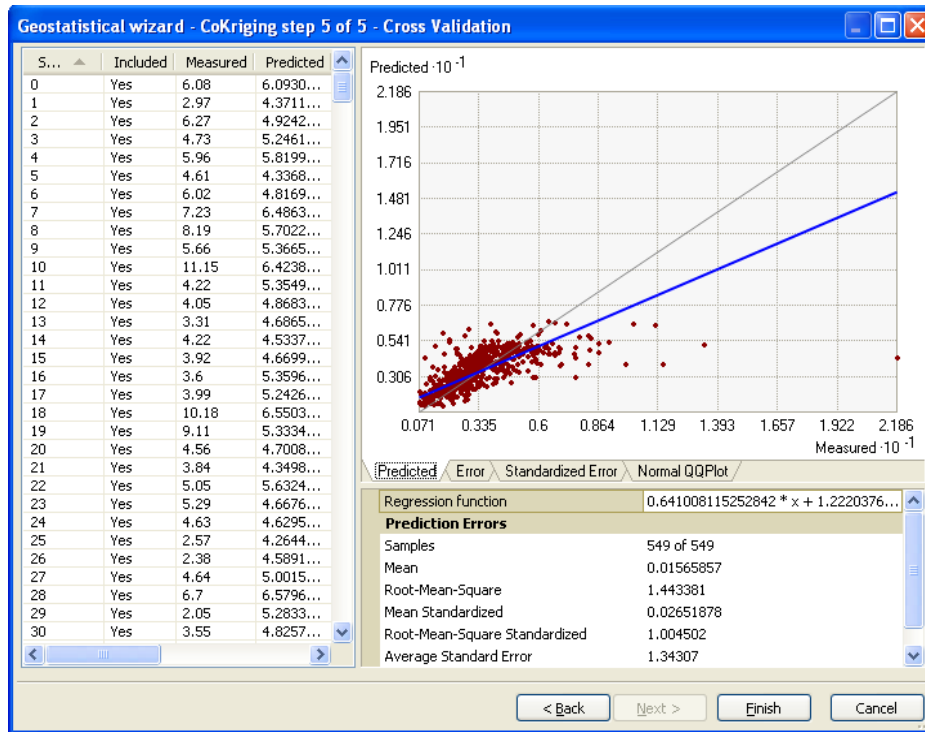
Figure 5-12: Predicted plot of Ordinary Cokriging (Predicted vs. Measured)
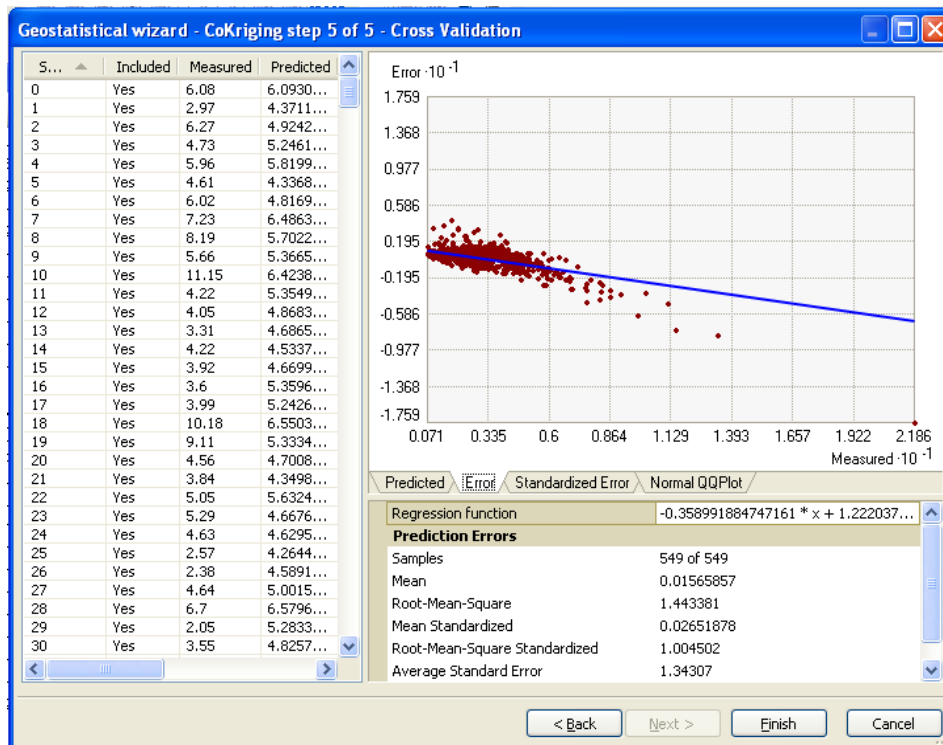
Figure 5-13: Error plot of Ordinary Cokriging (Error vs. Measured)
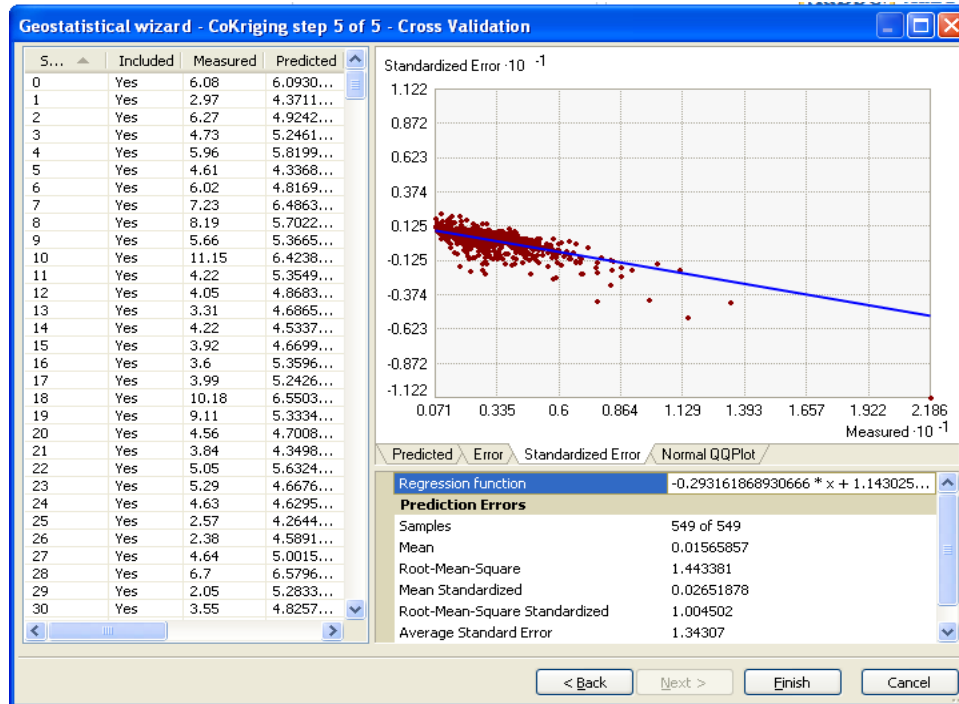
Figure 5-14: Standardized Error plot of Ordinary Cokriging (Standardized Error vs. Measured)
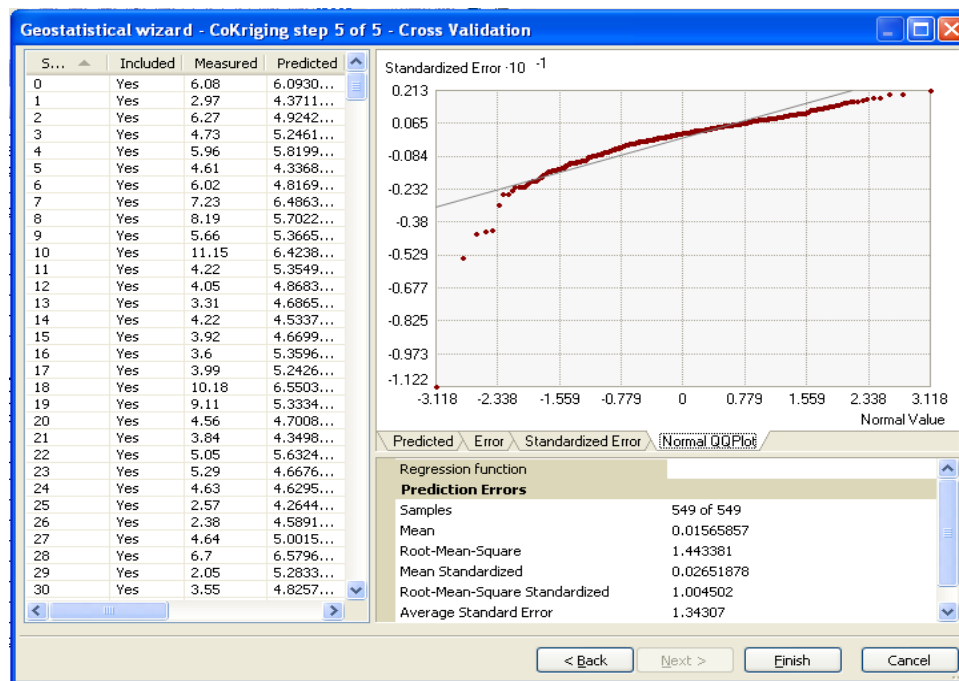
Figure 5-15: Normal QQ plot of Ordinary Cokriging

Prediction errors of ordinary cokriging available using the radon concentration training

dataset is presented in Table 5.2.

Table 5.2: Prediction errors using Ordinary Cokriging

Error	Value
Mean	0.01566
Root Mean Square	1.44338
Mean Standardized	0.02652
Root Mean Square Standardized	1.00450
Average Satndard Error	1.34307

After the cross validation process, the next step is the generation of the surface map.

Figure 5-16 shows the distribution of radon concentration for the State of Ohio using the

training dataset. The higher concentrations are represented by dark colors, and the lower

concentrations are represented by light colors.

Estimated Radon Concentration (pCi/l)

- 0.71 - 1.90
- 1.90 - 2.49
- 2.49 – 2.78
- 2.78 - 2.92
- 2.92 - 3.22
- 3.22 - 3.81
- 3.81 - 4.99
- 4.99 - 7.38
- 7.38 – 12.19
- 12.19 - 21.86
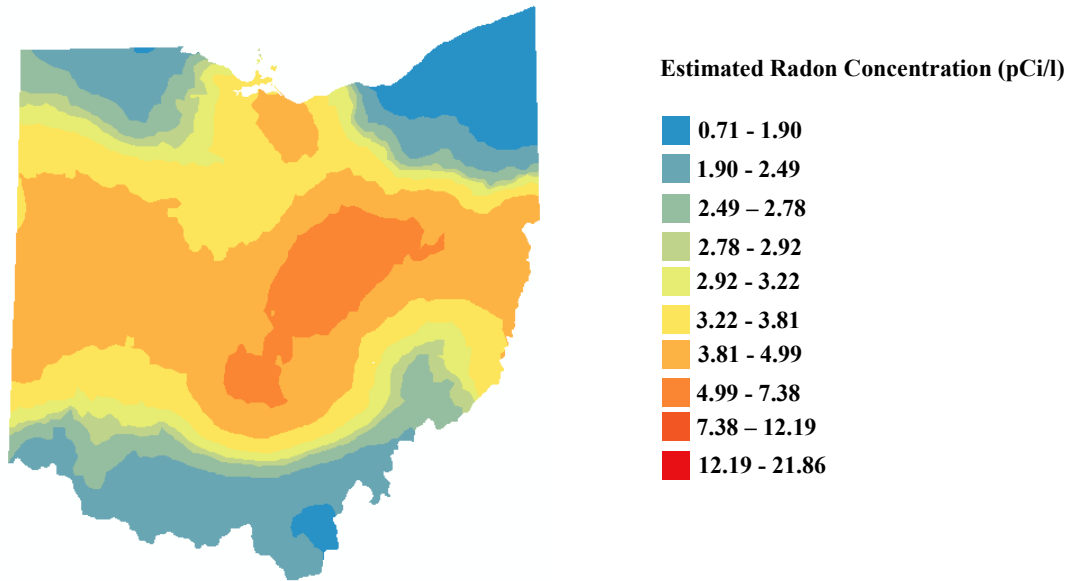
Figure 5-16: Prediction Map of Ordinary Cokriging using the Radon Concentration Training Data Set

5.2.3 Inverse Distance Weighting (IDW)

Inverse distance weighting assumes that things close to one another are more alike than those, which are farther apart. The first step in IDW is the searching neighborhood method, which is performed on the radon concentration dataset as shown in Figure 5-17. The power parameter 2 is selected which is the commonly used power parameter. The maximum and minimum numbers of neighboring points included are 15 and 10 respectively. The sector type selected is four sectors as shown in Figure 5-17.
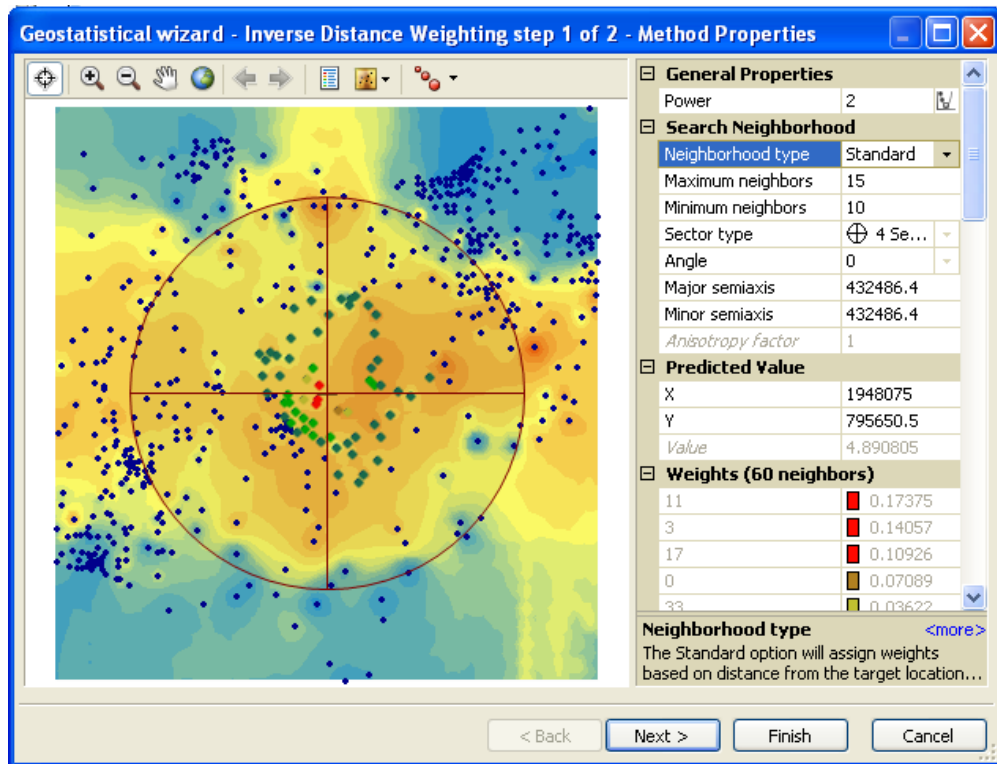
Figure 5-17: IDW Searching Neighborhood Dialogue Box

The last step is the cross validation tool, which gives the predicted, and error plot for the radon concentration training data set as shown in Figure 5-18 and Figure 5-19 respectively.
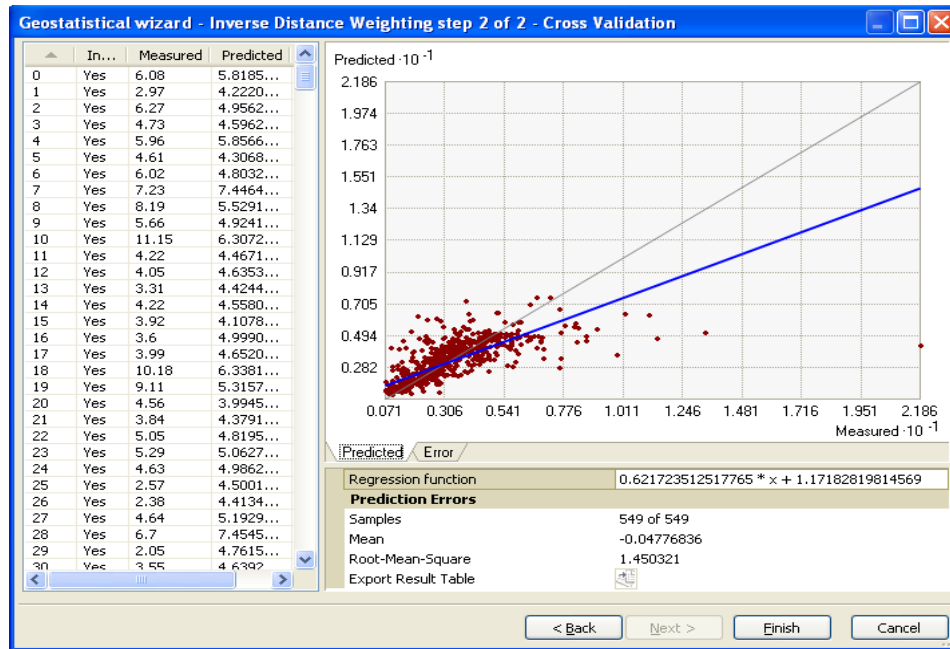
Figure 5-18: Predicted plot of IDW (Measured vs. Predicted)
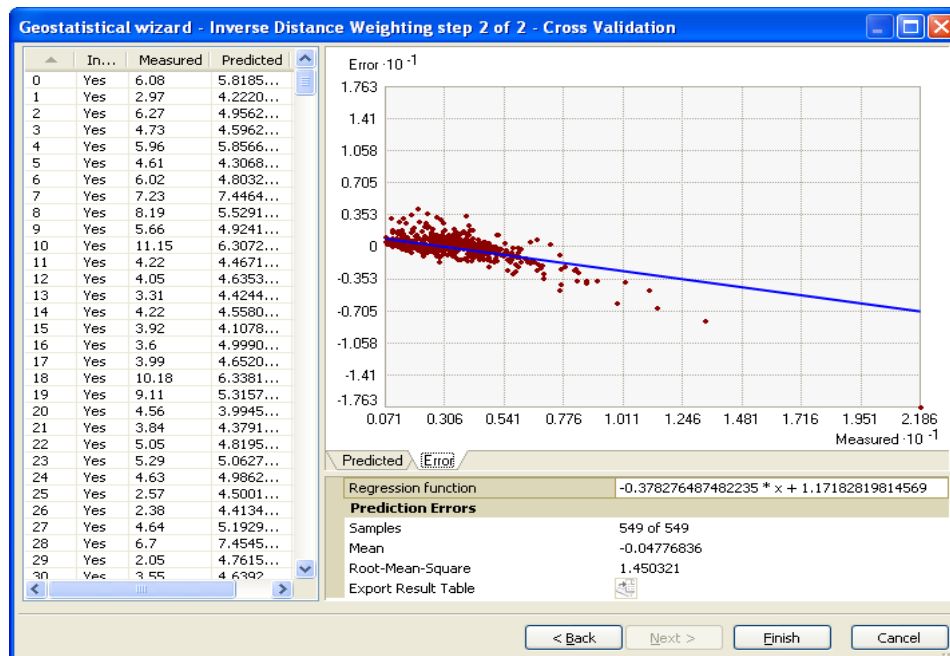
Figure 5-19: Error plot of IDW (Error vs. Measured)

For the IDW technique, prediction errors using the radon concentration training dataset is presented in Table 5.3.

Table 5.3: Prediction errors using IDW

Prediction	Errors
Mean	-0.04777
Root Mean Square	1.45032

The final predicted map after cross validation is shown in Figure 5-20 which shows the distribution of radon in the state of Ohio by using the IDW technique for the radon training dataset.

Estimated Radon Concentration (pCi/L)

- 0.71 - 1.90
- 1.90 - 2.49
- 2.49 – 2.78
- 2.78 - 2.92
- 2.92 - 3.22
- 3.22 - 3.81
- 3.81 - 4.99
- 4.99 - 7.38
- 7.38 – 12.19
- 12.19 - 21.86
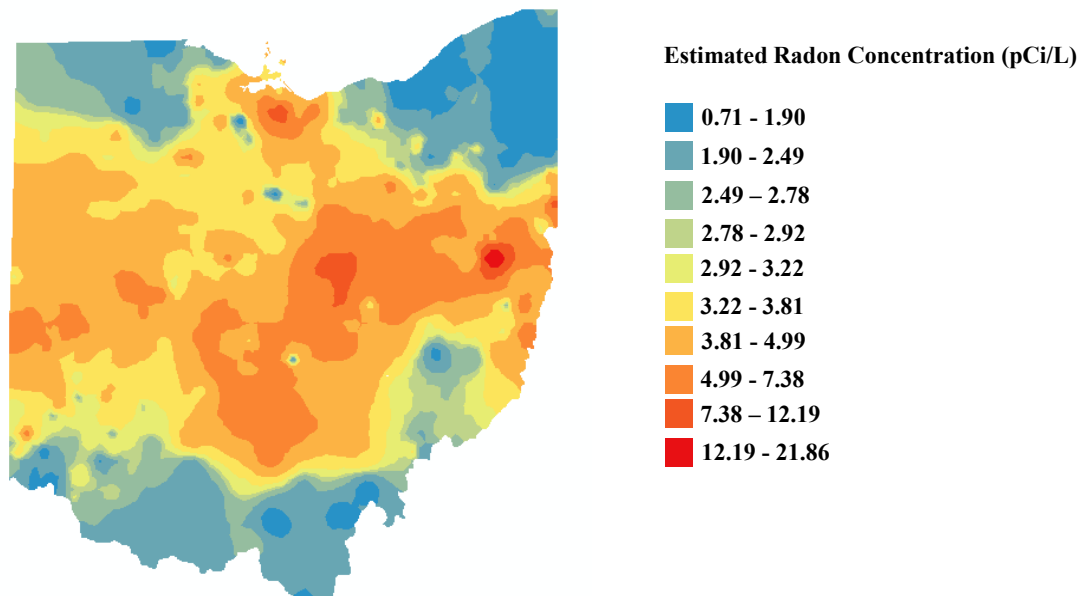
Figure 5-20: Prediction Map of Inverse Distance Weighting using the Radon Concentration Training Data Set

5.2.4 Radial Basis function (RBF)

The steps followed in the RBF techniques are similar to IDW. The first step is the searching neighborhood method, which is performed using a kernel function (completely regularized spline) with a kernel parameter value of 0.00056 on the radon training data

set as shown in Figure 5-21. In the search neighborhood option, the maximum and minimum number of data points included is 15 and 10 respectively along with 4 sectors.
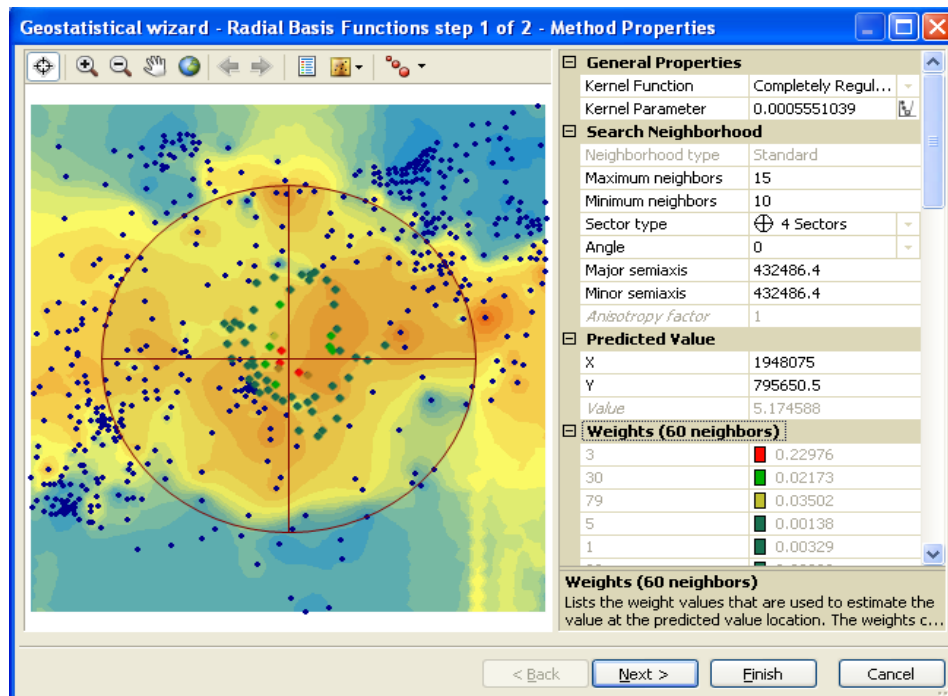
Figure 5-21: Searching Neighborhood Dialogue Box of Radial Basis Function

The last step is the cross validation tool, which gives the predicted, and error plots as shown in Figure 5-22 and Figure 5-23, respectively.
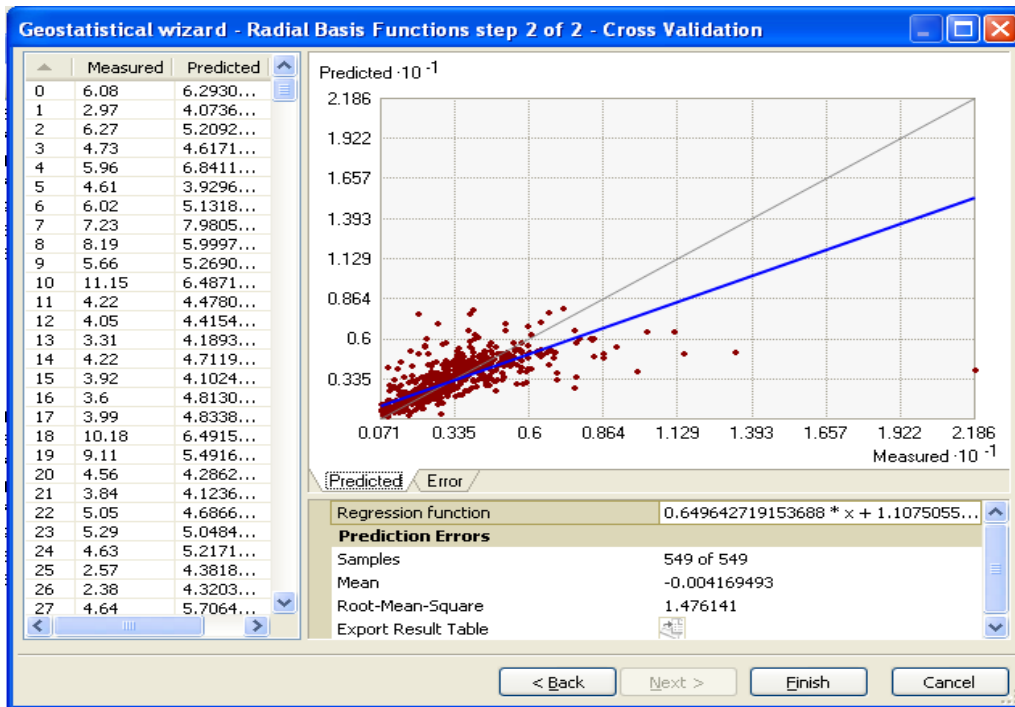
Figure 5-22: Predicted Plot of RBF (Predicted vs. Measured)
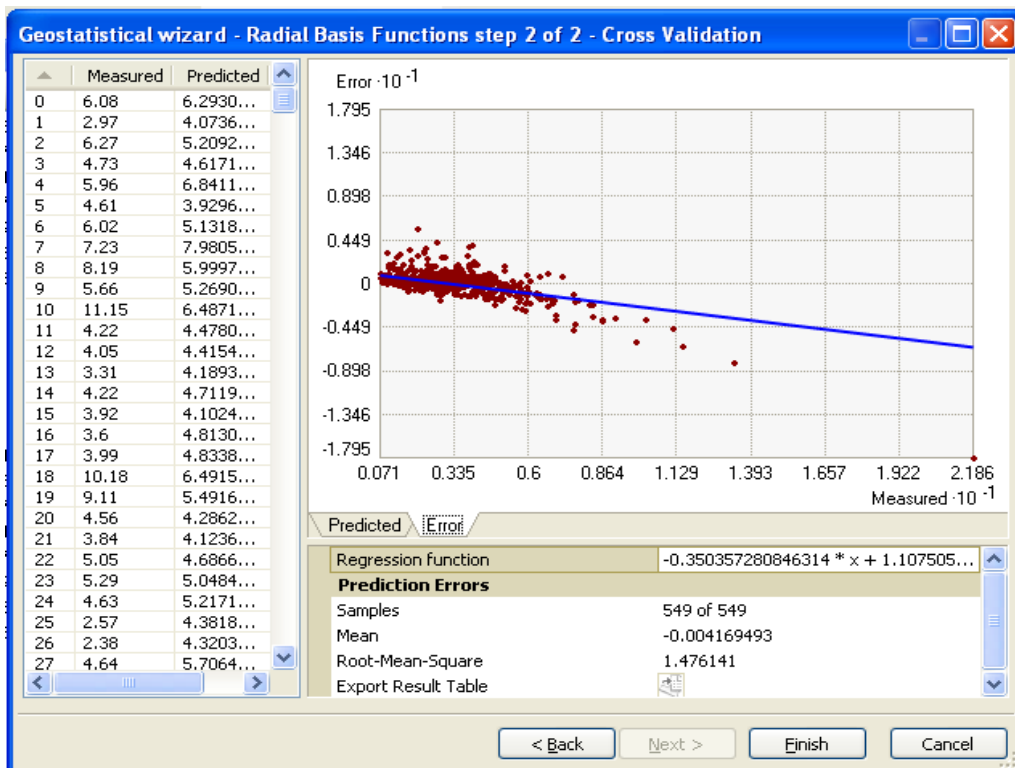
Figure 5-23: Error Plot of RBF (Error Vs. Measured)

For the RBF technique, prediction errors using the radon concentration training dataset is presented in Table 5.4.

Table 5.4: Prediction Errors using RBF

Prediction	Errors
Mean	-0.00417
Root Mean Square	1.47614

The final predicted map of RBF technique using the radon training data set for the State of Ohio is shown in Figure 5-24.

Estimated Radon Concentration (pCi/l)

- 0.71 - 1.90
- 1.90 - 2.49
- 2.49 – 2.78
- 2.78 - 2.92
- 2.92 - 3.22
- 3.22 - 3.81
- 3.81 - 4.99
- 4.99 - 7.38
- 7.38 – 12.19
- 12.19 - 21.86
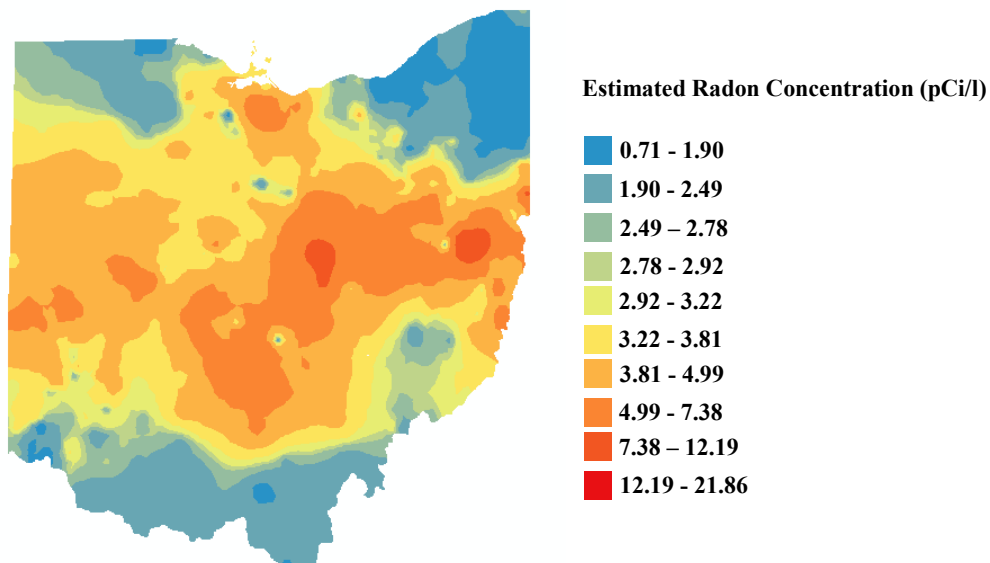
Figure 5-24: Prediction Map using Radial Basis Function

5.2.5 Global Polynomial Interpolation (GPI)

Global Polynomial Interpolation technique fits a smooth surface that represents gradual trends in the surface over the area of interest. The surface is defined by a polynomial. The order of polynomial is in the range 1-10. Since the polynomials of higher order show

greater root mean square error, a second order polynomial is selected as shown in Figure 5-25.
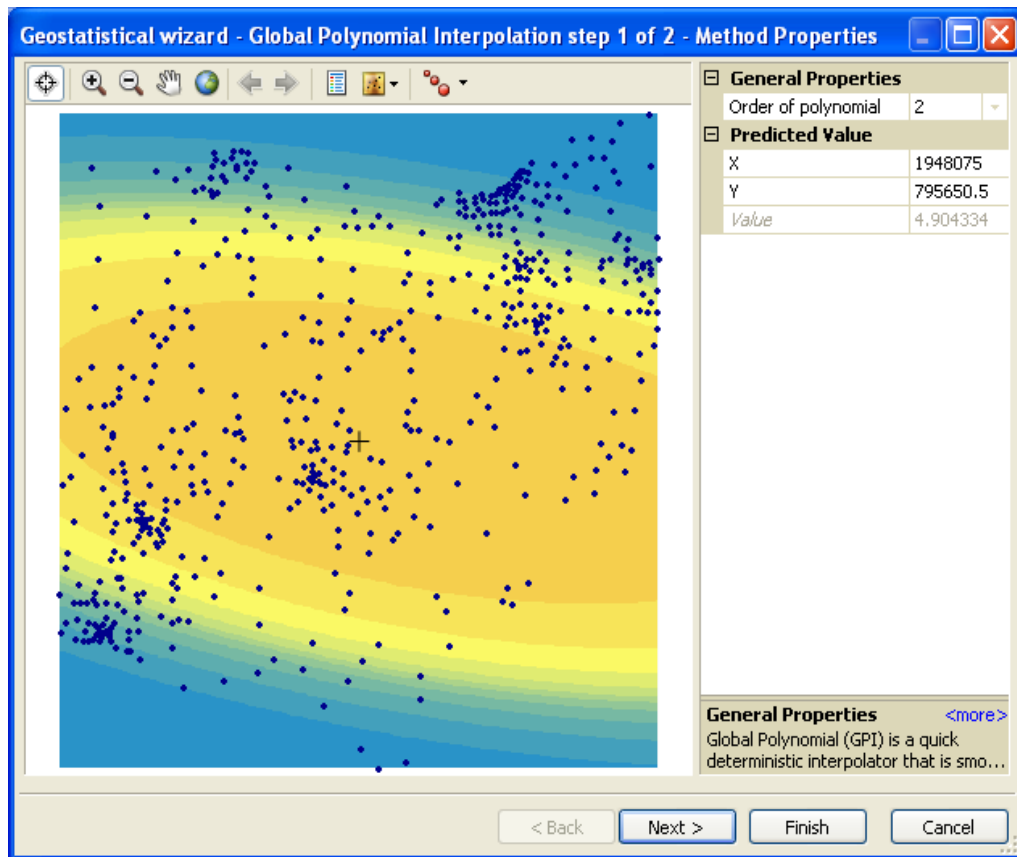
Figure 5-25: Setting of Polynomial in the Global Polynomial Interpolation Dialogue Box

The last step is the cross validation, which shows the measured and predicted error plots as shown in Figure 5-26, and Figure 5-27 respectively.
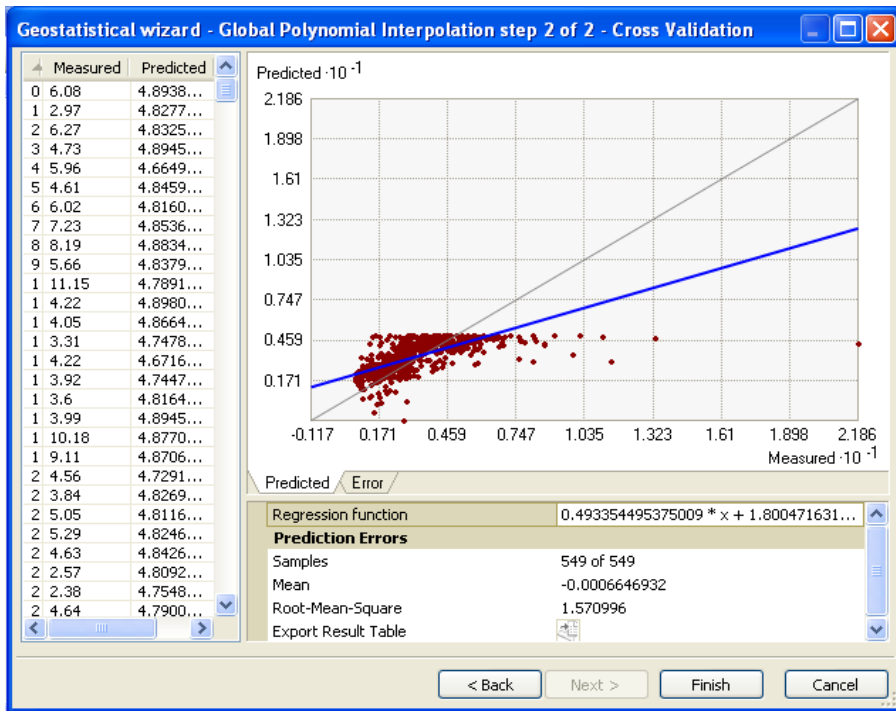
Figure 5-26: Predicted Plot of GPI (Predicted vs. Measured)
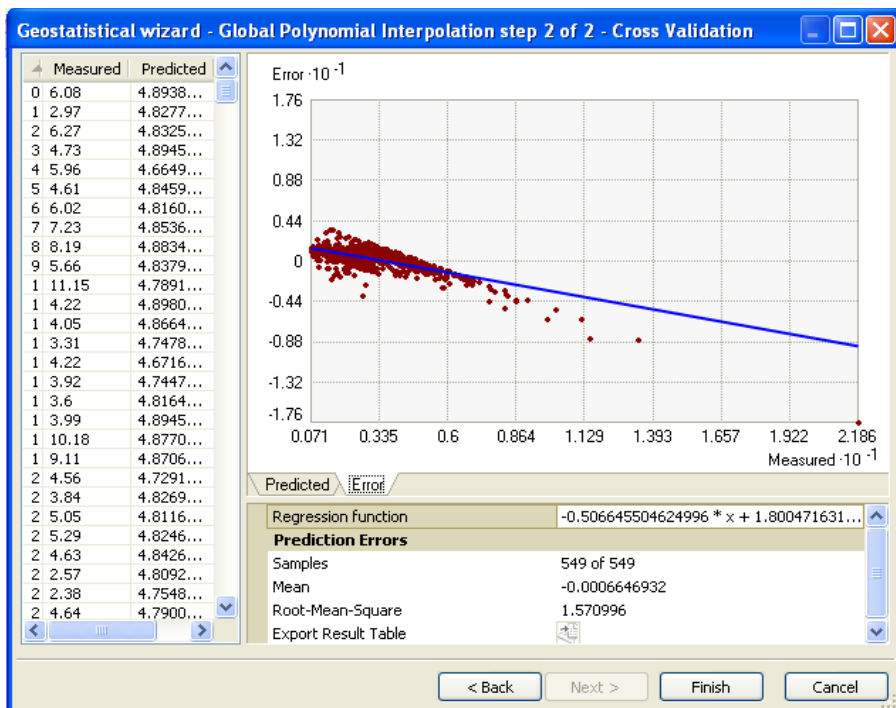
Figure 5-27: Error Plot of GPI (Error vs. Measured)

The radon concentration training data set prediction errors by GPI technique is presented in Table 5.5.

Table 5.5: Prediction Errors using Global Polynomial Interpolation Technique

Prediction	Errors
Mean	-0.00066
Root Mean Square	1.57100

The final prediction map by Global Polynomial interpolation Technique for the radon concentration training data set is shown in Figure 5-28.

Estimated Radon Concentration (pCi/L)

- 0.71 - 1.90
- 1.90 - 2.49
- 2.49 – 2.78
- 2.78 - 2.92
- 2.92 - 3.22
- 3.22 - 3.81
- 3.81 - 4.99
- 4.99 - 7.38
- 7.38 – 12.19
- 12.19 - 21.86
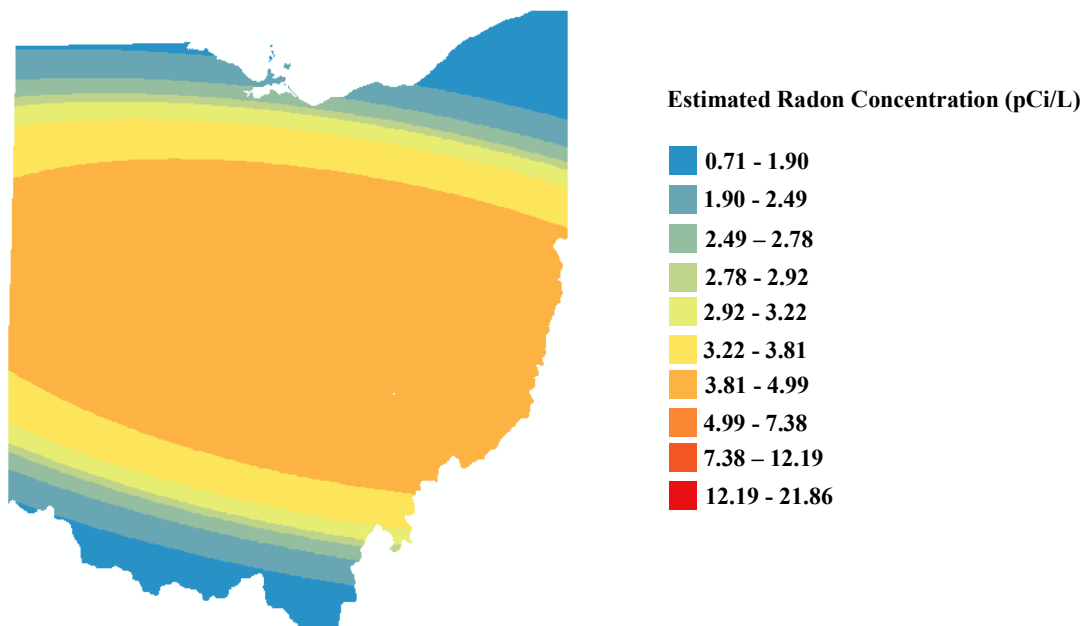
Figure 5-28: Prediction map using Global Polynomial Interpolation.

5.2.6 Local Polynomial Interpolation (LPI)

LPI produces a smooth surface and is best suited for data that exhibits short-range variation. Local polynomial interpolation is sensitive to the neighborhood distance, and

empty areas in the prediction surface may be created by a small searching neighborhood. In the first step, maximum neighbors, minimum neighbors and sector type selected are 1000, 10 and 4 respectively as shown in Figure 5-29. The predicted and error plots are shown in Figure 5-30 and 5-31 respectively.
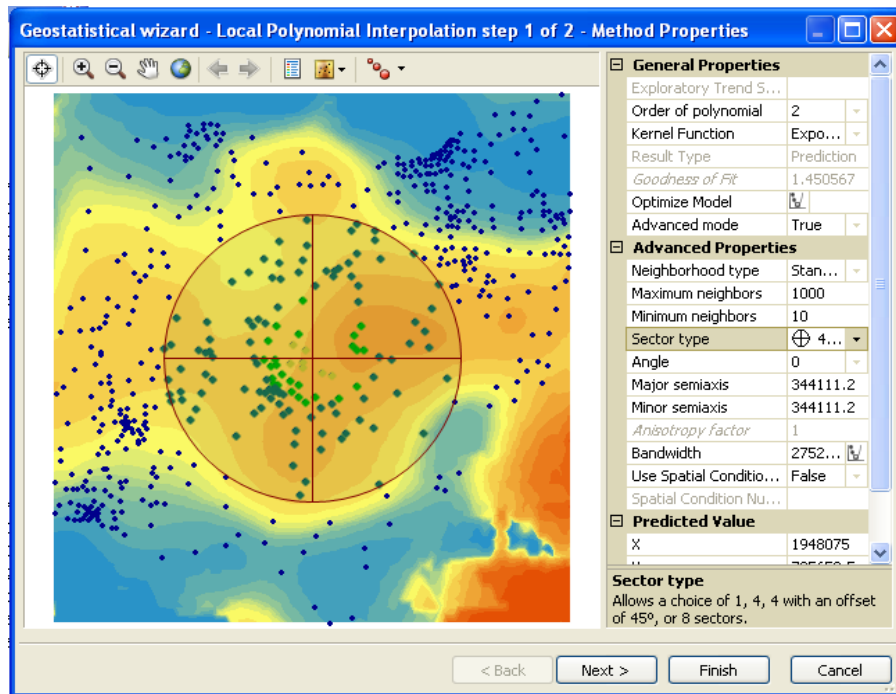
Figure 5-29: Local Polynomial Interpolation Searching Neighborhood Dialogue Box
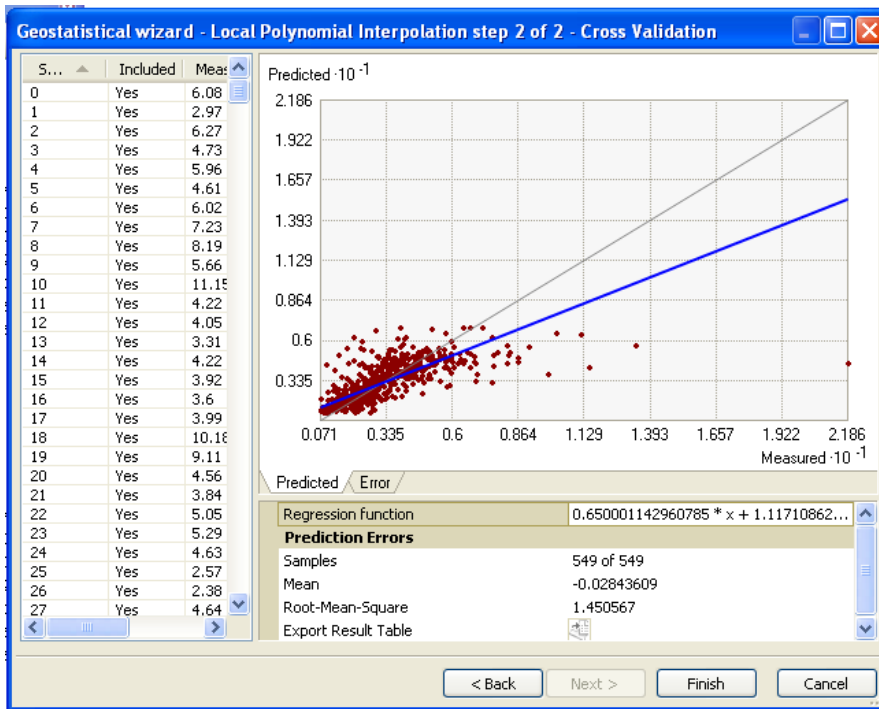
Figure 5-30: Prediction plot of LPI (Predicted vs. Measured)
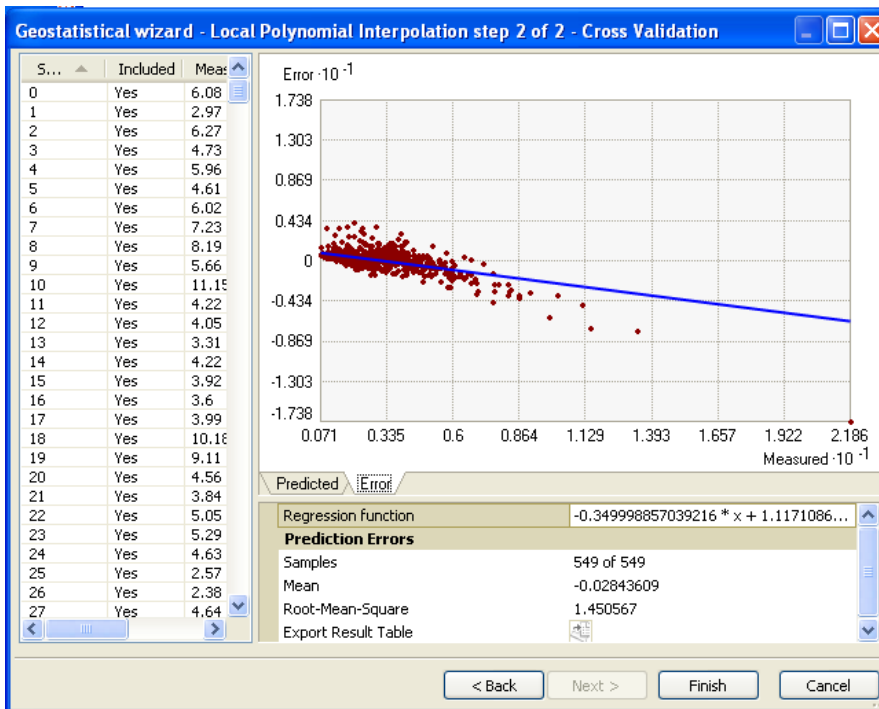
Figure 5-31: Error plot of LPI (Error vs. Measured)

The radon concentration training data set prediction errors by LPI technique is presented in Table 5.6.

Table 5.6: Prediction Errors using Local Polynomial Interpolation Technique

Prediction	Errors
Mean	-0.02844
Root Mean Square	1.45057

The final prediction map by LPI interpolation for the radon concentration training data set is shown in Figure 5-32.
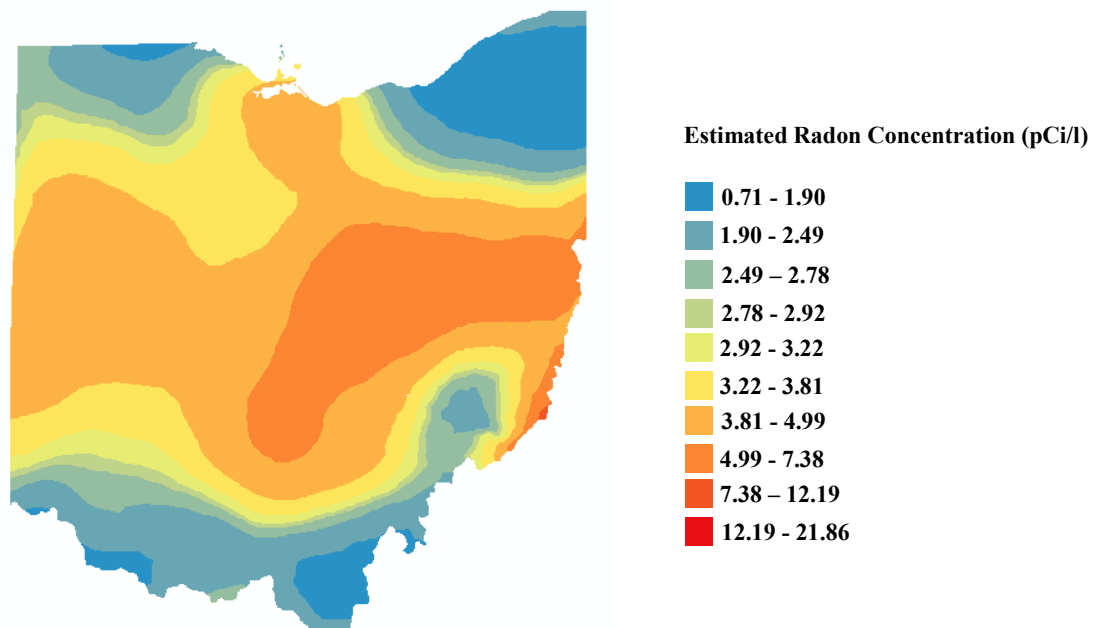
Figure 5-32: Prediction Map using Local Polynomial Interpolation.

5.3 Evaluation Criteria

Kadiyala and Kumar (2012) suggested a complete list of performance measures to validate indoor and outdoor air quality models. Our study deals with the indoor radon

concentrations. Therefore, this study uses the measures suggested for IAQ work by Kadiyala and Kumar (2012). These measures are based on the evaluation procedure established for extreme-end concentrations (i.e., peak-end/low-end) and the mid-range concentrations. Coefficient of correlation (r), Spearman correlation coefficient (ρ), slope of the regression line (m), ratio of the intercept of the regression line to the average observed concentrations (b/C_o), fractional variance (FV), fraction of prediction within a factor of two of the observations (FA$_2$), model comparison measure (MCM$_2$), geometric mean bias (MG), geometric mean variance (VG), normalized mean square error (NMSE), fractional bias (FB), revised index of agreement (IOA$_r$), accuracy for paired peak (A$_p$), maximum ratio (R$_{max}$), scatter plots, quantile – quantile (Q-Q) plots, and bootstrap 95% confidence interval estimates are the performance measures which are recommended for extreme-end concentrations (i.e., peak-end/low-end) and the mid-range concentrations of IAQ models. An IAQ model can be considered to be perfect if b/C_o, NMSE, FB, FV, MCM$_2$, A$_p$ statistics are equal to zero; ρ, m, FA$_2$, RHC$_{ratio}$, MG, VG, IOA$_r$, R$_{max}$ statistics are equal to one; and the scatter plots, Q-Q plots have the points plotted along the identity line i.e., along a 45^0 line. It is not possible to develop perfect models in real life. An IAQ model is deemed acceptable considering from both extreme-end and mid-range modeling perspectives, if it meets the ranked performance measures along with the recommended acceptable limits as presented in Table 5.7. The performance measures for m, b/C_0, FV, ρ, RHC$_{ratio}$, MCM$_2$, IOA$_r$, and A$_p$ are computed using Microsoft Excel, and r, NMSE, FB, FA$_2$, MG, VG, and bootstrap 95% confidence interval estimates over NMSE, r, FB, MG, and VG are computed using the BOOT v2.0 for this study. The scatter plots and the Q-Q plots are obtained from using MINITAB16 and MATLAB 2011b software.

Table 5.7: Ranked Performance Measures of IAQ Models.

Type	Rank	IAQ Models		
		Peak-End Estimates	**Low-End Estimates**	**Mid-Range Estimates**
Primary Performance Measures Set	1	$0.9 \leq \rho \leq 1.0$	$0.9 \leq \rho \leq 1.0$	$0.9 \leq r \leq 1.0$
	2	$0.75 \leq m \leq 1.25$	$0.75 \leq m \leq 1.25$	$0.75 \leq m \leq 1.25$
	3	$-25 \leq (b/C_0) \% \leq 25$	$-25 \leq (b/C_0) \% \leq 25$	$-25 \leq (b/C_0) \% \leq 25$
	4	$-0.5 \leq FV \leq 0.5$	$-0.5 \leq FV \leq 0.5$	$0 \leq NMSE \leq 0.25$
	5	$0.8 \leq FA_2 \leq 1.2$	$0.8 \leq FA_2 \leq 1.2$	$-0.25 \leq FB \leq 0.25$
	6	$0.8 \leq RHC_{ratio} \leq 1.2$	$0 \leq MCM_2 \leq 1.2$	$-0.5 \leq FV \leq 0.5$
	7	$0 \leq MCM_2 \leq 1.2$	$0.8 \leq MG \leq 1.2$	Bootstrap CI over r, NMSE, FB
	8	$0.8 \leq MG \leq 1.2$	$0.8 \leq VG \leq 1.2$	$0.8 \leq FA_2 \leq 1.2$
	9	$0.8 \leq VG \leq 1.2$	Bootstrap CI over MG, VG	$0 \leq MCM_2 \leq 1.2$
	10	Bootstrap CI over MG, VG	Scatter plots	$0.8 \leq MG \leq 1.2$
	11	Scatter plots	QQ plots	$0.8 \leq VG \leq 1.2$
	12	QQ plots	-	Bootstrap CI over MG, VG
	13	-	-	$0.85 \leq IOA_r \leq 1.0$
	14	-	-	Scatter plots
	15	-	-	QQ plots
Secondary Performance Measures Set	1	$0.85 \leq IOA_r \leq 1.0$	$0.85 \leq IOA_r \leq 1.0$	-
	2	$-15 \leq A_p \leq 15$	-	-
	3	$0.8 \leq R_{max} \leq 1.2$	-	-

Chapter 6

Results and Discussion

6.1 Summary

Table 6.1 shows the summary of statistical performance measures, which are used to compare the six interpolation techniques along with the mean (M) and standard deviations (SD). The performance measures, geometric mean bias (MG) and geometric mean variance (VG) which are based on logarithmic values cannot be calculated for the GPI technique due to the prediction of negative values at two locations. It can be observed from Table 6.1 that none of the six interpolation techniques meet the primary IAQ model acceptance criteria (Rank 1) $0.9 \leq \rho \leq 1.0$ (Peak End and Low-End) and $0.9 \leq r \leq 1.0$ (Mid-Range). Therefore, no interpolation techniques are statistically acceptable from a theoretical basis. However, we will examine the performance measures of the six interpolation techniques for peak-end, low-end and mid-range concentrations in the following sections using the ranking criteria presented in Table 5.7.

(1) Peak-end estimates

Considering the criteria for the primary performance measures (Table 5.7), none of the interpolation techniques meet the acceptance criteria of $0.9 \leq \rho \leq 1.0$, $0.75 \leq m \leq 1.25$ and $-25 \leq (b/C_0) \% \leq 25$ (Rank 1, 2, and 3) for peak end estimates (Table 6.1). Again, it

can be seen from Table 6.1 that all the techniques meet the primary acceptance criteria

for $-0.5 \leq FV \leq 0.5$, $0.8 \leq FA_2 \leq 1.2$, $0.8 \leq RHC_{ratio} \leq 1.2$, and $0 \leq MCM_2 \leq 1.2$ (Rank 4

to Rank 7) for peak end estimates. IDW, LPI, RBF, kriging, and cokriging also meet the

acceptable limits for $0.8 \leq MG \leq 1.2$ and $0.8 \leq VG \leq 1.2$ (Rank 8 and 9). Again, while

considering the criteria for secondary performance measures (Table 5.7), only GPI and

cokriging meet the acceptance criteria for $0.8 \leq R_{max} \leq 1.2$, and none of the interpolation

techniques meets the acceptance criteria of $0.85 \leq IOA_r \leq 1.0$ and $-15 \leq A_p \leq 15$. It can

be seen that (Table 6.1) the ideal values for the RBF technique are closer than the other

spatial interpolation techniques for most of the measures (FV, FA_2, RHC_{ratio}, MCM_2 and

VG) but it does not meet any of the secondary performance measures (IOA_r, A_P and

R_{max}) for peak end estimates. Between GPI and cokriging, the R_{max} value for GPI is

closer to the ideal value than cokriging; however, the ideal values of the cokriging

technique are closer for the primary performance measures (FV, FA_2 and RHC_{ratio}) than

the GPI technique. Therefore, the cokriging technique is a suitable technique while

considering the acceptable measures for the peak end estimate.

(2) Low-end estimates

While taking in to account the satisfactory limits for the primary performance measures

for low-end estimates (Table 5.7), none of the interpolation techniques meet the

acceptable criteria (Table 6.1) of $0.9 \leq \rho \leq 1.0$, $0.75 \leq m \leq 1.25$, and $-25 \leq (b/C_0) \% \leq 25$

(Rank 1, 2 and 3). Again, all the interpolation techniques meet the primary acceptance

criteria for $-0.5 \leq FV \leq 0.5$, $0.8 \leq FA_2 \leq 1.2$, and $0 \leq MCM_2 \leq 1.2$ (Rank 4 to Rank 6).

IDW, LPI, RBF, kriging, and cokriging also meet the acceptable criteria of $0.8 \leq MG \leq$

1.2 and $0.8 \leq VG \leq 1.2$ (Rank 7 and Rank 8). It can be seen from the Table 6.1 that none

of the interpolation techniques meets the secondary performance measure criteria $0.85 \leq IOA_r \leq 1.0$. Considering the closeness of the performance measures to their corresponding ideal values for most of the performance measures (FV, FA_2, MCM_2 and VG), the RBF technique performs relatively better compared to IDW, LPI, RBF, kriging and cokriging for low-end estimates.

(3) Mid-range estimates

As per the recommended measures for mid-range estimates (Table 5.7), none of the interpolation techniques meet the primary performance measures (Table 6.1) of $0.9 \leq r \leq 1.0$, $0.75 \leq m \leq 1.25$, and $-25 \leq (b/C_0) \% \leq 25$. Again, all the interpolation techniques meet the primary acceptance criteria for $0 \leq NMSE \leq 0.25$, $-0.25 \leq FB \leq 0.25$, $-0.5 \leq FV \leq 0.5$ (Rank 4 to 6), and $0.8 \leq FA_2 \leq 1.2$ (Rank 8). None of the techniques meets the criteria of $0.85 \leq IOA_r \leq 1.0$ (Rank 13). Like peak-end estimates and low-end estimates, IDW, LPI, RBF, kriging, and cokriging also meet the acceptable limits for of $0.8 \leq MG \leq 1.2$ and $0.8 \leq VG \leq 1.2$ (Rank 7 and Rank 8). Again, considering the proximity for most of the performance measures (NMSE, FB, FV, FA_2, MCM_2, and VG) to their respective ideal values, it is seen that the RBF technique is the ideal technique for mid-range estimates as compared to the other five interpolation techniques.

Table 6.1: Statistical performance measures computed for the six interpolation techniques

MODEL (S)	M	SD	R	m	$(b/C_o)\%$	NMSE	FB	FV	FA$_2$
Arithmetic Values									
OBS	3.560	1.970	1.000	1.000	0.000	0.000	0.000	0.000	1.000
IDW	3.390	1.340	0.635	0.431	52.197	0.200	0.048	0.383	0.942
GPI	3.330	1.190	0.608	0.368	56.832	0.210	0.066	0.492	0.883
LPI	3.360	1.290	0.648	0.423	52.238	0.190	0.056	0.419	0.942
RBF	3.430	1.370	0.666	0.462	50.331	0.180	0.036	0.362	0.942
KRIG	3.410	1.240	0.676	0.426	53.398	0.180	0.041	0.454	0.927
COKRIG	3.420	1.200	0.678	0.412	54.916	0.180	0.039	0.487	0.942

Table 6.1 (Contd.): Statistical performance measures computed for the six interpolation techniques

MODEL (s)	MCM$_2$	IOA$_r$	ρ	RHC$_{ratio}$	A$_p$	R$_{max}$	MG	VG
Arithmetic Values							Log Values	
OBS	0.000	1.000	1.000	1.000	0.000	1.000	1.000	1.000
IDW	0.717	0.659	0.746	0.819	-68.523	2.620	0.987	1.140
GPI	1.082	0.523	0.694	0.735	-62.419	1.110		
LPI	0.746	0.486	0.721	0.787	-65.625	2.270	0.995	1.160

MODEL (s)	MCM$_2$	IOA$_r$	ρ	RHC$_{ratio}$	A$_p$	R$_{max}$	MG	VG
RBF	0.695	0.558	0.764	0.842	-67.514	2.380	0.977	1.130
KRIG	0.723	0.564	0.742	0.789	-63.983	0.580	0.971	1.150
COKRIG	0.732	0.531	0.744	0.782	-64.037	1.170	0.965	1.150

Bootstrap 95 % confidence interval (CI) over NMSE, FB, r, MG and VG for individual model comparisons and among model comparisons, are obtained from running bootstrap resampling techniques, are as shown in Table 6.2 and Table 6.3 respectively.

Table 6.2: Bootstrap CI Estimates over NMSE, FB, r, MG, and VG

(Individual model comparison)

Model (s)	Measures	Student's 95% confidence limits.		Student t	Mean	SD
		LL	UL			
IDW	NMSE	0.114	0.280	4.682	0.197	0.042
	FB	-0.020	0.120	1.402	0.050	0.035
	r	0.522	0.745	11.195	0.634	0.057
	VG	0.099	0.170	7.482	0.135	0.018
	MG	-0.067	0.053	-0.229	-0.007	0.030
GPI	NMSE	0.130	0.291	5.165	0.210	0.041
	FB	-0.006	0.146	1.832	0.070	0.038
	r	0.522	0.708	13.124	0.615	0.047
	VG					
	MG					
LPI	NMSE	0.115	0.270	4.893	0.193	0.039
	FB	-0.013	0.129	1.624	0.058	0.036
	r	0.555	0.740	13.873	0.648	0.047
	VG	0.114	0.187	8.181	0.151	0.018
	MG	-0.065	0.070	0.065	0.002	0.034
RBF	NMSE	0.101	0.259	4.053	0.180	0.040
	FB	-0.031	0.105	1.071	0.037	0.034
	r	0.556	0.772	12.171	0.664	0.055

Model (s)	Measures	Student's 95% confidence limits.		Student t	Mean	SD
		LL	UL			
	VG	0.092	0.161	7.210	0.126	0.017
	MG	-0.077	0.041	-0.596	-0.018	0.030
KRIG	**NMSE**	0.101	0.251	4.614	0.176	0.038
	FB	-0.025	0.112	1.247	0.043	0.035
	r	0.583	0.771	14.251	0.677	0.048
	VG	0.100	0.170	7.598	0.135	0.018
	MG	-0.087	0.040	-0.723	-0.023	0.032
COKRIG	**NMSE**	0.102	0.250	4.685	0.176	0.037
	FB	-0.027	0.111	1.202	0.042	0.035
	r	0.595	0.764	15.870	0.679	0.043
	VG	0.101	0.174	7.432	0.137	0.018
	MG	-0.094	0.037	-0.867	-0.029	0.033

Table 6.3: Bootstrap CI Estimates over NMSE, FB, r, MG, and VG

(Among model Comparison)

Model (s)	Measures (s)	Student's 95% confidence limits.		Student t	Mean	SD
		LL	UL			
IDW – LPI	**NMSE**	-0.013	0.022	0.516	0.004	0.009
	FB	-0.025	0.008	-0.999	-0.009	0.009
	R	-0.049	0.021	-0.792	-0.014	0.018
	VG	-0.030	-0.003	-2.346	-0.016	0.007
	MG	-0.029	0.011	-0.900	-0.009	0.010
IDW – RBF	**NMSE**	0.008	0.026	3.800	0.017	0.004
	FB	0.004	0.022	2.861	0.013	0.005
	R	-0.050	-0.011	-3.115	-0.030	0.010
	VG	0.004	0.013	3.604	0.008	0.002
	MG	0.003	0.019	2.608	0.011	0.004
IDW – KRIG	**NMSE**	-0.003	0.045	1.743	0.021	0.012
	FB	-0.011	0.024	0.746	0.006	0.009
	R	-0.095	0.008	-1.684	-0.044	0.026
	VG	-0.017	0.015	-0.089	-0.001	0.008
	MG	0.000	0.033	1.956	0.016	0.008
IDW- COKRIG	**NMSE**	-0.004	0.047	1.670	0.021	0.013

Model (s)	Measures (s)	Student's 95% confidence limits.		Student t	Mean	SD
		LL	UL			
	FB	-0.012	0.028	0.748	0.008	0.010
	R	-0.100	0.008	-1.699	-0.046	0.027
	VG	-0.022	0.016	-0.291	-0.003	0.010
	MG	0.002	0.041	2.230	0.022	0.010
LPI – RBF	NMSE	-0.004	0.028	1.508	0.012	0.008
	FB	0.005	0.038	2.546	0.021	0.008
	R	-0.049	0.017	-0.976	-0.016	0.017
	VG	0.012	0.037	3.825	0.024	0.006
	MG	0.000	0.040	1.958	0.020	0.010
LPI – KRIG	NMSE	0.000	0.034	1.930	0.017	0.009
	FB	0.002	0.028	2.353	0.015	0.006
	R	-0.073	0.013	-1.376	-0.030	0.022
	VG	0.005	0.026	2.939	0.015	0.005
	MG	0.012	0.039	3.803	0.025	0.007
LPI – COKRIG	NMSE	0.003	0.031	2.370	0.017	0.007
	FB	0.003	0.029	2.428	0.016	0.007
	R	-0.068	0.004	-1.747	-0.032	0.018
	VG	0.001	0.025	2.115	0.013	0.006
	MG	0.016	0.045	4.232	0.031	0.007

Model (s)	Measures (s)	Student's 95% confidence limits.		Student t	Mean	SD
		LL	UL			
RBF – KRIG	NMSE	-0.017	0.026	0.398	0.004	0.011
	FB	-0.022	0.009	-0.822	-0.006	0.008
	R	-0.057	0.030	-0.611	-0.013	0.022
	VG	-0.024	0.005	-1.242	-0.009	0.007
	MG	-0.011	0.022	0.657	0.005	0.008
RBF– COKRIG	NMSE	-0.018	0.027	0.404	0.005	0.011
	FB	-0.024	0.013	-0.574	-0.005	0.009
	R	-0.060	0.029	-0.681	-0.015	0.023
	VG	-0.029	0.007	-1.249	-0.110	0.009
	MG	-0.008	0.030	1.120	0.011	0.010
KRIG- COKRIG	NMSE	-0.011	0.011	0.054	0.000	0.006
	FB	-0.006	0.009	0.311	0.001	0.004
	R	-0.026	0.022	-0.166	-0.002	0.012
	VG	-0.008	0.004	-0.693	-0.002	0.003
	MG	0.000	0.011	1.186	0.005	0.003

The summaries of the confidence limits between individual models comparison and among models comparison are shown in Table 6.4 and Table 6.5, respectively. It can be seen from the results that NMSE, coefficient of correlation (r) and VG values are

significantly different from zero, but FB and MG values are not when each technique is considered individually (Table 6.4). Again, when the NMSE, FB, r, VG, and MG values are compared among the techniques, it is observed that (Table 6.5) NMSE values are significantly different from zero for IDW and RBF, LPI and cokriging and RBF and cokriging. FB values are significantly different from zero for IDW and RBF, LPI and RBF, LPI and kriging, LPI and cokriging. Coefficient of correlation (r) values are significantly different from zero for IDW and RBF. Similarly, VG values are significantly different from zero for IDW and LPI, IDW and RBF, LPI and RBF, LPI and kriging, and LPI and cokriging, and MG values are significantly different from zero for IDW and RBF, IDW and cokriging, LPI and kriging, and LPI and cokriging.

Table 6.4: Summaries of Bootstrap Confidence Limit Analyses on Each Technique

(NMSE, FB, r, MG & VG)

Measures	Cokriging	Kriging	IDW	RBF	GPI	LPI
NMSE	X	X	X	X	X	X
FB						
r	X	X	X	X	X	X
VG	X	X	X	X		X
MG						

*X indicates significantly different from zero.

*Blank indicates not significantly different from zero.

Table 6.5: Summary of Bootstrap Confidence Limits Analyses among Techniques (NMSE, FB, r, VG & MG)

Interpolation Technique	Among Techniques									
	NMSE		FB		r		VG		MG	
	Yes	No	Yes	No	Yes	No	Yes	No	Yes	No
IDW-GPI										
IDW-LPI							X			
IDW-RBF	X		X		X		X		X	
IDW-KRIG										
IDW-COKRIG									X	
GPI-IDW										
GPI-LPI										
GPI-RBF										
GPI-KRIG										
GPI-COKRIG										
LPI-IDW										
LPI-GPI										
LPI-RBF			X				X			
LPI-KRIG			X				X		X	
LPI-COKRIG	X		X				X		X	
RBF-IDW										
RBF-GPI										
RBF-LPI										

Interpolation Technique	Among Techniques									
	NMSE		FB		r		VG		MG	
	Yes	No	Yes	No	Yes	No	Yes	No	Yes	No
IDW-GPI										
IDW-LPI							X			
RBF-KRIG										
RBF-COKRIG	X									
KRIG – IDW										
KRIG – GPI										
KRIG-LPI										
KRIG - RBF										
KRIG – COKRIG										

*X indicates significantly different from zero.

*Blank indicates not significantly different from zero.

The graphical representation for the scatter plots and QQ plots for IDW, GPI, LPI, RBF, kriging and cokriging interpolation techniques are shown in Figure 6-1 and Figure 6-2, respectively. It can be seen that the scatter plots (Figure 6 -1) are of the same pattern for all the interpolation techniques. The plotted points are closer to the 1:1 identity line for the RBF technique as compared to the other interpolation techniques, which can be seen from the QQ plots (Figure 6-2).
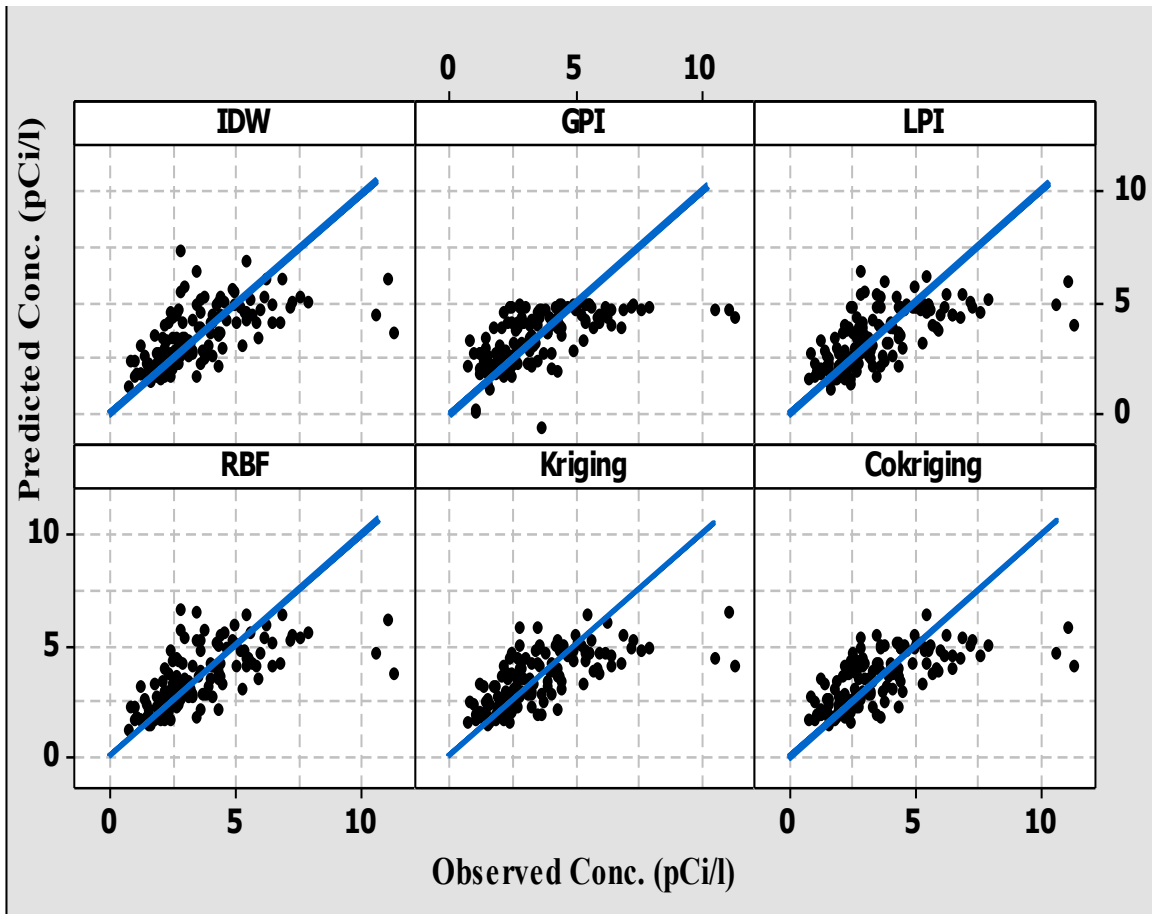
Figure 6-1: Scatter plots for the six interpolation techniques
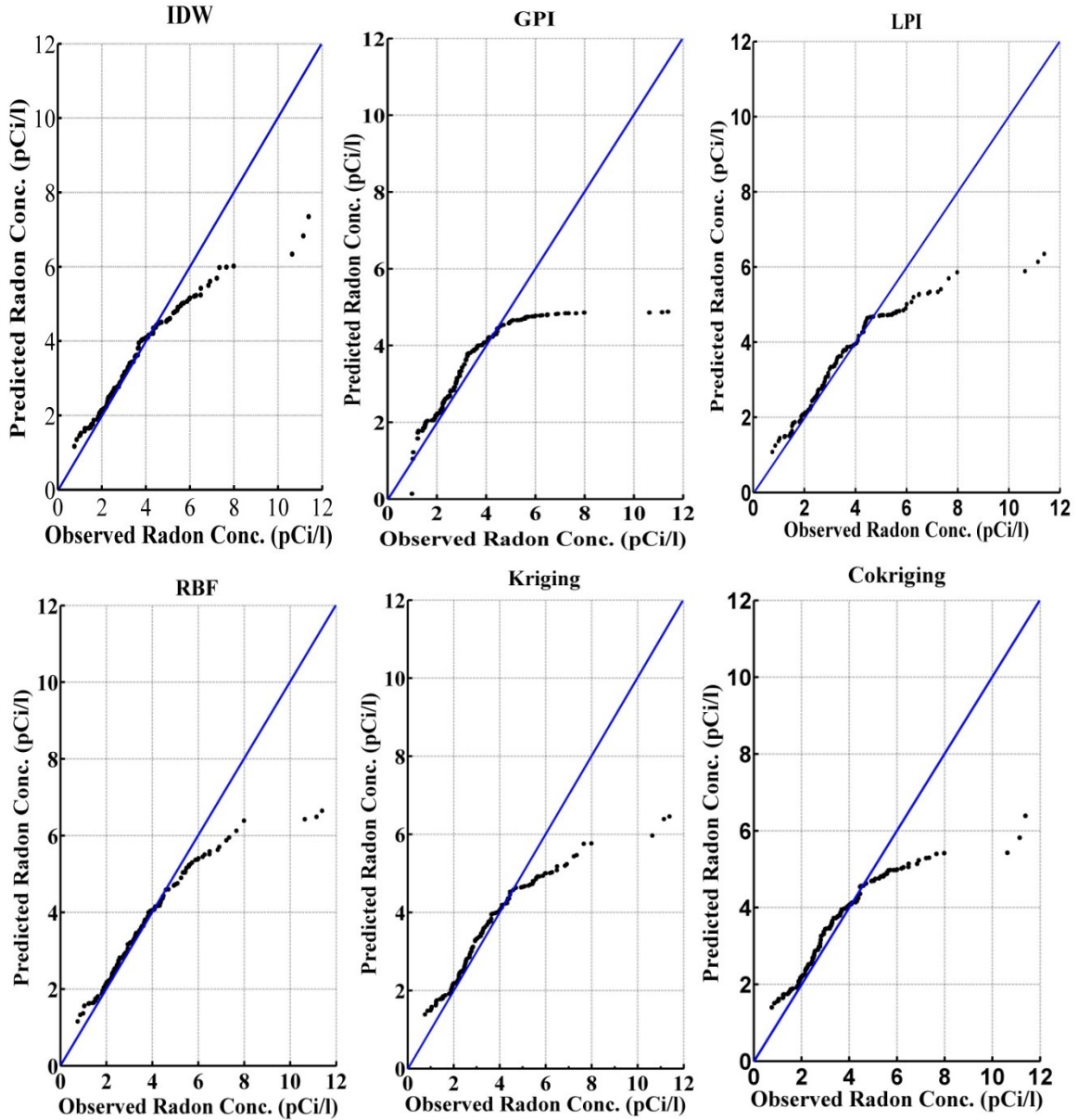
Figure 6-2: QQ plots for the six interpolation techniques

Now considering the closeness of the greater number of measures to their respective ideal values, graphical representations of the scatter plots and QQ plots, the RBF technique surpasses the other six interpolation techniques. Again, the bootstrap confidence interval estimates among the techniques (Table 6.5) indicate that the RBF technique is not significantly different from the other five interpolation techniques under all situations.

This finding clearly indicates that it can be possible that other techniques will be better than the RBF if used with another data set. Therefore, the RBF technique may not be the best technique always when applied to similar datasets from other states and countries. The RBF technique can be tentatively suggested to predict radon concentrations for the unknown zip codes in Ohio based on its performance with other statistical indicators. Figure 6-3 shows the prediction map created by using the RBF technique using the whole radon data set. Table A.1 (Appendix A) shows the geometric mean of radon concentrations that are predicted for the unmeasured 1176 zip codes using the RBF interpolation technique.
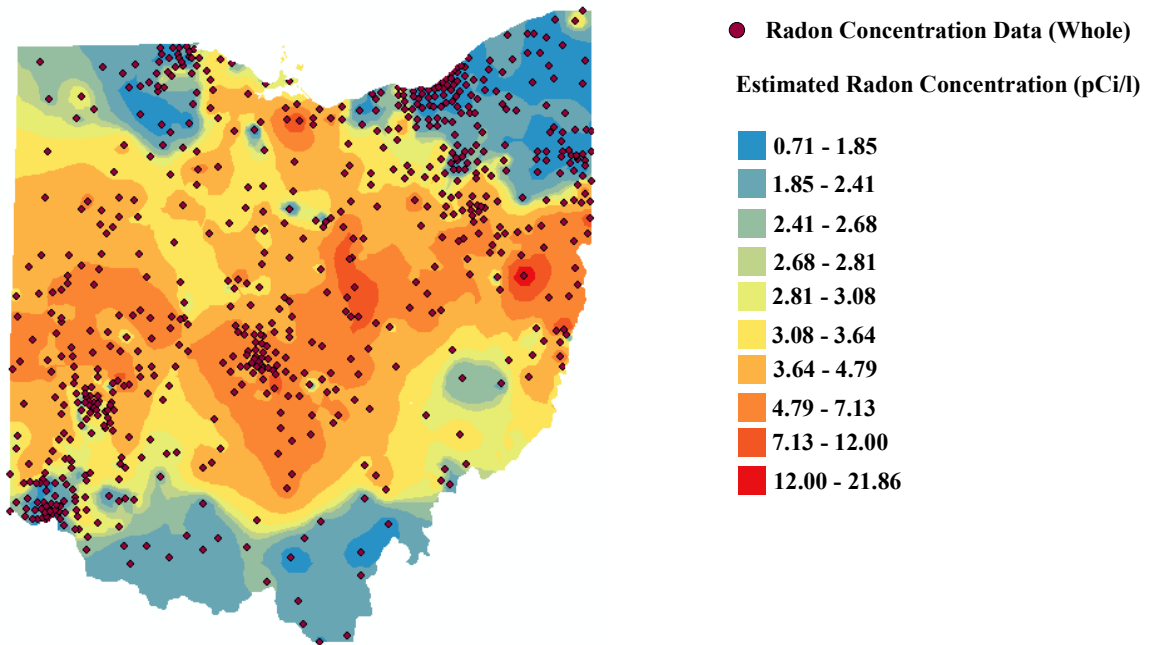
Figure 6-3: Radon Concentration Prediction Map using RBF technique for the whole Radon data set.

6.2 Analysis based on zip codes

Manthena et al. (2011) analyzed the zip codes based on the radon concentrations greater than 2.7 pCi/l, 4 pCi/l, 8 pCi/l, and 20 pCi/l. This study uses the zip codes with number of

radon concentrations greater than 20; on the other hand, Manthena et al. (2011) considered all the zip codes. The zip code based analysis results predicted by this study are shown in Table 6.6 along with the results by Manthena et al. (2011). It can be seen that the number of zip codes exceeding 4 pCi/l and 8 pCi/l increases after prediction for the present analysis as compared to Manthena et al (2011). Again, number of zip codes exceeding 8 pCi/l and 20 pCi/l decreases after predictions as compared to Manthena et al. (2011) and the cokriging technique shows no concentration at all for 8 pCi/l and 20 pCi/l after prediction. The predicted radon concentration data by RBF technique shows that 37.22% zip codes have radon concentrations more than 4 pCi/l (US EPA action limit) as compared to 18.61% zip codes based on the measured data. Similarly, 69.82% of zip codes have radon concentrations more than 2.7 pCi/l (WHO recommended limit) as compared to 36.58% of zip codes based on the measured data. Although the number of zip codes exceeding 8 pCi/l and 20 pCi/l are decreasing for this analysis, the number of zip codes exceeding 4 pCi/l and 2.7 pCi/l are increasing as compared to the study by Manthena et al (2011). It can be inferred from the analysis that more mitigation work is needed to lower the radon concentrations to the recommended limits for the State of Ohio.

Table 6.6: Zip code based analysis results

Criteria	Present Study			Manthena et al.	
	Measured	Predicted (RBF)	Predicted (Cokriging)	Measured	Predicted (Cokriging)
No. of zip codes with radon concentration greater than 2.7 pCi/l	574	1300	1361	529	1070
No. of zip codes with radon concentration greater than 4 pCi/l	292	693	693	296	594
No. of zip codes with radon concentration greater than 8 pCi/l	28	28	-	53	105
No. of zip codes with radon concentration greater than 20 pCi/l	2	2	-	2	4

6.3 Analysis based on Counties

The percentage change in radon concentrations in the counties as predicted by the RBF technique is presented in Table 6.7. The estimated radon level in a particular county may either increase or decrease due to prediction by the interpolation techniques. The positive and negative sign indicates the percentage increase and decrease in radon concentrations respectively. The percentage change in estimated radon levels in the counties varies from -64.29% to 72.71% after prediction as compared to -34.74% to 30.59% by Manthena et al. (2011).

Table 6.7: County based analysis of radon gas concentrations

County	Radon Conc. Based On Monitored Data (pCi/l)	Radon Conc. After Prediction using RBF	Percentage Change Due To RBF Prediction
ADAMS	5.83	2.08	-64.29
ALLEN	2.48	3.98	60.35
ASHLAND	3.60	4.53	25.86
ASHTABULA	1.48	1.49	0.50
ATHENS	2.66	3.19	19.65
AUGLAIZE	2.67	4.55	70.70
BELMONT	3.57	3.72	4.04
BROWN	2.39	2.31	-3.41
BUTLER	3.67	2.94	-19.70
CARROLL	3.81	5.58	46.67
CHAMPAIGN	4.05	4.83	19.09
CLARK	4.29	4.25	-0.91
CLERMONT	1.83	2.63	44.18
CLINTON	2.76	2.94	6.72
COLUMBIA	4.71	4.00	-15.10
COSHOCTON	6.96	5.61	-19.40
CRAWFORD	0.10	3.35	33.50
CUYAHOGA	1.37	1.56	14.08
DARKE	4.88	4.81	-1.33
DEFIANCE	4.40	2.84	-35.44
DELAWARE	4.29	4.29	-0.09
ERIE	3.50	4.50	28.54
FAIRFIELD	6.56	5.22	-20.38
FAYETTE	0.10	3.55	35.50
FRANKLIN	4.75	5.02	5.70
FULTON	2.04	2.08	2.16
GALLIA	2.07	1.88	-9.27
GEAUGA	2.10	1.90	-9.46
GREENE	4.60	3.69	-19.76
GUERNSEY	2.52	3.00	19.35
HAMILTON	2.05	2.03	-1.21
HANCOCK	6.91	3.35	-51.62
HARDIN	3.19	3.57	11.78
HARRISON	3.94	5.12	29.85

County	Radon Conc. Based On Monitored Data (pCi/l)	Radon Conc. After Prediction using RBF	Percentage Change Due To RBF Prediction
HENRY	2.81	2.32	-17.46
HIGHLAND	2.64	2.54	-3.61
HOCKING	5.34	4.45	-16.60
HOLMES	5.99	5.23	-12.63
HURON	4.79	4.10	-14.42
JACKSON	1.70	2.17	27.46
JEFFERSON	4.04	5.89	46.04
KNOX	4.75	6.38	34.31
LAKE	1.69	1.73	2.50
LAWRENCE	1.21	2.02	66.49
LICKING	5.30	5.99	12.95
LOGAN	3.98	4.25	6.79
LORAIN	2.66	2.72	2.22
LUCAS	2.04	2.11	3.10
MADISON	4.03	4.40	9.02
MAHONING	1.91	1.60	-16.29
MARION	4.24	3.81	-10.15
MEDINA	3.25	3.19	-1.64
MEIGS	1.49	2.02	35.65
MERCER	3.23	4.39	36.15
MIAMI	4.77	4.85	1.76
MONROE	2.37	3.16	33.06
MONTGOMEY	3.65	3.39	-7.13
MORGAN	0.10	3.30	33.00
MORROW	3.78	3.93	4.17
MUSKINGUM	4.24	4.13	-2.63
NOBLE	1.62	2.79	72.71
OTTAWA	2.12	3.30	55.92
PAULDING	2.34	3.32	41.99
PERRY	3.24	4.36	34.81
PICKAWAY	6.22	5.24	-15.88
PIKE	3.30	2.48	-24.81
PORTAGE	2.38	2.33	-2.08
PREBLE	4.21	4.35	3.26
PUTNAM	3.27	3.61	10.59

County	Radon Conc. Based On Monitored Data (pCi/l)	Radon Conc. After Prediction using RBF	Percentage Change Due To RBF Prediction
RICHLAND	4.20	3.85	-8.24
ROSS	4.55	4.26	-6.41
SANDUSKY	3.37	3.53	4.77
SCIOTO	2.10	2.14	1.83
SENECA	2.90	3.30	13.73
SHELBY	4.49	4.86	8.08
STARK	3.44	4.12	19.76
SUMMIT	2.29	2.33	1.75
TRUMBULL	1.59	1.48	-7.31
TUSCARAWAS	4.47	5.14	15.14
UNION	3.96	4.09	3.28
VAN WERT	2.41	4.01	66.14
VINTON	2.33	3.33	43.10
WARREN	2.89	2.94	1.85
WASHINGTON	2.10	2.97	41.59
WAYNE	3.66	4.01	9.78
WILLIAMS	2.56	2.61	2.26
WOOD	2.28	2.22	-2.54
WYANDOT	3.49	3.59	3.02

6.4 Limitations of the results:

The first law of geography (Waldo Tobler 1970) states that everything is related to everything else, but near things are more related than distant things. This law is the basis of spatial interpolation and the nearby points are assigned more weights as compared to the far away points. Figure 6-4 shows the distribution of radon concentrations for the observed radon concentration dataset with light green color representing number of radon concentrations greater than 20 (N>20) and blue color representing number of radon concentrations less than 20 or else no measured radon concentrations ($0 \leq N \leq 20$). It can be seen that pattern of the occurrence radon data is not similar for the State of Ohio with

some places more closely placed data, while in case of other places, concentration of radon data are sparse. The uncertainty lies in the predictions by the interpolation techniques where concentration of radon data are thinly scattered.
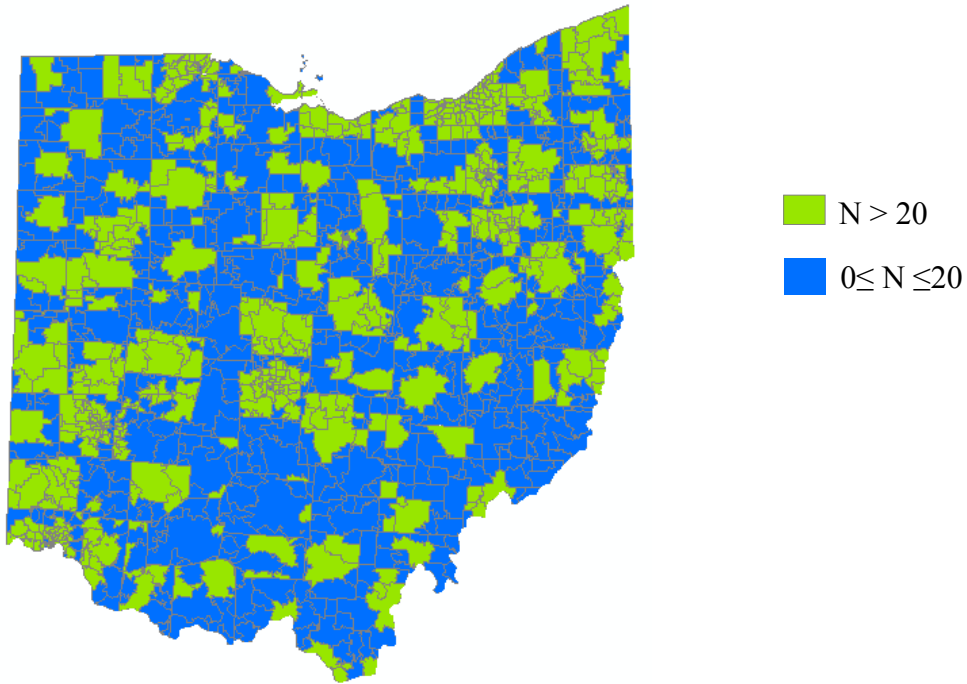
Figure 6-4: Map of Ohio for the observed radon concentrations data set

Chapter 7

Conclusions and Future Recommendations

7.1 Conclusions

In this study, six GIS based spatial interpolation techniques are evaluated by dividing the data into training and test data points. The interpolation techniques are applied on the training data points and validations are done for the test data points. The prediction maps are created for each technique and statistical parameters are used to evaluate the best interpolation technique. The radial basis function (RBF) technique performs better than the other five techniques: IDW, GPI, LPI, kriging, and cokriging after considering the required statistical indicator. However, this technique is not significantly different from the other five interpolation techniques based on the analysis of the bootstrap confidence interval estimates among the techniques given in section 6.1. Therefore, the RBF technique is provisionally suggested to predict radon concentrations in the unknown zip codes in Ohio.

A Prediction Map is created for the whole radon data set by using the RBF technique and geometric means of radon concentrations are evaluated for the unmeasured 1176 zip codes in the Ohio zip code shape file as shown in Table A.1 (Appendix A). The zip code

based analysis using the RBF technique shows that the number of zip codes exceeding 2.7 pCi/l (WHO recommended limit) , 4 pCi/l (US EPA action limit), 8 pCi/l and 20 pCi/l are 1300, 693, 28 and 2 respectively. The zip code based analysis also shows that 37.22 % of zip codes have radon concentration greater than 4 pCi/l after prediction as compared to 18.61% zip codes based on observed data, and 69.82% of zip codes have radon concentrations greater than 2.7 pCi/l after prediction as compared to 36.58% of zip codes based on the observed data. This clearly indicates that more work is ahead for radon planners in Ohio. The percentage decrease and increase in the radon levels changes from -64.29 to 72.71 % after prediction in the counties, which is found from the county-based analysis for the State of Ohio.

7.2 Future Recommendations

There are other interpolation techniques available under the ArcGIS geostatistical analysts that are not used in the present analysis. The deterministic interpolation techniques: kernel interpolation with barriers and diffusion interpolation with barriers, and geostatistical interpolation techniques: simple, universal, probability, and disjunctive, which are available under kriging/cokriging methods, could be applied in the future studies to estimate radon concentrations.

The radon concentration dataset consists of 212,653 data points for 1569 zip codes, but for the present analysis, 208,097 data points for 708 zip codes with 20 or more radon concentration measurements are used. Twenty-two zip codes are not shown in the Ohio zip code shape file, so only 686 zip codes are inputted into the Ohio zip code shape file. Therefore, additional monitoring should be done in the 861 (1569 -708) zip codes to

increase the number of readings for those zip codes in the State of Ohio and these zip

codes are within the blue color region of Figure 6-4.

References

1. "ArcGIS geostatistical Analyst: Statistical Tools for Data Exploration, Modeling, and Advanced Surface Generation". An ESRI White paper, August (2001).

2. **Ahmadi, S. H., and Sedghamiz, A.** "Application and evaluation of kriging and cokriging methods on groundwater depth mapping". *Environmental Monitoring and Assessment* 2008, vol. 138, pp. 357-368.

3. **Akkala, A., Devabhaktuni, V.K., & Kumar, A.** "Interpolation Techniques and Associated Software for Environmental Data". *Environmental Progress & Sustainable Energy* 2010, vol. 29, no. 2, pp. 134-141.

4. **Akkala, A., Devabhaktuni, V.K., & Kumar, A.** "Spatial Interpolation Techniques for Environmental Data: Theory to Practice". *Advances in Environmental Research* 2011, vol. 10, Chapter 2, pp. 33-66, Editor: Justin A. Daniels, Nova Science Publishers, Inc., ISBN: 978-1-61761-895-6.2011. (invited)

5. **Akkala, A., Devabhaktuni, V.K., & Kumar, A.** "Knowledge Based Neural Network Approaches for Modeling and Estimating Radon Concentrations". *Environmental Progress & Sustainable Energy* 2012 (in press).

6. **Akkala, A., Devabhaktuni, V.K., Kumar, A., & Bhatt, D.** "Development of an ANN interpolation scheme for estimating missing radon concentrations in Ohio". *The Open Environmental & Biological Monitoring Journal* 2011, vol. 4, pp. 21-30. (invited)

7. **Duval, J. S.** Aerial radiometric contour maps of Ohio: US Geological Survey, Geophysical Investigations Map GP-968. 1985.

8. **Ersahin, S.** "Comparing Ordinary Kriging and Cokriging to Estimate Infiltration Rate". *Soil Science Society of America Journal* 2003, vol. 67, pp. 1848-1855.

9. **Erxleben, J., Elder, K., & Davis, R.** "Comparison of spatial interpolation methods for estimating snow distribution in the Colorado Rocky Mountains". *Hydrological Processes* 2002, vol. 16, pp. 3627-3649.

10. **Harrell, J. A., & Kumar, A.** "Multivariate Stepwise Regression Analysis of Indoor Radon Data from Ohio, U.S.A.", *Journal of Official Statistics* 1989, vol. 5, pp. 409-420.

11. **Harrell, J. A., Belsito, M. E., & Kumar, A.** "Radon Hazards Associated with the Ohio Shale". *Environmental Geology and Water Sciences* 1991, vol. 18, no. 1, pp. 17-26.

12. **Heydinger, A., Kumar, A., & Harrell, J. A.** "An Indoor Radon Information System", *Environmental Software* 1991, vol. 6, no. 4, pp. 194-201.

13. **Hooshmand, A., Delghandi, M., Izadi, A., & Aali, A.** "Application of kriging and cokriging in spatial estimation of groundwater quality parameters". *African Journal of Agricultural Research* 2011, vol.6, no.14, pp. 3402-3408.

14. **Kadiyala, A., & Kumar, A.** "Guidelines for Operational Evaluation of Air Quality Models". *Saarbrücken: LAP LAMBERT Academic Publications* 2012. ISBN: 978-3-8465-3277-5.

15. **Kumar, A., & Varadarajan, C.** "Development of Ohio Radon Information System". *Proceedings of Environmental Data Analysis-Assessing Health and Environmental Impacts, Developing Policy, and Achieving Regulatory Compliance Conference, Air & Waste Management Association*, October 2005, Oak Brook, IL.

16. **Kumar, A., Heydinger, A., Harrell, J. A.** "Development of an Indoor Radon Information System for Ohio and its Application in the Study of the Geology of Radon in Ohio", Toledo, OH, November, 1990.

17. **Kumar, A., Kadiyala, A., Devabhaktuni, V. K., Akkala, A., & Manthena, D.V.** "Examination of Ohio indoor radon data". *American Association of Radon Scientists and Technologists (AARST) Proceedings of 22nd International Radon Symposium*, Columbus, OH, October 2010.

18. **Kumar, A., Maroju, S., & Bhat, A.** "Application of ArcGIS Geostatistical Analyst for Interpolating Environmental Data from Observations". *Environmental Progress* 2007, vol. 26, no.3, pp. 220-225.

19. **Kumar, A., Varadarajan, C., & Kadiyala, A.** "Management of Radon Data in the State of Ohio, U.S.A". *The Open Environmental & Biological Monitoring Journal* 2011, vol.4, pp. 57-71 (invited).

20. **Li, X., Cheng, G., & Lu, L.** "Spatial Analysis of Air Temperature in the Qinghai-Tibet Plateau". *Arctic, Antarctic, and Alpine Research* 2005, vol. 37, no.2, pp. 246-252.

21. **Liu, X., Wu, J., & Xu, J.** "Characterizing the risk assessment of heavy metals and sampling uncertainty analysis in paddy field by geostatistics and GIS". *Environmental Pollution* 2006, vol.141, pp. 257-264.

22. **Luo, W., Taylor, M. C., & Parker, S.R.** "A comparison of spatial interpolation methods to estimate continuous wind speed surfaces using irregularly distributed data from England and Wales". *International Journal of Climatology* 2008, vol. 28, pp. 947-959.

23. **Manthena, D. V, Kumar, A., & Kadiyala, A.** "Development of an Approach to Predict Radon Gas Concentrations for Unmeasured Zip Codes Using GIS Based Interpolation Techniques". *Advances in Mathematics Research* 2011, vol. 15, Chapter 2, ISBN: 978-1-61324-179-0, Editor: Albert R. Baswell, *Nova Science Publishers, Inc. (invited)*

24. **Manthena, D.V., Kadiyala, A., & Kumar, A.** "Interpolation of Radon Concentrations Using GIS Based Kriging and Cokriging Techniques". *Environmental Progress & Sustainable Energy* 2009, vol.28, no.4, pp. 487- 492.

25. **Maroju, Suman,** "Evaluation of Five GIS Based Interpolation Techniques for Estimating the Radon Concentration for Unmeasured Zip Codes in the State of Ohio". Master's Thesis, The University of Toledo, Toledo, August 2007.

26. **Moral, F. J.** "Comparison of different geostatistical approaches to map climate variables: application to precipitation". *International Journal of Climatology* 2010, vol.30, pp. 620-631.

27. **Nas, B., & Berktay, A.** "Groundwater quality mapping in urban groundwater using GIS". *Environmental Monitoring and Assessment* 2010, vol.160, pp. 215-227.

28. National Cancer Institute Fact sheet (http://www.cancer.gov/cancertopics/factsheet/Risk/radon)

29. **Salih M, I., Pettersson, H.B.L., Sivertun, A., & Lund, E.** "Spatial correlation between radon (222Rn) in groundwater and bedrock uranium (238U): GIS and geostatistical analyses". *Journal of Spatial Hydrology* 2002, vol.2, no. 2.

30. **Sarmadian, F., Keshavarzi, A., & Malekian, A.** "Continuous mapping of topsoil calcium carbonate using geostatistical techniques in a semi-arid region". *Australian Journal of Crop Science* 2010, vol. 4, pp. 603-608.

31. **Sud**, **A.** "Update and Analysis of a Residential Radon Database for the State of Ohio". Master's Thesis, The University of Toledo, Toledo, 1998.

32. United States Environmental Protection Agency (USEPA): A Citizen's Guide to Radon (http://www.epa.gov/radon/pubs/citguide.html)

33. **Ustrnul, Z., & Czekierda, D.** "Application of GIS for the development of climatological air temperature maps: an example from Poland". *Meteorological Applications* 2005, vol.12, pp. 43-50.

34. WHO (World Health Organization) Handbook on Indoor Radon: A public health Perspective, 2009.

35. **Yang, J.S., Wang, Y.Q., & August, P.V.** "Estimation of Land Surface Temperature Using Spatial Interpolation and Satellite-Derived Surface Emissivity". *Journal of Environmental Informatics* 2004, vol.4, no. 1, pp. 37-44.

Appendix A

Radon Concentrations in the unmeasured zip codes

Table A.1: Prediction of Radon Concentration using Radial Basis Function

ZIP CODE	COUNTY	RADON CONC.	ZIP CODE	COUNTY	RADON CONC.
45144	ADAMS	2.24	43728	ATHENS	3.23
45684	ADAMS	2.14	45723	ATHENS	2.74
45650	ADAMS	2.17	45724	ATHENS	3.00
45616	ADAMS	2.16	45735	ATHENS	2.85
45679	ADAMS	2.32	45766	ATHENS	3.26
45657	ADAMS	2.11	45772	ATHENS	2.56
45168	ADAMS	2.12	45776	ATHENS	2.61
45693	ADAMS	2.22	45778	ATHENS	3.12
45167	ADAMS	2.10	43331	AUGLAIZE	4.92
45646	ADAMS	1.96	43333	AUGLAIZE	4.85
45671	ADAMS	1.80	45896	AUGLAIZE	4.46
45812	ALLEN	3.83	45805	AUGLAIZE	3.96
45887	ALLEN	4.27	45806	AUGLAIZE	4.26
45896	ALLEN	4.03	45850	AUGLAIZE	4.25
45877	ALLEN	3.91	45887	AUGLAIZE	4.07
45850	ALLEN	3.73	43901	BELMONT	5.15
45868	ALLEN	3.75	43971	BELMONT	5.82
44866	ASHLAND	3.54	43719	BELMONT	3.22
44880	ASHLAND	3.68	43747	BELMONT	3.27
44628	ASHLAND	4.78	43902	BELMONT	4.00
44638	ASHLAND	4.39	43933	BELMONT	3.93

ZIP CODE	COUNTY	RADON CONC.	ZIP CODE	COUNTY	RADON CONC.
44837	ASHLAND	3.86	43942	BELMONT	3.64
44878	ASHLAND	3.86	43973	BELMONT	3.76
44676	ASHLAND	4.34	43977	BELMONT	3.92
44840	ASHLAND	4.50	43983	BELMONT	3.95
44082	ASHTABULA	2.12	43773	BELMONT	2.83
44064	ASHTABULA	1.52	43788	BELMONT	2.16
44093	ASHTABULA	1.49	45118	BROWN	2.67
44099	ASHTABULA	1.36	45133	BROWN	2.52
44450	ASHTABULA	1.51	45148	BROWN	2.81
44046	ASHTABULA	1.38	45154	BROWN	2.60
44032	ASHTABULA	1.33	45697	BROWN	2.27
43766	ATHENS	3.74	45101	BROWN	2.12
43730	ATHENS	3.69	45120	BROWN	2.10
45651	ATHENS	3.37	45130	BROWN	2.03
45761	ATHENS	3.87	45144	BROWN	2.13
45711	ATHENS	3.42	45167	BROWN	2.06
45732	ATHENS	3.64	45168	BROWN	2.09
45064	BUTLER	3.76	44455	COLUMBIANA	6.20
45003	BUTLER	3.06	43945	COLUMBIANA	5.99
43986	CARROLL	13.65	44454	COLUMBIANA	5.22
43903	CARROLL	10.90	44423	COLUMBIANA	4.96
44695	CARROLL	7.80	43930	COLUMBIANA	4.51
44651	CARROLL	6.18	44625	COLUMBIANA	4.11
44427	CARROLL	5.62	44657	COLUMBIANA	3.80
44675	CARROLL	4.43	43932	COLUMBIANA	3.69
43319	CHAMPAIGN	5.09	44634	COLUMBIANA	2.94
43343	CHAMPAIGN	4.85	44490	COLUMBIANA	2.84
43084	CHAMPAIGN	4.80	44609	COLUMBIANA	2.51
43029	CHAMPAIGN	4.67	43014	COSHOCTON	7.67
45317	CHAMPAIGN	4.45	43843	COSHOCTON	7.61
45344	CLARK	6.14	43006	COSHOCTON	6.80
43072	CLARK	5.81	43840	COSHOCTON	6.57
43078	CLARK	4.50	43844	COSHOCTON	6.43
43044	CLARK	4.05	43804	COSHOCTON	6.28
45502	CLARK	4.04	44637	COSHOCTON	5.88
43153	CLARK	3.03	43749	COSHOCTON	4.82

ZIP CODE	COUNTY	RADON CONC.	ZIP CODE	COUNTY	RADON CONC.
45111	CLERMONT	3.17	43762	COSHOCTON	4.77
45160	CLERMONT	3.09	43802	COSHOCTON	4.75
45154	CLERMONT	2.93	43811	COSHOCTON	4.65
45176	CLERMONT	2.89	44865	CRAWFORD	3.84
45118	CLERMONT	2.71	43335	CRAWFORD	3.68
45107	CLERMONT	2.38	44807	CRAWFORD	3.56
45106	CLERMONT	2.33	44854	CRAWFORD	3.48
45153	CLERMONT	2.32	44887	CRAWFORD	3.29
45120	CLERMONT	2.21	44127	CUYAHOGA	1.41
45130	CLERMONT	2.17	45845	DARKE	5.58
45122	CLERMONT	2.07	45332	DARKE	5.29
45107	CLINTON	3.06	45388	DARKE	5.07
45148	CLINTON	2.87	45321	DARKE	5.05
45142	CLINTON	2.83	45382	DARKE	4.88
45146	CLINTON	2.81	45303	DARKE	4.87
45135	CLINTON	2.79	45362	DARKE	4.58
45162	CLINTON	2.46	45348	DARKE	4.36
45122	CLINTON	2.34	43548	DEFIANCE	3.21
44427	COLUMBIANA	6.38	43526	DEFIANCE	2.95
43557	DEFIANCE	2.93	43222	FRANKLIN	4.25
43536	DEFIANCE	2.90	43103	FRANKLIN	3.18
43556	DEFIANCE	2.88	43502	FULTON	2.52
43527	DEFIANCE	2.79	43570	FULTON	2.51
43517	DEFIANCE	2.77	43521	FULTON	2.41
43549	DEFIANCE	2.69	43545	FULTON	2.22
43040	DELAWARE	3.49	43533	FULTON	2.10
44826	ERIE	4.99	43540	FULTON	1.99
43464	ERIE	3.78	43504	FULTON	1.94
43438	ERIE	3.15	45623	GALLIA	2.04
43154	FAIRFIELD	7.17	45659	GALLIA	2.01
43102	FAIRFIELD	7.05	45678	GALLIA	2.01
43150	FAIRFIELD	4.81	45688	GALLIA	1.99
43155	FAIRFIELD	4.77	45695	GALLIA	1.97
43160	FAYETTE	3.56	45658	GALLIA	1.96
43106	FAYETTE	3.52	45656	GALLIA	1.92
43145	FAYETTE	3.37	45685	GALLIA	1.90

ZIP CODE	COUNTY	RADON CONC.	ZIP CODE	COUNTY	RADON CONC.
45135	FAYETTE	3.27	45686	GALLIA	1.87
43128	FAYETTE	3.20	45741	GALLIA	1.82
45335	FAYETTE	3.16	45620	GALLIA	1.73
45169	FAYETTE	3.04	45760	GALLIA	1.72
43110	FRANKLIN	7.13	44202	GEAUGA	2.09
43235	FRANKLIN	6.79	44040	GEAUGA	2.07
43147	FRANKLIN	5.99	44023	GEAUGA	2.05
43064	FRANKLIN	5.86	44057	GEAUGA	2.04
43002	FRANKLIN	5.82	44022	GEAUGA	2.01
43140	FRANKLIN	5.70	44491	GEAUGA	1.99
43016	FRANKLIN	5.61	44086	GEAUGA	1.81
43017	FRANKLIN	5.51	44064	GEAUGA	1.75
43062	FRANKLIN	5.41	44062	GEAUGA	1.73
43065	FRANKLIN	5.39	44139	GEAUGA	1.65
43054	FRANKLIN	5.10	44046	GEAUGA	1.55
43081	FRANKLIN	5.03	44099	GEAUGA	1.38
43068	FRANKLIN	4.98	45323	GREENE	4.83
43240	FRANKLIN	4.69	45387	GREENE	4.47
43082	FRANKLIN	4.68	45068	GREENE	4.42
43031	FRANKLIN	4.63	45385	GREENE	4.27
43137	FRANKLIN	4.46	45502	GREENE	4.22
45324	GREENE	4.05	45069	HAMILTON	2.38
45341	GREENE	3.79	45242	HAMILTON	2.25
45314	GREENE	3.56	45241	HAMILTON	2.24
45424	GREENE	3.54	45225	HAMILTON	2.11
45177	GREENE	3.49	45246	HAMILTON	1.90
45368	GREENE	3.39	45014	HAMILTON	1.89
45335	GREENE	3.25	45251	HAMILTON	1.88
43153	GREENE	3.12	45228	HAMILTON	1.86
43160	GREENE	3.06	45231	HAMILTON	1.71
45169	GREENE	2.98	45221	HAMILTON	1.65
44699	GUERNSEY	4.26	45204	HAMILTON	1.24
43973	GUERNSEY	3.92	45210	HAMILTON	1.23
43832	GUERNSEY	3.74	45240	HAMILTON	1.13
43983	GUERNSEY	3.67	43359	HANCOCK	3.87
43749	GUERNSEY	3.60	45867	HANCOCK	3.76

ZIP CODE	COUNTY	RADON CONC.	ZIP CODE	COUNTY	RADON CONC.
43837	GUERNSEY	3.58	45814	HANCOCK	3.69
43762	GUERNSEY	3.43	45817	HANCOCK	3.63
43755	GUERNSEY	3.09	45841	HANCOCK	3.61
43713	GUERNSEY	3.07	45868	HANCOCK	3.61
43773	GUERNSEY	3.02	45881	HANCOCK	3.49
43778	GUERNSEY	2.84	44804	HANCOCK	3.48
43732	GUERNSEY	2.69	45890	HANCOCK	3.23
43723	GUERNSEY	2.47	43516	HANCOCK	2.69
43780	GUERNSEY	2.34	45889	HANCOCK	2.62
43772	GUERNSEY	2.16	43310	HARDIN	4.41
45174	HAMILTON	3.76	45850	HARDIN	4.21
45150	HAMILTON	3.71	43346	HARDIN	4.08
45013	HAMILTON	3.40	45812	HARDIN	3.76
45111	HAMILTON	3.04	45836	HARDIN	3.69
45030	HAMILTON	3.02	45814	HARDIN	3.66
45053	HAMILTON	2.90	45843	HARDIN	3.64
45140	HAMILTON	2.84	43347	HARDIN	3.59
45243	HAMILTON	2.73	45817	HARDIN	3.59
45244	HAMILTON	2.63	45841	HARDIN	3.58
45040	HAMILTON	2.62	45810	HARDIN	3.57
45001	HAMILTON	2.58	45835	HARDIN	3.57
45255	HAMILTON	2.46	43332	HARDIN	3.44
45252	HAMILTON	2.44	43340	HARDIN	3.40
43345	HARDIN	3.29	45679	HIGHLAND	2.40
43986	HARRISON	9.24	45697	HIGHLAND	2.37
43988	HARRISON	8.96	45171	HIGHLAND	2.36
43908	HARRISON	8.02	45660	HIGHLAND	2.16
43976	HARRISON	6.81	45646	HIGHLAND	2.13
44695	HARRISON	6.63	43102	HOCKING	6.06
43907	HARRISON	5.44	43130	HOCKING	5.92
43901	HARRISON	5.38	43149	HOCKING	5.28
43977	HARRISON	4.54	43135	HOCKING	5.26
44699	HARRISON	4.43	43152	HOCKING	4.67
43917	HARRISON	4.35	43155	HOCKING	4.66
43973	HARRISON	4.28	45622	HOCKING	4.26
43983	HARRISON	4.23	43748	HOCKING	4.25

ZIP CODE	COUNTY	RADON CONC.	ZIP CODE	COUNTY	RADON CONC.
44621	HARRISON	3.36	43138	HOCKING	4.23
43950	HARRISON	3.27	43107	HOCKING	4.10
43548	HENRY	3.23	43766	HOCKING	3.87
43524	HENRY	3.19	45654	HOCKING	3.79
43557	HENRY	3.05	45732	HOCKING	3.73
43527	HENRY	2.87	45764	HOCKING	3.67
43502	HENRY	2.83	45651	HOCKING	3.46
43516	HENRY	2.81	43014	HOLMES	6.86
43567	HENRY	2.52	43843	HOLMES	6.64
43535	HENRY	2.45	43006	HOLMES	6.63
43545	HENRY	2.40	43824	HOLMES	6.21
43511	HENRY	1.87	43844	HOLMES	6.02
43515	HENRY	1.80	44628	HOLMES	5.69
43534	HENRY	1.68	44689	HOLMES	5.56
43522	HENRY	1.62	44637	HOLMES	5.51
43532	HENRY	1.32	43804	HOLMES	5.47
45123	HIGHLAND	3.21	44608	HOLMES	5.37
45135	HIGHLAND	3.01	44624	HOLMES	4.91
45169	HIGHLAND	2.94	44611	HOLMES	4.81
45146	HIGHLAND	2.75	44633	HOLMES	4.72
45142	HIGHLAND	2.72	44676	HOLMES	4.65
45118	HIGHLAND	2.70	44627	HOLMES	4.57
45159	HIGHLAND	2.68	44638	HOLMES	4.55
45154	HIGHLAND	2.63	43812	HOLMES	4.49
45133	HIGHLAND	2.49	44654	HOLMES	4.45
44842	HOLMES	4.38	43932	JEFFERSON	5.85
44811	HURON	6.11	43901	JEFFERSON	5.62
44847	HURON	5.77	43944	JEFFERSON	5.29
44857	HURON	4.78	43913	JEFFERSON	5.18
44855	HURON	4.35	43910	JEFFERSON	5.14
44826	HURON	4.17	43907	JEFFERSON	5.03
44859	HURON	4.04	43938	JEFFERSON	4.93
44865	HURON	3.99	43930	JEFFERSON	4.26
44851	HURON	3.87	43968	JEFFERSON	4.05
44875	HURON	3.86	43822	KNOX	9.18
44837	HURON	3.86	44822	KNOX	9.08

ZIP CODE	COUNTY	RADON CONC.	ZIP CODE	COUNTY	RADON CONC.
44854	HURON	3.80	43843	KNOX	7.99
44807	HURON	3.77	43014	KNOX	7.59
44878	HURON	3.74	43037	KNOX	7.31
44846	HURON	3.56	43006	KNOX	6.63
44889	HURON	3.49	44628	KNOX	5.32
45672	JACKSON	3.55	43074	KNOX	5.27
45601	JACKSON	3.38	43011	KNOX	5.19
45651	JACKSON	3.06	43013	KNOX	5.15
45634	JACKSON	2.44	44813	KNOX	4.81
45613	JACKSON	2.29	44842	KNOX	4.00
45695	JACKSON	2.14	44086	LAKE	2.27
45686	JACKSON	2.02	44077	LAKE	2.20
45685	JACKSON	1.98	44024	LAKE	2.17
45658	JACKSON	1.91	44057	LAKE	2.15
45656	JACKSON	1.87	44143	LAKE	1.94
45682	JACKSON	1.62	44040	LAKE	1.91
43935	JEFFERSON	10.15	44060	LAKE	1.77
43986	JEFFERSON	9.65	44094	LAKE	1.55
43903	JEFFERSON	8.65	44026	LAKE	1.54
44615	JEFFERSON	7.94	44132	LAKE	0.91
43908	JEFFERSON	7.51	45629	LAWRENCE	2.23
43943	JEFFERSON	6.65	45659	LAWRENCE	2.10
43917	JEFFERSON	6.55	45682	LAWRENCE	2.03
43963	JEFFERSON	6.45	45623	LAWRENCE	2.02
43976	JEFFERSON	6.32	45696	LAWRENCE	2.01
43971	JEFFERSON	6.16	45678	LAWRENCE	2.01
43945	JEFFERSON	5.98	45688	LAWRENCE	2.01
45658	LAWRENCE	1.99	43347	LOGAN	3.87
45645	LAWRENCE	1.99	43345	LOGAN	3.48
45656	LAWRENCE	1.95	43340	LOGAN	3.45
45675	LAWRENCE	1.94	43319	LOGAN	3.19
45619	LAWRENCE	1.92	43040	LOGAN	3.07
43822	LICKING	8.18	44859	LORAIN	4.31
43843	LICKING	7.82	44851	LORAIN	4.01
43844	LICKING	7.38	44028	LORAIN	3.80
43055	LICKING	7.07	44880	LORAIN	3.60

ZIP CODE	COUNTY	RADON CONC.	ZIP CODE	COUNTY	RADON CONC.
43071	LICKING	7.00	44090	LORAIN	3.34
43080	LICKING	6.46	44275	LORAIN	3.32
43076	LICKING	6.42	44889	LORAIN	2.77
43050	LICKING	5.99	44012	LORAIN	2.70
43004	LICKING	5.91	44011	LORAIN	2.65
43025	LICKING	5.84	44089	LORAIN	2.61
43062	LICKING	5.57	44039	LORAIN	2.52
43054	LICKING	5.54	44053	LORAIN	1.85
43011	LICKING	5.47	43618	LUCAS	3.27
43031	LICKING	5.36	43445	LUCAS	3.02
43760	LICKING	5.17	43610	LUCAS	2.73
43068	LICKING	5.17	43620	LUCAS	2.16
43147	LICKING	5.16	43504	LUCAS	1.91
43013	LICKING	5.07	43558	LUCAS	1.88
43046	LICKING	4.59	43522	LUCAS	1.82
43105	LICKING	4.48	43624	LUCAS	1.35
43357	LOGAN	6.16	43602	LUCAS	1.06
43318	LOGAN	5.31	43026	MADISON	6.15
43343	LOGAN	5.23	43002	MADISON	5.83
45340	LOGAN	5.07	43162	MADISON	5.60
45365	LOGAN	5.02	43119	MADISON	5.45
43311	LOGAN	4.98	43064	MADISON	5.44
43333	LOGAN	4.92	43123	MADISON	5.37
43348	LOGAN	4.81	43044	MADISON	4.90
43331	LOGAN	4.78	43029	MADISON	4.76
45895	LOGAN	4.71	43045	MADISON	4.75
43360	LOGAN	4.48	43140	MADISON	4.45
43310	LOGAN	4.36	43143	MADISON	4.25
43326	LOGAN	3.94	45369	MADISON	3.98
43106	MADISON	3.69	44235	MEDINA	3.48
45368	MADISON	3.67	44028	MEDINA	3.45
43153	MADISON	3.38	44276	MEDINA	3.45
43128	MADISON	3.31	44275	MEDINA	3.39
45335	MADISON	3.12	44090	MEDINA	3.37
45314	MADISON	3.00	44214	MEDINA	3.35
44443	MAHONING	5.25	44044	MEDINA	3.06

ZIP CODE	COUNTY	RADON CONC.	ZIP CODE	COUNTY	RADON CONC.
44454	MAHONING	4.80	44253	MEDINA	3.03
44408	MAHONING	3.05	44256	MEDINA	2.94
44437	MAHONING	2.72	44212	MEDINA	2.60
44436	MAHONING	2.36	44233	MEDINA	2.51
44460	MAHONING	2.30	45735	MEIGS	2.51
44601	MAHONING	2.16	45772	MEIGS	2.45
44672	MAHONING	2.08	45723	MEIGS	2.38
44609	MAHONING	2.08	45701	MEIGS	2.35
44429	MAHONING	2.05	45695	MEIGS	2.33
44449	MAHONING	1.97	45776	MEIGS	2.22
44411	MAHONING	1.84	45743	MEIGS	2.21
44506	MAHONING	1.56	45770	MEIGS	2.20
44507	MAHONING	0.11	45710	MEIGS	2.05
44504	MAHONING	0.10	45771	MEIGS	2.02
44510	MAHONING	0.10	45741	MEIGS	1.89
43342	MARION	5.32	45686	MEIGS	1.87
43356	MARION	4.00	45620	MEIGS	1.76
43302	MARION	3.97	45775	MEIGS	1.76
44833	MARION	3.85	45614	MEIGS	1.75
43341	MARION	3.70	45760	MEIGS	1.71
43337	MARION	3.69	45845	MERCER	5.85
43335	MARION	3.68	45865	MERCER	5.20
43003	MARION	3.67	45860	MERCER	4.93
43344	MARION	3.66	45869	MERCER	4.64
43314	MARION	3.66	45883	MERCER	4.40
45843	MARION	3.64	45874	MERCER	4.23
44820	MARION	3.57	45894	MERCER	4.20
43332	MARION	3.52	45887	MERCER	4.16
44287	MEDINA	3.54	45862	MERCER	4.15
44280	MEDINA	3.53	45882	MERCER	4.13
44880	MEDINA	3.51	45898	MERCER	4.01
45846	MERCER	4.01	45305	MONTGOMERY	3.71
45885	MERCER	3.95	45344	MONTGOMERY	3.41
45380	MIAMI	5.99	45424	MONTGOMERY	3.33
45344	MIAMI	5.78	45005	MONTGOMERY	3.22
45318	MIAMI	5.35	45432	MONTGOMERY	3.21

ZIP CODE	COUNTY	RADON CONC.	ZIP CODE	COUNTY	RADON CONC.
45363	MIAMI	5.18	45459	MONTGOMERY	3.17
45308	MIAMI	5.13	45430	MONTGOMERY	3.08
45333	MIAMI	5.03	45440	MONTGOMERY	3.07
45337	MIAMI	4.92	45433	MONTGOMERY	2.88
45304	MIAMI	4.57	45420	MONTGOMERY	2.80
45365	MIAMI	4.54	45458	MONTGOMERY	2.78
43072	MIAMI	4.00	45068	MONTGOMERY	2.66
45424	MIAMI	3.93	45370	MONTGOMERY	2.60
45317	MIAMI	3.85	45324	MONTGOMERY	2.54
43716	MONROE	4.00	45341	MONTGOMERY	2.42
43942	MONROE	3.71	43777	MORGAN	3.90
43915	MONROE	3.69	43731	MORGAN	3.84
43747	MONROE	3.60	43730	MORGAN	3.64
43946	MONROE	3.51	43758	MORGAN	3.51
43793	MONROE	3.25	45732	MORGAN	3.50
45767	MONROE	3.11	45711	MORGAN	3.38
45734	MONROE	3.09	43728	MORGAN	3.31
45789	MONROE	3.07	43787	MORGAN	3.21
45745	MONROE	3.05	45715	MORGAN	3.13
43724	MONROE	2.86	45724	MORGAN	3.08
43754	MONROE	2.81	43724	MORGAN	3.05
43788	MONROE	2.56	45786	MORGAN	3.03
43773	MONROE	2.36	43732	MORGAN	2.92
45304	MONTGOMEY	4.84	43011	MORROW	4.77
45327	MONTGOMEY	4.60	43050	MORROW	4.63
45337	MONTGOMEY	4.48	44813	MORROW	4.27
45338	MONTGOMEY	4.47	43334	MORROW	4.19
45042	MONTGOMEY	4.25	44833	MORROW	4.02
45311	MONTGOMEY	4.21	44903	MORROW	3.87
45383	MONTGOMEY	4.08	43019	MORROW	3.86
45371	MONTGOMEY	4.05	43074	MORROW	3.80
45431	MONTGOMEY	4.00	43321	MORROW	3.75
45377	MONTGOMEY	3.92	43335	MORROW	3.70
43315	MORROW	3.69	43773	NOBLE	2.50
43320	MORROW	3.65	43780	NOBLE	2.36
43314	MORROW	3.63	43772	NOBLE	2.13

ZIP CODE	COUNTY	RADON CONC.	ZIP CODE	COUNTY	RADON CONC.
43003	MORROW	3.47	43442	OTTAWA	3.77
43076	MUSKINGUM	5.50	43416	OTTAWA	3.67
43739	MUSKINGUM	5.27	43412	OTTAWA	3.38
43056	MUSKINGUM	5.25	43445	OTTAWA	3.30
43746	MUSKINGUM	4.98	43449	OTTAWA	3.21
43055	MUSKINGUM	4.77	43456	OTTAWA	3.21
43822	MUSKINGUM	4.73	43436	OTTAWA	3.20
43760	MUSKINGUM	4.62	43432	OTTAWA	3.17
43749	MUSKINGUM	4.60	45827	PAULDING	3.87
43811	MUSKINGUM	4.49	45849	PAULDING	3.70
43830	MUSKINGUM	4.36	45886	PAULDING	3.67
43802	MUSKINGUM	4.25	45851	PAULDING	3.55
43777	MUSKINGUM	4.04	45880	PAULDING	3.46
43821	MUSKINGUM	4.04	45831	PAULDING	3.43
43812	MUSKINGUM	4.03	45873	PAULDING	3.41
43731	MUSKINGUM	3.83	45813	PAULDING	3.18
43767	MUSKINGUM	3.74	43526	PAULDING	3.10
43762	MUSKINGUM	3.69	43512	PAULDING	3.10
43734	MUSKINGUM	3.64	45821	PAULDING	3.02
43771	MUSKINGUM	3.62	43536	PAULDING	3.00
43756	MUSKINGUM	3.54	43556	PAULDING	2.98
43720	MUSKINGUM	3.34	43025	PERRY	5.86
43727	MUSKINGUM	3.33	43107	PERRY	5.16
43732	MUSKINGUM	2.95	43739	PERRY	4.98
45715	NOBLE	3.25	43076	PERRY	4.83
45746	NOBLE	3.15	43150	PERRY	4.75
45727	NOBLE	3.09	43760	PERRY	4.67
45745	NOBLE	3.01	43046	PERRY	4.62
43756	NOBLE	2.95	43148	PERRY	4.58
43754	NOBLE	2.89	43748	PERRY	4.54
43724	NOBLE	2.82	43138	PERRY	4.31
43732	NOBLE	2.68	43777	PERRY	4.06
43778	NOBLE	2.62	43782	PERRY	4.02
43788	NOBLE	2.58	43731	PERRY	3.99
43779	NOBLE	2.52	43766	PERRY	3.98
43758	PERRY	3.73	44491	PORTAGE	1.95

ZIP CODE	COUNTY	RADON CONC.	ZIP CODE	COUNTY	RADON CONC.
43730	PERRY	3.70	44288	PORTAGE	1.92
45732	PERRY	3.64	44444	PORTAGE	1.82
43154	PICKAWAY	7.81	45332	PREBLE	5.11
43110	PICKAWAY	6.89	45309	PREBLE	5.07
43102	PICKAWAY	6.17	45346	PREBLE	5.00
43103	PICKAWAY	6.14	45304	PREBLE	4.88
43135	PICKAWAY	5.75	45382	PREBLE	4.86
43113	PICKAWAY	5.74	45321	PREBLE	4.85
43140	PICKAWAY	5.49	45347	PREBLE	4.84
43125	PICKAWAY	5.41	45338	PREBLE	4.67
43146	PICKAWAY	5.29	45325	PREBLE	4.57
45601	PICKAWAY	5.18	45327	PREBLE	4.53
43137	PICKAWAY	4.73	45345	PREBLE	4.48
43164	PICKAWAY	4.72	45381	PREBLE	4.32
43143	PICKAWAY	4.56	45064	PREBLE	3.85
43115	PICKAWAY	4.30	45042	PREBLE	3.84
43160	PICKAWAY	3.91	45311	PREBLE	3.72
43145	PICKAWAY	3.71	45056	PREBLE	3.17
45601	PIKE	3.54	45003	PREBLE	3.15
45612	PIKE	2.65	45844	PUTNAM	4.52
45661	PIKE	2.61	45807	PUTNAM	4.42
45613	PIKE	2.53	45830	PUTNAM	4.28
45660	PIKE	2.28	45827	PUTNAM	3.92
45657	PIKE	2.24	45877	PUTNAM	3.75
45133	PIKE	2.16	43524	PUTNAM	3.70
45646	PIKE	2.03	45868	PUTNAM	3.66
45671	PIKE	1.96	45856	PUTNAM	3.58
44243	PORTAGE	2.38	45840	PUTNAM	3.47
44234	PORTAGE	2.25	45831	PUTNAM	3.45
44023	PORTAGE	2.23	43548	PUTNAM	3.27
44255	PORTAGE	2.18	43512	PUTNAM	3.22
44087	PORTAGE	2.15	45858	PUTNAM	3.21
44411	PORTAGE	2.07	43516	PUTNAM	3.13
44412	PORTAGE	2.05	44822	RICHLAND	8.94
44231	PORTAGE	2.03	44864	RICHLAND	7.40
44202	PORTAGE	2.00	44843	RICHLAND	6.38

ZIP CODE	COUNTY	RADON CONC.	ZIP CODE	COUNTY	RADON CONC.
44449	PORTAGE	1.97	44813	RICHLAND	5.28
44904	RICHLAND	4.30	44830	SANDUSKY	3.05
43019	RICHLAND	4.17	43406	SANDUSKY	2.96
44887	RICHLAND	4.01	43457	SANDUSKY	2.90
44859	RICHLAND	3.84	45661	SCIOTO	2.48
44865	RICHLAND	3.77	45648	SCIOTO	2.45
44805	RICHLAND	3.74	45652	SCIOTO	2.42
44837	RICHLAND	3.71	45663	SCIOTO	2.36
44878	RICHLAND	3.64	45629	SCIOTO	2.26
44833	RICHLAND	3.62	45657	SCIOTO	2.24
44875	RICHLAND	3.31	45638	SCIOTO	2.23
44827	RICHLAND	2.79	45684	SCIOTO	2.22
44903	RICHLAND	2.15	45694	SCIOTO	2.20
43152	ROSS	5.15	45616	SCIOTO	2.19
43135	ROSS	5.12	45659	SCIOTO	2.18
45672	ROSS	4.99	45660	SCIOTO	2.11
45644	ROSS	4.99	45671	SCIOTO	2.04
43113	ROSS	4.94	45613	SCIOTO	1.98
43164	ROSS	4.62	45682	SCIOTO	1.91
45601	ROSS	4.41	45653	SCIOTO	1.89
45628	ROSS	4.25	45656	SCIOTO	1.87
43115	ROSS	4.19	45640	SCIOTO	1.22
45673	ROSS	4.16	44802	SENECA	4.74
43160	ROSS	4.04	43316	SENECA	4.26
45123	ROSS	3.83	44811	SENECA	4.24
45681	ROSS	3.55	44844	SENECA	3.89
45690	ROSS	3.47	44890	SENECA	3.87
45612	ROSS	3.00	44841	SENECA	3.59
43145	ROSS	2.97	44807	SENECA	3.58
44811	SANDUSKY	5.40	44854	SENECA	3.55
44824	SANDUSKY	5.38	43407	SENECA	3.54
43464	SANDUSKY	4.44	44830	SENECA	3.47
44870	SANDUSKY	3.88	44883	SENECA	3.46
43416	SANDUSKY	3.85	44882	SENECA	3.28
43469	SANDUSKY	3.79	44818	SENECA	3.23
43442	SANDUSKY	3.77	43420	SENECA	3.01

ZIP CODE	COUNTY	RADON CONC.	ZIP CODE	COUNTY	RADON CONC.
43407	SANDUSKY	3.71	43457	SENECA	2.78
43420	SANDUSKY	3.69	43410	SENECA	1.69
44841	SANDUSKY	3.19	44836	SENECA	1.68
45860	SHELBY	5.74	44720	SUMMIT	4.03
45306	SHELBY	5.13	44685	SUMMIT	3.72
45871	SHELBY	5.12	44230	SUMMIT	3.28
43343	SHELBY	5.07	44256	SUMMIT	3.28
45845	SHELBY	5.02	44281	SUMMIT	3.11
45340	SHELBY	5.02	44216	SUMMIT	2.93
45869	SHELBY	4.99	44614	SUMMIT	2.92
45388	SHELBY	4.99	44312	SUMMIT	2.90
45334	SHELBY	4.96	44087	SUMMIT	2.85
45356	SHELBY	4.94	44260	SUMMIT	2.55
43333	SHELBY	4.93	44240	SUMMIT	2.54
45318	SHELBY	4.93	44233	SUMMIT	2.54
45365	SHELBY	4.86	44278	SUMMIT	2.51
45895	SHELBY	4.86	44286	SUMMIT	2.40
45865	SHELBY	4.84	44645	SUMMIT	2.38
45333	SHELBY	4.73	44056	SUMMIT	2.34
45380	SHELBY	4.50	44224	SUMMIT	2.29
45326	SHELBY	4.20	44236	SUMMIT	2.18
45317	SHELBY	4.18	44067	SUMMIT	2.16
45363	SHELBY	4.13	44304	SUMMIT	2.07
44608	STARK	6.68	44141	SUMMIT	2.07
44643	STARK	6.16	44202	SUMMIT	1.90
44689	STARK	5.63	44308	SUMMIT	1.90
44662	STARK	5.22	44325	SUMMIT	1.88
44613	STARK	4.95	44125	SUMMIT	1.86
44260	STARK	4.50	44146	SUMMIT	1.80
44685	STARK	4.42	44311	SUMMIT	1.70
44688	STARK	4.25	44307	SUMMIT	1.44
44730	STARK	4.13	44440	TRUMBULL	2.23
44704	STARK	4.06	44437	TRUMBULL	2.05
44702	STARK	3.99	44418	TRUMBULL	1.99
44657	STARK	3.94	44404	TRUMBULL	1.93
44632	STARK	3.78	44491	TRUMBULL	1.89

ZIP CODE	COUNTY	RADON CONC.	ZIP CODE	COUNTY	RADON CONC.
44669	STARK	3.70	44231	TRUMBULL	1.85
44634	STARK	3.03	44417	TRUMBULL	1.83
44201	STARK	2.71	44288	TRUMBULL	1.80
44601	STARK	2.70	44470	TRUMBULL	1.74
44411	STARK	2.22	44428	TRUMBULL	1.69
44444	TRUMBULL	1.67	43045	UNION	4.37
44062	TRUMBULL	1.58	43342	UNION	3.82
44450	TRUMBULL	1.58	43040	UNION	3.79
44425	TRUMBULL	1.40	43302	UNION	3.73
44430	TRUMBULL	1.37	43319	UNION	3.52
44076	TRUMBULL	1.36	43332	UNION	3.43
44099	TRUMBULL	1.23	43060	UNION	3.42
44420	TRUMBULL	1.01	43340	UNION	3.38
44481	TRUMBULL	0.91	43344	UNION	3.36
44505	TRUMBULL	0.10	43358	UNION	3.35
43824	TUSCARAWAS	7.68	43067	UNION	3.07
44626	TUSCARAWAS	6.76	43066	UNION	2.98
44680	TUSCARAWAS	6.59	45833	VAN WERT	4.47
43804	TUSCARAWAS	6.40	45844	VAN WERT	4.38
44643	TUSCARAWAS	6.12	45894	VAN WERT	4.31
44608	TUSCARAWAS	5.85	45887	VAN WERT	4.19
43840	TUSCARAWAS	5.82	45863	VAN WERT	4.11
44612	TUSCARAWAS	5.70	45874	VAN WERT	4.11
44624	TUSCARAWAS	5.61	45898	VAN WERT	4.01
44629	TUSCARAWAS	5.28	45827	VAN WERT	3.99
44681	TUSCARAWAS	5.12	45849	VAN WERT	3.80
44654	TUSCARAWAS	5.08	45832	VAN WERT	3.79
44683	TUSCARAWAS	4.97	45886	VAN WERT	3.73
44656	TUSCARAWAS	4.97	45851	VAN WERT	3.66
44699	TUSCARAWAS	4.44	45880	VAN WERT	3.63
43837	TUSCARAWAS	4.41	45647	VINTON	5.20
44620	TUSCARAWAS	4.37	43135	VINTON	4.97
43832	TUSCARAWAS	4.08	43152	VINTON	4.65
44621	TUSCARAWAS	3.64	45601	VINTON	4.64
44675	TUSCARAWAS	3.56	43138	VINTON	4.23
43017	UNION	5.85	45672	VINTON	4.12

ZIP CODE	COUNTY	RADON CONC.	ZIP CODE	COUNTY	RADON CONC.
43002	UNION	5.80	45622	VINTON	3.97
43065	UNION	5.60	45654	VINTON	3.62
43064	UNION	5.26	45764	VINTON	3.48
43015	UNION	5.10	45651	VINTON	3.24
43029	UNION	4.68	45766	VINTON	2.94
43061	UNION	4.62	45692	VINTON	2.79
43044	UNION	4.60	45634	VINTON	2.68
45710	VINTON	2.40	45778	WASHINGTON	3.05
45695	VINTON	2.25	45788	WASHINGTON	3.01
45686	VINTON	2.07	45786	WASHINGTON	2.98
45741	VINTON	2.00	45768	WASHINGTON	2.84
45177	WARREN	4.14	45723	WASHINGTON	2.83
45370	WARREN	3.97	45773	WASHINGTON	2.81
45327	WARREN	3.78	45742	WASHINGTON	2.80
45068	WARREN	3.53	44662	WAYNE	4.81
45042	WARREN	3.32	44624	WAYNE	4.46
45054	WARREN	3.15	44840	WAYNE	4.40
45005	WARREN	3.13	44633	WAYNE	4.34
45036	WARREN	3.13	44676	WAYNE	4.31
45152	WARREN	3.11	44611	WAYNE	4.30
45066	WARREN	3.07	44691	WAYNE	4.27
45140	WARREN	3.01	44842	WAYNE	4.22
45044	WARREN	3.00	44627	WAYNE	4.05
45342	WARREN	2.94	44618	WAYNE	4.02
45458	WARREN	2.90	44276	WAYNE	3.96
45050	WARREN	2.85	44287	WAYNE	3.81
45249	WARREN	2.75	44866	WAYNE	3.72
45069	WARREN	2.62	44217	WAYNE	3.69
45241	WARREN	2.53	44214	WAYNE	3.65
45040	WARREN	2.46	44270	WAYNE	3.52
45162	WARREN	2.30	44645	WAYNE	3.51
45122	WARREN	1.68	44230	WAYNE	3.47
45744	WASHINGTON	3.36	44666	WAYNE	3.46
43724	WASHINGTON	3.35	44614	WAYNE	3.07
45715	WASHINGTON	3.22	43557	WILLIAMS	2.80
45711	WASHINGTON	3.20	43517	WILLIAMS	2.74

ZIP CODE	COUNTY	RADON CONC.	ZIP CODE	COUNTY	RADON CONC.
43728	WASHINGTON	3.18	43518	WILLIAMS	2.69
45746	WASHINGTON	3.18	43502	WILLIAMS	2.64
45734	WASHINGTON	3.11	43506	WILLIAMS	2.63
45767	WASHINGTON	3.10	43570	WILLIAMS	2.60
45727	WASHINGTON	3.10	43554	WILLIAMS	2.54
45745	WASHINGTON	3.09	43501	WILLIAMS	2.47
43787	WASHINGTON	3.08	43521	WILLIAMS	2.46
45789	WASHINGTON	3.07	43431	WOOD	3.11
45724	WASHINGTON	3.06	43412	WOOD	3.08
43469	WOOD	2.91	43566	WOOD	1.80
43430	WOOD	2.88	43451	WOOD	1.73
43447	WOOD	2.83	43522	WOOD	1.57
44830	WOOD	2.77	43569	WOOD	1.40
43537	WOOD	2.72	44802	WYANDOT	4.02
43460	WOOD	2.71	44844	WYANDOT	3.83
43406	WOOD	2.62	43332	WYANDOT	3.71
43551	WOOD	2.57	43316	WYANDOT	3.66
45889	WOOD	2.48	45843	WYANDOT	3.66
44817	WOOD	2.44	43302	WYANDOT	3.65
43516	WOOD	2.42	43359	WYANDOT	3.63
43457	WOOD	2.41	44820	WYANDOT	3.62
45872	WOOD	2.20	43337	WYANDOT	3.60
43609	WOOD	2.19	43351	WYANDOT	3.58
43605	WOOD	2.10	45867	WYANDOT	3.53
43402	WOOD	1.92	43326	WYANDOT	3.50
43403	WOOD	1.85	44882	WYANDOT	3.46
43511	WOOD	1.80	44849	WYANDOT	3.42